AN ABSTRACT OF THE DISSERTATION OF

Yu-Jung Chu for the degree of Doctor of Philosophy in Electrical and Computer Engineering presented on May 15, 2020.

Title: Channel Estimation, Modulation Techniques and Decoding Algorithms for Hybrid WiFi-FSO (WiFO) WLAN of Femtocells

Abstract approved: _____

Thinh P. Nguyen

Due to the limitation of the radio frequency (RF) spectrum, it is increasingly more difficult to support billions of wireless devices in the age of Internet-of-Things. Consequently, many recent wireless indoor communication systems have been developed using free space optical (FSO) communication technologies that exploit the extremely large light spectrum to transmit data. This dissertation contributes three physical layer techniques to an FSO system called WiFO, which is integrated with the existing WiFi transmission. (1) We proposed a Pulse Amplitude Modulation (PAM) decoding scheme that estimates the channel parameters and determine the optimal decoding thresholds to minimize the average bit error rate (BER). The conditions on channel parameters for which signal recovery is impossible, are also determined. (2) A pre-shaping technique called Adaptive Sending Duration Algorithm (ASDA), that modifies the dura-

tions of input bits dynamically, is proposed to be used at an LED-transmitter. Simulation results show that ASDA working with equalization successfully improves the performance of BERs. (3) We propose a decoding scheme called Memory Decoding Algorithm (MDA) used at a receiver and show that it effectively reduces the bit error rates via maximum likelihood decoding principle.

Channel Estimation, Modulation Techniques and Decoding Algorithms for Hybrid WiFi-FSO (WiFO) WLAN of Femtocells

by

Yu-Jung Chu

A DISSERTATION

submitted to

Oregon State University

in partial fulfillment of
the requirements for the
degree of

Doctor of Philosophy

Presented May 15, 2020
Commencement June 2020

Doctor of Philosophy dissertation of Yu-Jung Chu presented on May 15, 2020.

APPROVED:

Major Professor, representing Electrical and Computer Engineering

---

Head of the School of Electrical Engineering and Computer Science

---

Dean of the Graduate School

I understand that my dissertation will become part of the permanent collection of Oregon State University libraries. My signature below authorizes release of my dissertation to any reader upon request.

Yu-Jung Chu, Author

ACKNOWLEDGEMENTS

This dissertation is dedicated to my dad, mom and my beloved family. Thanks to everyone in my life who had contributed, at varying levels, to help make me who I am today. Biggest thanks to my advisor, Dr. Nguyen, who has been the most supportive of me for the past six years.

Glory to GOD.

TABLE OF CONTENTS

TABLE OF CONTENTS (Continued)

LIST OF FIGURES

LIST OF FIGURES (Continued)

LIST OF FIGURES (Continued)

LIST OF ALGORITHMS

Chapter 1: Introduction

In recent years, the products of hand-held portable devices, such as smart phones and tablets, increased in both quality and quantity. In the other aspect, as the price of broadband access service becomes more affordable, the number of homes with WiFi and public WiFi hotspots in the US are increasing significantly. Therefore, people tend to own multiple devices for various purposes from work and school to personal entertainment. For example, other than a smart phone, one might have a tablet for recreation and another laptop for work or study. Even kids watch cartoons on tablets more than on TVs nowadays. These consumer devices with applied software have indeed bound up with people's daily life inseparably. Thousands of miscellaneous apps for those devices have also sprung up everyday. Consequently, future Wireless Local Area Networks (WLAN) must be able to accommodate such explosive increase in wireless usage. Cisco reported that the yearly global mobile data traffic will reach 930 exabytes and 59 percent of the total mobile data traffic will be offloaded through WiFi by 2022 [1]. Such statistics indicate that WiFi continues to be an indispensable and pervasive technology. However, limited capacity of existing WiFi networks fail to provide adequate bandwidth for densely populated areas such as airports, conference venues, and hotel lobbies. That said, this chapter will discuss the shortcomings of current WiFi and introduce a novel

communication system called WiFO. WiFO is a hybrid WiFi Free Space Optical Local Wireless Area Network of Femtocells.

1.1 Motivation

With the rapid growth in wireless communication usage, WiFi has become an indispensable and important part of people's daily lives. However, if with lack of the access of internet, especially WiFi, the convenience and usefulness it brings to us will be sharply diminished. The main problem with typical WiFi systems is the Radio Frequency (RF) interference that allows only a single pair of sender and receiver to communicate with each other at the same time and on the same frequency band. This severely limits the WiFi capacity. For example, while the most popular WiFi standard, IEEE 802.11g has the maximum theoretical data rate of 54Mbps, only a fraction of the maximum capacity, e.g, 30 Mbps can be obtained in practice due to the MAC protocol overhead and the distances between the receivers and the Access Point (AP). Furthermore, if there are 20 users, 30 Mbps has to be divided among the 20 users. Consequently, the throughput per user is only 1.5 Mbps which cannot support high definition video streaming applications.

Due to the fundamental limitation of the radio frequency (RF) spectrum induced by the laws of physics, the shared RF spectrum cannot be unboundedly expanded. The emerging markets for smart homes and the Internet of Things also make it increasingly more difficult to support billions of wireless devices

competing for the limited shared bandwidth. The shortcoming of limited wireless capacities makes current WiFi networks fail to provide adequate bandwidth in densely populated areas, thus, it is becoming a critical problem to find new ways of providing sufficient access to wireless Internet for accommodating such explosive increase in wireless usage. Consequently, recent research efforts on RF-based communications have focused on expanding RF spectrum communications and using RF spectrum more efficiently. Like [2] to [4] work on efficient use of radio frequency bands, but these efforts have not overcome fundamental limitations caused by restricted bandwidths. For the recent WiFi standard 802.11ad, it promises to deliver a significant increase in capacity of up to 6 Gbps in approximately 2 GHz of spectrum at 60 GHz. This is a significant departure from the today 2.4 and 5 GHz wireless bands which are already heavily congested. However, due to 60 GHz transmission, 802.11ad suffers from large attenuation when propagating through walls, and therefore are used primarily for short distance transmissions. Circuitry for 802.11ad transceivers are also complex and have yet been demonstrated to be economically viable. There have been numerous techniques to increase spectrum efficiency, ranging from physical layer techniques such as Multiple Input Multiple Output (MIMO) transmissions to higher level approaches such as Dynamic Spectrum Access (DSA). Although the DSA approach allows the wireless device operating band to change dynamically in both spatial and temporal dimensions in order to utilize spectrum more efficiently, such an approach requires increasingly advanced and complicated RF circuitry and algorithms for dynamically allocating spectrum based on tem-

poral and spatial dimensions. Therefore, due to many economic and technical issues, the proliferation of DSA remain to be seen.

On the other hand, recent remarkable research in Free Space Optical (FSO), which is an approach to increasing wireless capacity with minimal changes to the existing WiFi architecture, promises a complementary system. Importantly, this system can be realized because FSO communication technology does not interfere with the RF transmissions [5]. Specifically, the solid state light sources such as Light Emitting Diode (LED) and Vertical Cavity Surface Emitting Laser (VCSEL) are now able to transmit data at high bit rates (> 1 Gbps) reliably with low energy consumption using simple modulation schemes such as On-OFF Keying [6] [7]. However, the main factors that limit the capacities of FSO communication systems are technologies, such as integration with the existing WiFi. FSO communication transmits information by modulating light. In practice, LED transmitters have maximum modulation frequency before the output signals become too distorted. There is also an inherent trade-off between the output power (light intensity) and the modulation frequency. The LEDs that are capable of modulating light at a high data rate, tend to have lower emission power while ones with low modulation bandwidth have a higher emission power. As for the receiving side, a photo-diode is used to turn light intensity into current/voltage, i.e., decoding. The demodulation rate of a photo-diode depends on the area used to collect the light signals. A larger area collects more light, resulting in a more reliable signal, but at the expense of lower demodulation speed due to larger capacitance. Thus, FSO communication systems are

designed with the appropriate transmitters, receivers, and usage scenarios to maximize the transmission rate. Therefore, how to modulate light efficiently and how to decode a light signal reliably are also worthy to investigate.

1.2 Related Work

It is important to note that the previous work and other excellent researchers' contributions play a key role of inspiring us to have the proposed WiFO system in section 1.3. Recently, solid state light sources such as Light Emitting Diodes (LEDs) and laser diodes are sufficiently mature enough so that it is practical to transmit high data rates at reliably short ranges. LEDs also have exceptional features such as low power consumption, low cost, light-weight, and small volume. Besides these remarkable features, LEDs enhance communication security, which is highly desirable in many applications [8] and have great accuracy with indoor positioning [9]. As such, there has been work on outdoor and long-distance implementations of hybrid FSO/RF communication systems [10] by O. Bouchet, [11] by H. Wu, [12] by S. Bloom and [13] by I. Kim where the transmissions are subjected to attenuation and fading due to distances, weather conditions and scintillation. In the work of H. Al Hajjar et al. [14] and K. Wang et al. [15], the implementation of a physical layer with a large bandwidth is employed to provide high speed data links for a small number of users in a base station. Much less research effort is devoted to indoor free-space optical communications. An example of indoor FSO communication system is the work of

M. Kavehrad et al. [16] which uses white light emitting diodes (WLEDs) for simultaneous illumination and free-space optical communication. [17] is the other example of indoor visible light communication using MIMO-OFDM scheme. Although this solution is potentially energy efficient, it is not easy to integrate with the existing WiFi systems, and offers low bandwidth. There have also been recent researches on optimization of joint data transmission on both RF and FSO channels. For example, the works in [18] by A. Eslami, [19] by Y. Tang, [20] by N. Letzepis, [21] by F. Ahdi, [22] by A. Abdulhussein and [23] by D. Wang address joint coding schemes for both FSO and RF channels. There are also some interesting applications with light communications including underwater optical transmission [24] and vehicular applications [25] [26]. Li-Fi [27] by H. Hans et al. is another notable technology using visible light communication that can achieve high data rate for short range communication. FSO communication systems are not well integrated with WiFi and are therefore of limited mobility. Thus, the general theme of using FSO and RF for communication has been extensively studied. For example, Wang et al. have characterized the throughput and delay of hybrid FSO/RF networks [28], while others research into point-to-point architecture based on board-level and chip-level optical interconnects [29] for super computers. The WiFO (WiFi Free-Space Optical) system we proposed is the other novel communication system based on FSO utilizing inexpensive IR LEDs that are invisible to the human eye and well integrated with existing WiFi networks, while most of other works focus on visible light communications [30] [31] [32]. Specifically, WiFO resolved both capacity

and mobility issues that the present WiFi and FSO technologies are facing. To the best knowledge, the WiFO system [33] [34] [35] is the first to integrate WiFi and FSO seamlessly at a low cost using inexpensive components while providing both high capacity and mobility.

1.3 WiFO

WiFO consists of an array of FSO transmitters attached to the ceiling. These FSO transmitters use inexpensive LEDs or slightly more expensive VCSELs to modulate light for digital transmissions. Fig. 1.1 illustrates a typical setting for the proposed WiFO system. These include airport terminals, offices, entertainment centres, and other indoor communications where WiFi bandwidth is potentially inadequate. In this setting, the focus will be on the common downlink scenario where most of users will download contents from the Internet via an AP. A network of FSO transmitters LEDs, with the high-speed Ethernet infrastructure can be deployed directly above the appropriate spots to provide local high-rate FSO transmissions most of the time, in addition to the WiFi transmission. To transmit data, each FSO transmitter creates an invisible beam cone of light about one square meter that covers a small area, and then a laptop or a PC located in this area equipped with a silicon photodiode (PDs) can receive data via local FSO transmissions with rates depending on the distances to the center of the projected cone. Digital bits “1” and “0” can be transmitted by switching the LEDs or VCSELs on and off rapidly. And

then each WiFO receiver equipped with a silicon pin photodiode converts light intensity into electrical currents that can be interpreted as the digital bits ”0” and ”1”. The hardware and software architectures of WiFO will be described briefly as follow.

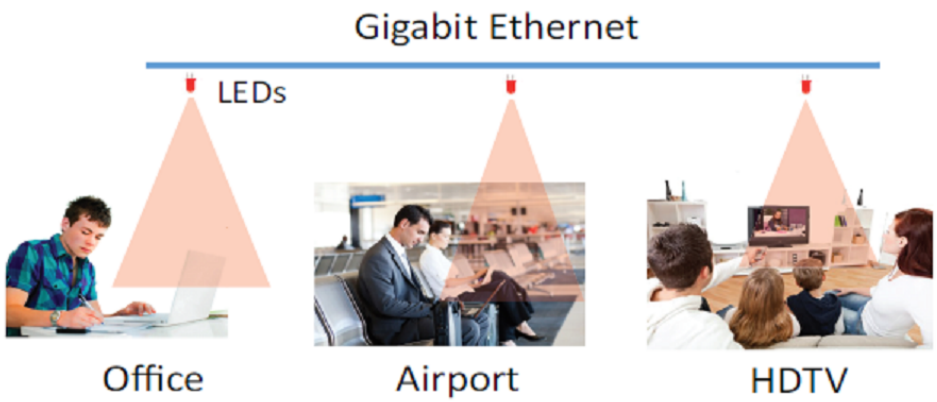

Figure 1.1: WiFO Usage Scenarios

1.3.1 Hardware Architecture and Software Design

1.3.1.1 Hardware Architecture

We used BeagleBone microcontrollers as a signal source and as an interface between the receiver circuitry and terminal computer. The transmitter uses a 100mW 850nm infrared LED that is driven using NMOS transistors. The receiver consists of two main components: 1) a receiver circuit connected to a

FDS-100 silicon pin photodiode from Thorlabs and 2) a comparator connected to an amplifier. The amplifier converts the current signal produced by a photo diode into an amplified voltage signal and provide extra signal strength while also removing the unwanted DC component created by the photo diode. The comparator checks whether the filtered signal is greater then or less then zero and then outputs a square wave with a value of 0V or 3V based on that comparison. Fig. 1.2 and Fig. 1.3 show the block diagram and realization for the WiFO hardware architecture.

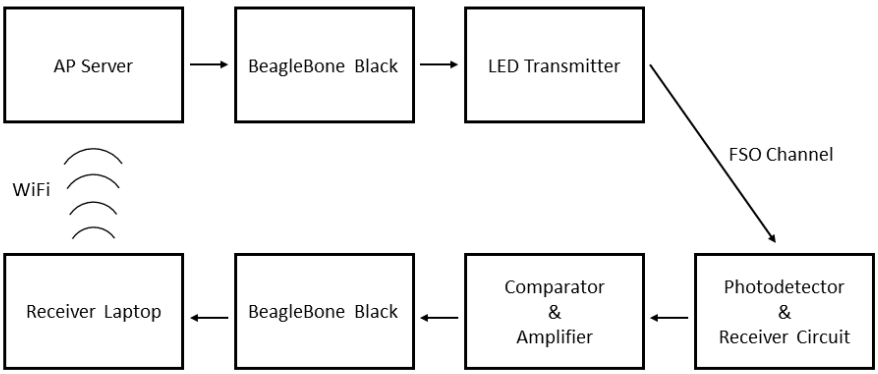

Figure 1.2: WiFO System Block Diagram

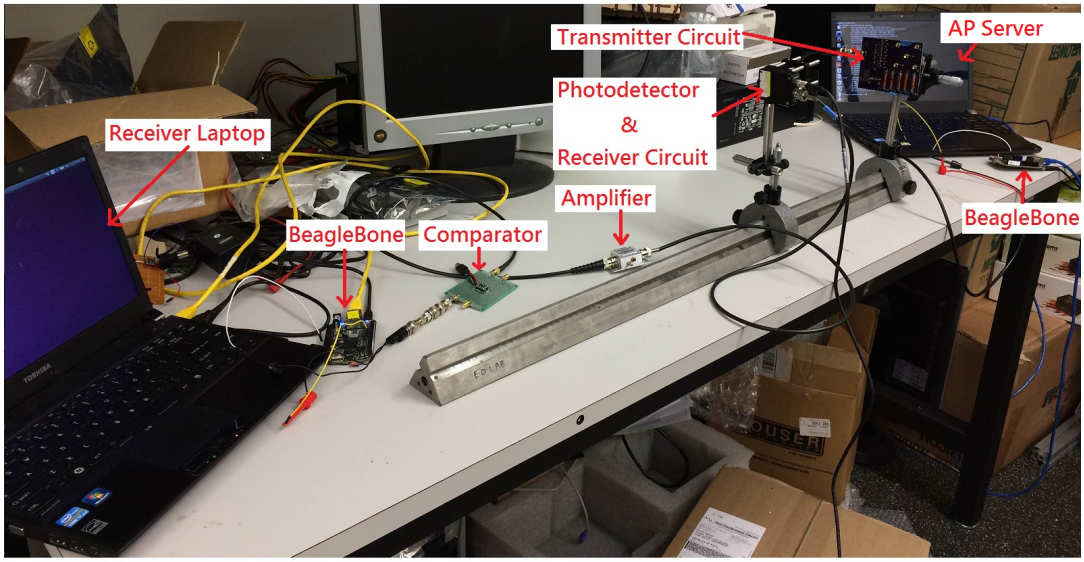

Figure 1.3: WiFO Hardware Architecture

1.3.1.2 Software Design

The OSI model consists of seven layers in conceptual network stacks. Fig. 1.4 shows the software design of the functions used for FSO transmissions in each layer.

- Physical Layer: A 32-bit preamble is prefixed to each frame used to distinguish between frames. Then the transmitter uses OOK (On-Off Keying) to modulate ”0” to low optical intensity and ”1” to high optical intensity. The received signals are four-time oversampled, then a Majority decoder is implemented at the receiver to avoid bit flips.

- MAC/Data Link Layer: Manchester Code [36] is implemented here for eliminating DC components. When receiving data, the corresponding decoding is implemented.

- Network Layer: An AP server is used to regulate packet flow. It uses a mechanism to decide whether the FSO or the WiFi channel is used to transmit the packet.

- Transport Layer: Since WiFO is a one-way FSO transmission focusing on the down-link scenario, the ACKs are sent back via the WiFi channel from the receivers to the AP server to implement the retransmission mechanism. Packet IDs are also checked here to examine the order the packets are received and ensure the data are reconstructed correctly in order.

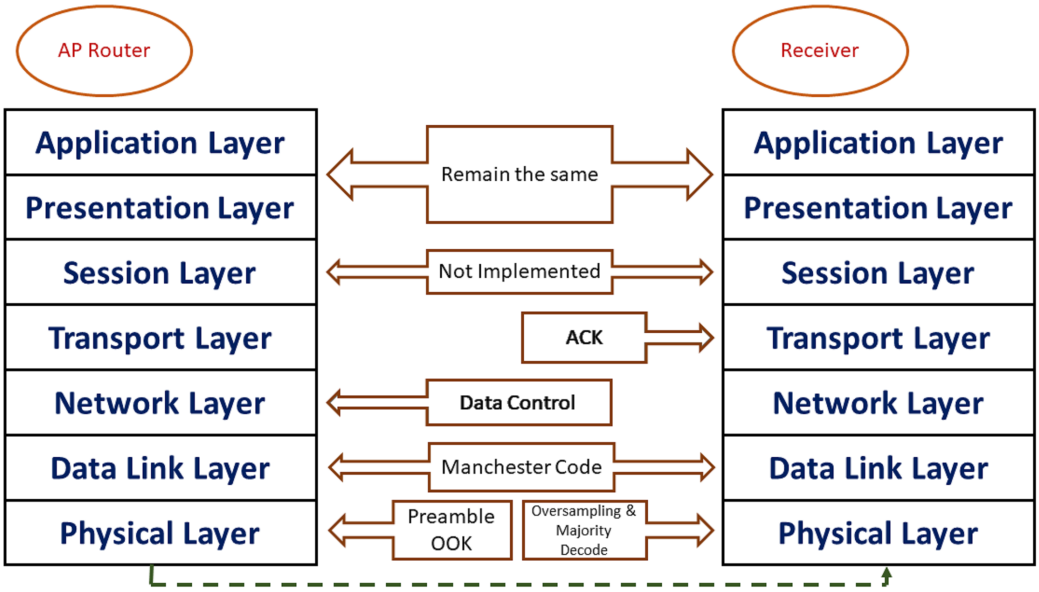

Figure 1.4: WiFO Software Design

- Session Layer: This layer of WiFO has not been implemented. In the future, this can be addressed with a mechanism for authentication and permission on users connected to each WiFO transmitter.

- Presentation Layer and Application Layer: One of the best advantages of WiFO is that everything remains the same in the application layer. This means, programmers do not need to make any changes with high level APIs when systems are integrated with WiFO. And WiFO is compatible with all existing network protocols, such as HTTP, FTP, TELNET...ext.

1.3.2 Video Demo

Please watch our WiFO demo videos at
https://www.youtube.com/watch?v=Pf6TMwor8qM&feature=youtu.be
and
https://www.youtube.com/watch?v=qVzJ0aj80PA&feature=youtu.be
.

1.4 Outline of The Thesis

With the descriptions of the motivation, related works and the prototype of WiFO in the previous sections, this section is going to briefly go over the following chapters. This thesis is divided into 6 chapters. Chapter 2 will propose an optimal Pulse Amplitude Modulation (PAM) scheme to address the scenario when light cones overlap. In Chapter 3, a mathematical model to accurately capture the distortion of the output for a given input to an LED-based transmitter is introduced and the memory property of the light response is discussed. Chapter 4 propose a pre-distortion technique called Adaptive Sending Duration Algorithm (ASDA) to be used at an LED-transmitter that modifies the durations of input bits dynamically in order to compensate for the distortions of output bis. And Chapter 5 propose a called Memory Decoding Algorithm (MDA) to be used at a receiver that exploits the distortion model to reduce the bit error rates via Maximum Likelihood decoding principle. Finally, a conclusion will be made in Chapter 6.

Chapter 2: FSO Channel Characterization and Optimal Pulse Amplitude Modulation/Demodulation

To provide high bit rates and large coverage, WiFO employs an array of LED-based transmitters. Each modulates a beam of invisible light using a Pulse Amplitude Modulation (PAM) scheme. A WiFO receiver is capable of receiving signals from multiple transmitters simultaneously to achieve higher bit rates. In this chapter, we describe a PAM decoding scheme that estimates the channel parameters, then use them to determine the optimal decoding thresholds for minimizing the average bit error rate. Furthermore, we characterize the conditions on channel parameters for perfect signal recovery. Simulations and theoretical analyses are provided to validate the proposed scheme. That said, the primary contribution of this chapter is on the design and analysis of an optimal Pulse Amplitude Modulation (PAM) decoding scheme used in the WiFO system. Using the proposed PAM decoding scheme, the receiver first estimates the channel parameters, then uses them to determine the optimal decoding thresholds for minimizing the average bit error rate.

Each FSO transmitter creates an invisible cone of light about one square meter directly below in which the data can be received to transmit data. Fig. 2.1 shows an example of a coverage area with seven FSO transmitters. Digital bits ”1” and ”0” can be transmitted by switching the LEDs or VCSELs on

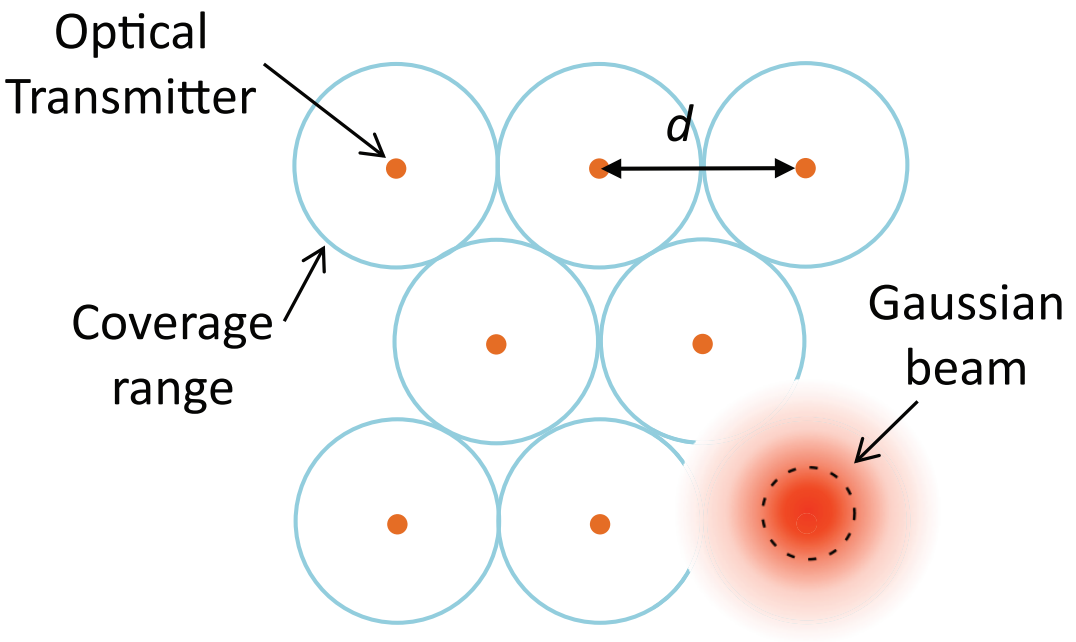

Figure 2.1: Configuration of the optical transmitter array

and off rapidly. For the general PAM, signals of more than two levels can be transmitted. The switching rate can be up to 100 MHz for LED-based transmitters and $>$ 1 GHz for VCSEL-based transmitters. Fig. 2.2 shows the light intensity as the function of the position measured from the center of the cone. High intensity results in more reliable transmissions.

In this chpter, we will (1) characterize the FSO channel empirically (2) use it to propose a channel model; (3) estimate the channel parameters based on the model; (4) propose an optimal PAM decoding scheme based on the channel parameters; and (5) analyze the conditions for data irrecoverability.

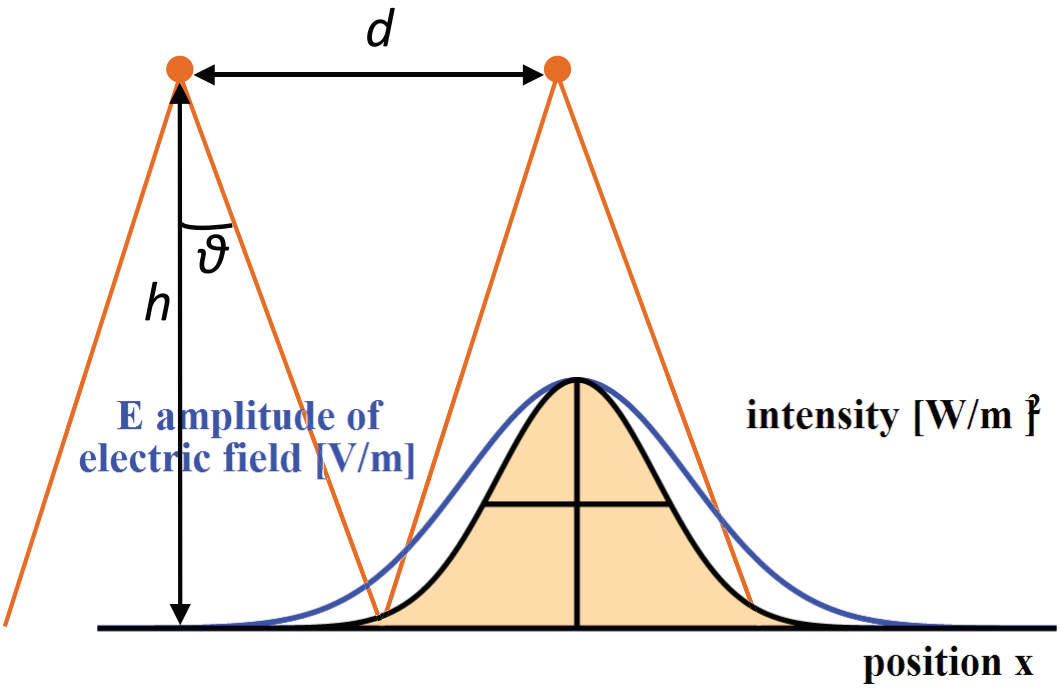

Figure 2.2: coverage of optical transmitters with a divergent angle of ϑ

2.1 Channel Characterization and Modeling

We study the FSO channel using the setup shown in Fig. 2.3. The setup consists of a transmitter board and receiver board located on a rail at a distance of 1 meter away from each other. The transmitter board contains two LEDs inches apart. For the first part of the experiment, at any one time, only one of the two LEDs emits a constant power at wavelength of 890 nm under the regular white light illumination. The receiver is then moved to different positions along the line perpendicular to the rail. The received power levels were measured at each position. This part of the experiment aims to characterize the power signal received at the receiver at different divergent angles. As seen in Fig. 2.4, the power intensities (power) at the receiver due to each separate LED decreases as the distance from the center of the cone increases, i.e., the divergent angle ϑ increases. Furthermore, the light intensities follows a Gaussian-like shape as predicted by the theory of FSO [37].

In the second part of the experiment, we aim to verify whether the FSO channel is an additive channel. In this setup, both LEDs emit light simultaneously. Fig. 2.5 shows the power at the receiver as a function of divergent angle. Importantly, this power is approximately equal to the sum of the individual powers observed from the two LEDS shown in Fig. 2.4. Therefore, the FSO channel can be modeled very well as an additive channel. This is an important property to be exploited in the proposed PAM to increase a receiver's throughput when it is in the coverage of more than one light cones.

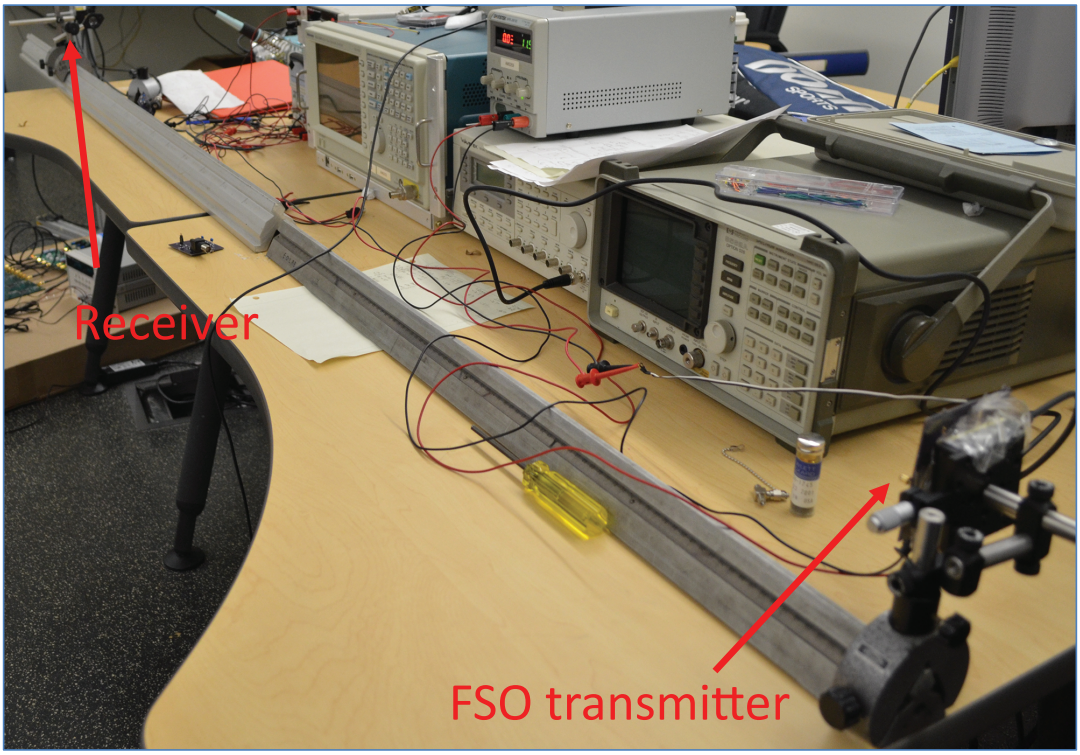

Figure 2.3: Experiment setup for channel characterization

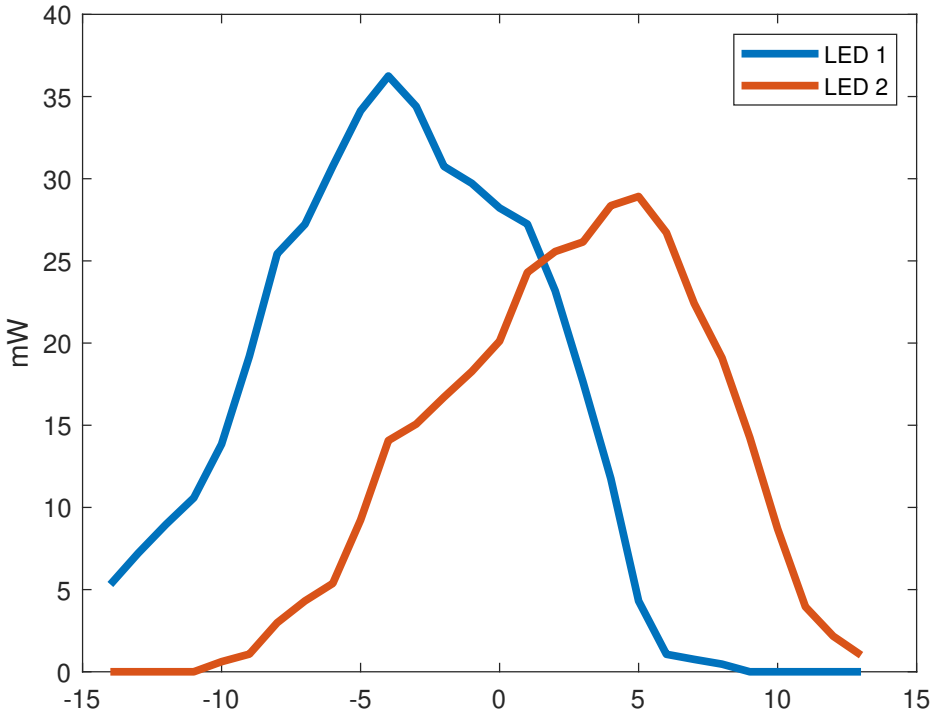

Figure 2.4: Power measurements of two LEDs measured separately

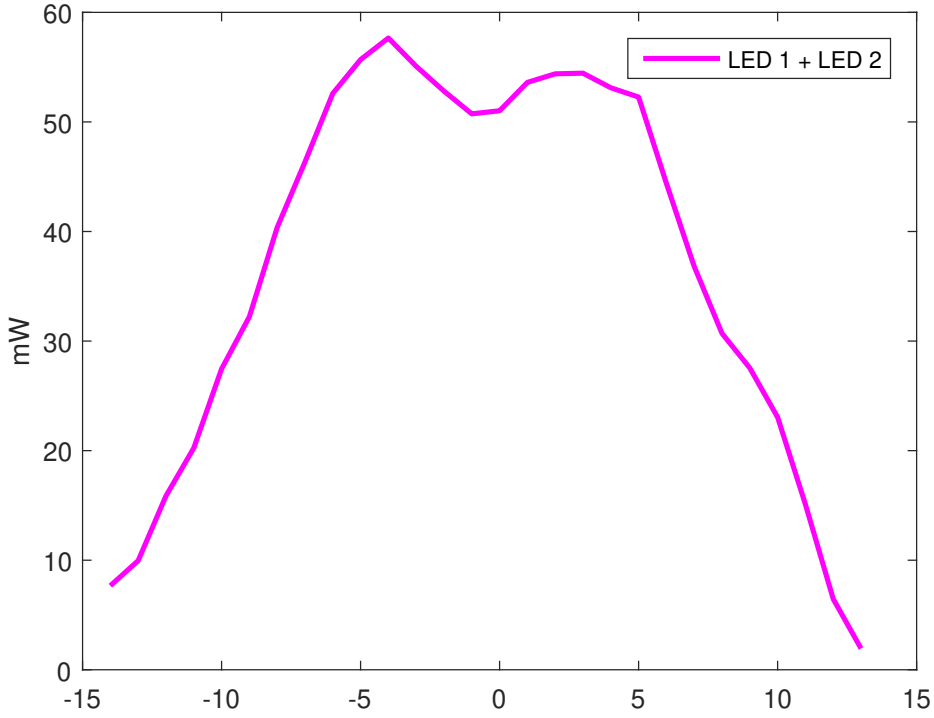

Figure 2.5: Power measurements of two LEDs measured at the same time

Based on the discussion above, we propose the following free space optical (FSO) communication model. We note that, due to the femtocell architecture, all WiFO's transmissions are short and line of sight transmissions. In addition, fading due to reflected light is negligible. That said, let $x_i(t)$ be the transmitted signal by the transmitter i, and $y_{ij}(t)$ be the received signal by the receiver j due solely to transmitter i as shown in Fig. 2.6(a), then

$$y_{ij}(t) = \alpha_{ij} x_i(t) + n_j, \tag{2.1}$$

where $\alpha_{ij} \in (0, 1)$ and n_j denote the attenuation factor and the thermal Gaussian noise respectively. α_{ij} is small (large) when the receiver j is at a large (small) distance or large (small) divergent angle from the transmitter i. We note that since fading is negligible, there is no delayed version of $x_i(t)$ in Eq. (2.1) as often is the case when modeling RF transmissions. For digital transmissions as is the case for WiFO, an equivalent digital version of Eq. (2.1) is:

$$y_{ij}[k] = \alpha_{ij} x_i[k] + n_j. \tag{2.2}$$

In general, if a receiver receives signals from n transmitters simultaneously as shown in Fig. 2.6(b) (for $n = 2$), then due to the additive property, the signal received at the receiver j is:

$$y_j[k] = \sum_{i}^{n} \alpha_{ij} x_{ij}[k] + n_j = \mathbf{x}_j^T \boldsymbol{\alpha}_j + n_j, \tag{2.3}$$

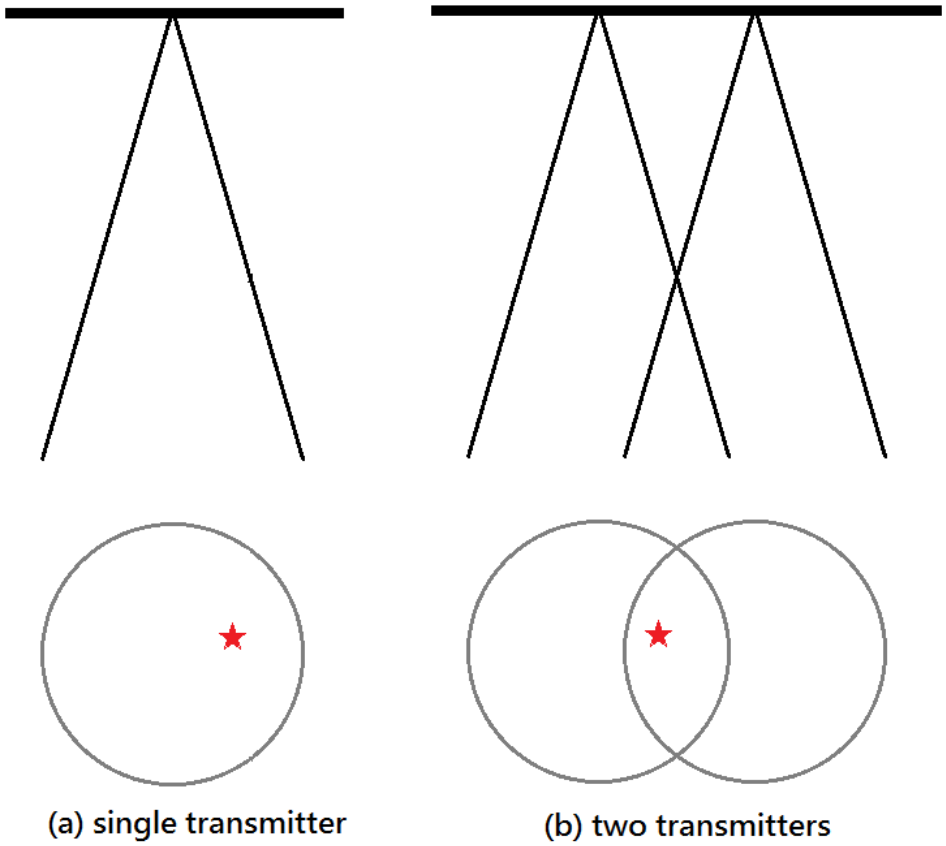

Figure 2.6: Single/Multiple Transmitters Scenario

where $\mathbf{x}_j = (x_{1j}, x_{2j}, \ldots, x_{nj})^T$, and $\boldsymbol{\alpha}_j = (\alpha_{1j}, \alpha_{2j}, \ldots, x_{nj})^T$. We note that if a receiver j is not located in the light cone of a transmitter i, then effectively, $\alpha_{ij} = 0$.

2.2 Optimal Pulse Amplitude Modulation/Demodulation

We now describe the modulation and demodulation of WiFO.

Modulation. WiFO sends information digitally by pulsing light at m discrete levels of light intensities. Furthermore, a receiver can receive light from multiple transmitters simultaneously. If there are n transmitters, each capable of pulsing light at m discrete levels, then depending on the values of α_{ij}, an ideal receiver j can observe a total of m^n of possible distinct patterns. For example, Fig. 2.7 shows the scenario consisting of a single receiver receiving signals simultaneously from two transmitters ($n = 2$), each capable of transmitting three levels (m=3). Assuming no thermal noise and the given α_1 α_2 as the attenuated factors from the two transmitters to the receiver, there are 9 possible discrete light intensity levels observed by the receiver. An ideal receiver will be able to distinguish all of these levels and correctly infer the transmitted patterns. However, for some values of α_i, it is not possible to infer the transmitted signals correctly, regardless of whether noise is present or not. For example, in the same scenario when $\alpha_1 = 1$ and $\alpha_2 = 0$, it is straightforward to see that the total number of distinct light intensity levels at the receiver is 3. However, there can be a total of 9 transmitted patterns, and thus it is not possible to recover the transmitted signals. We will consider this issue in Section 2.5.

Demodulation. Given the received signal, the receiver j infers the transmitted patterns using the following procedure. First, the receiver j estimates the values of α_{ij}, i.e. channel estimation. The channel estimation procedure is

described in Section 2.3. Next, using α_{ij}, the receiver constructs a table similar to Fig. 2.7 for all the possible values of a received signal. If there are k possible discrete levels, the receiver will find k optimal non-overlapped intervals, i.e., *thresholds* corresponding to the k possible transmitted patterns. If the received signal y_j is within a specified interval, the receiver will decode the transmitted patterns that correspond to that interval. We discuss the method for determining the optimal thresholds in Section 2.4.

The bit rate of a receiver depends on the number of distinct levels that a receiver can decode per unit time. Specifically, if there are k different patterns per unit time, then the maximum amount of information per unit time can be sent to a receiver is $\log k$ bits, assuming noise is not present. Thus, by allowing more transmitters to cooperate to transmit the information to a receiver, the receiver can obtain a higher bit rate.

2.3 Channel Estimation

In this section, we describe the linear regression method for estimating α_{ij} at the receivers that minimizes the mean square error (MSE). In WiFO, the n transmitters are controlled by the AP. Multiple receivers might be located in the light cones of multiple transmitters as shown Fig. 2.8. The estimation method begins with each transmitter sending out its l training data points (training sequence) simultaneously to all r receivers within their coverage. Let $\boldsymbol{\alpha}_j = (\alpha_{1j}, \alpha_{2j}, \ldots, \alpha_{nj})^T$. Then, all r receivers estimate $\boldsymbol{\alpha}_1, \boldsymbol{\alpha}_2, \ldots, \boldsymbol{\alpha}_r$ simultaneously

	$\alpha_1 = 0.3$	$\alpha_2 = 0.9$	$\underline{x}_i^T \underline{\alpha}$
$\underline{x}_9$	2	2	2.4
$\underline{x}_8$	1	2	2.1
$\underline{x}_7$	0	2	1.8
$\underline{x}_6$	2	1	1.5
$\underline{x}_5$	1	1	1.2
$\underline{x}_4$	0	1	0.9
$\underline{x}_3$	2	0	0.6
$\underline{x}_2$	1	0	0.3
$\underline{x}_1$	0	0	0

$m = 3 \quad n = 2$

Figure 2.7: The received levels

based on their received signals. Let us consider a single receiver j that can receive the signal from n transmitters. By sending l training symbols from the n transmitters, the received signal at the receiver j is:

$$\mathbf{y}_j = \mathbf{X}\boldsymbol{\alpha}_j + \mathbf{n}_j, \tag{2.4}$$

where

$$\mathbf{X} = \begin{bmatrix} x_1[1] & x_2[1] & \dots & x_n[1] \\ x_1[2] & x_2[2] & \dots & x_n[2] \\ \dots & \dots & \dots & \\ x_1[l] & x_2[l] & \dots & x_n[l] \end{bmatrix}$$

is the training matrix whose $x_i[k]$ denotes the kth training symbol sent out by transmitter i , $\mathbf{y}_j = (y_j[1], y_j[2], \dots, y_j[l])^T$ denotes the vector of l observations, and $\mathbf{n}_j = (n_j[1], n_j[2], \dots, n_j[l])^T$ denotes a vector of i.i.d thermal noise.

Next, we define the sum of square error (SSE) as:

$$\mathbf{S}(\boldsymbol{\alpha}_j) = \|\mathbf{y}_j - \mathbf{X}\boldsymbol{\alpha}_j\|^2 = \mathbf{y}_j^T\mathbf{y}_j - 2\boldsymbol{\alpha}_j^T\mathbf{X}^T\mathbf{y}_j + \boldsymbol{\alpha}_j^T\mathbf{X}^T\mathbf{X}\boldsymbol{\alpha}_j. \tag{2.5}$$

Now, since MSE is equal to SSE divided by l, minimizing MSE is equivalent to minimizing SSE. We want to determine $\hat{\boldsymbol{\alpha}}_j$ that minimizes SSE. This is done by taking derivative of $\mathbf{S}(\boldsymbol{\alpha}_j)$ with respect to $\boldsymbol{\alpha}_j$ and set it to zero, we have:

$$-\mathbf{X}^T\mathbf{y}_j + \mathbf{X}^T\mathbf{X}\boldsymbol{\alpha}_j = \mathbf{0}. \tag{2.6}$$

Multiplying $(\mathbf{X}^T\mathbf{X})^{-1}$ on both sides of Eq. (2.6), we obtain:

$$\hat{\boldsymbol{\alpha}}_j = (\mathbf{X}^T\mathbf{X})^{-1}\mathbf{X}^T\mathbf{y}_j. \tag{2.7}$$

Note that the training sequences, i.e., $\mathbf{X}$ should be chosen such that $\mathbf{X}^T\mathbf{X}$ is invertible. Equivalently, the rank of $\mathbf{X}$ should equal n.

Plugging $\hat{\boldsymbol{\alpha}}_j$ back into Eq. (2.5), the resulted SSE is:

$$\mathbf{S}(\hat{\boldsymbol{\alpha}}_j) = \|\mathbf{y}_j - \mathbf{X}\hat{\boldsymbol{\alpha}}_j\|^2 = \|\mathbf{y}_j - \mathbf{X}(\mathbf{X}^T\mathbf{X})^{-1}\mathbf{X}^T\mathbf{y}_j\|^2$$

$$= \|(\mathbf{I}_{l\times l} - \mathbf{X}(\mathbf{X}^T\mathbf{X})^{-1}\mathbf{X}^T)\mathbf{y}_j\|^2. \tag{2.8}$$

For r users, Eq. (2.4) can be extended as:

$$\mathbf{Y} = \mathbf{X}\mathbf{A} + \mathbf{N}, \tag{2.9}$$

where

$$\mathbf{N} = \begin{bmatrix} \mathbf{n}_1 & \mathbf{n}_2 & \dots & \mathbf{n}_r \end{bmatrix}$$

denotes the $l \times r$ matrix whose columns consist of thermal noise from each receiver,

$$\mathbf{A} = \begin{bmatrix} \boldsymbol{\alpha}_1 & \boldsymbol{\alpha}_2 & \dots & \boldsymbol{\alpha}_r \end{bmatrix},$$

and

$$\mathbf{Y} = \begin{bmatrix} \mathbf{y}_1 & \mathbf{y}_2 & \dots & \mathbf{y}_r \end{bmatrix}.$$

Similarly, the linear regression estimation of A is:

$$\hat{\mathbf{A}} = (\mathbf{X}^T\mathbf{X})^{-1}\mathbf{X}^T\mathbf{Y}. \tag{2.10}$$

2.4 Optimal Decoding Thresholds

In Section 2.2, we briefly discussed the method for recovering the transmitted patterns based on the received signals. In this section, we describe in detail the decoding method based on a thresholding procedure. Here we assume the transmission rate remains the same over the time and source patterns. Thus, the bit rate is constant. Let us first consider a setting consisting of a single receiver that can receive signal from $n = 2$ transmitters. Each transmitter can modulate light at $m = 2$ different intensity levels. Assume that α_{ij} have already been estimated, a receiver can construct a table shown in Fig. 2.9. We note that there are a total of 4 possible distinct transmitted patterns from the two transmitters. Depending on the values of $\boldsymbol{\alpha}$, 4 distinct transmitted patterns could result in 4 different received signals, then the receiver can recover the transmitted signal perfectly assuming there is no noise. For some values of α_{ij}, two or more distinct transmitted patterns might result in the same value at the receiver. In this case, it is impossible to recover the transmitted pattern correctly even without the presence of noise. We will consider this situation in Section 2.5. On the other hand, if noise is present, the received signal is a random variable.

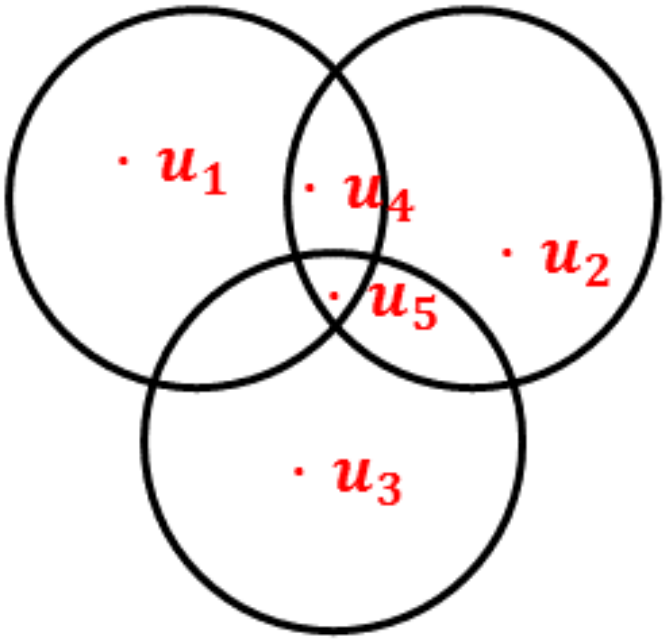

Figure 2.8: Multiple receivers in multiple light cones

In this case, the receiver will try to determine the transmitted patterns by binning a received signal to the correct bin of the transmitted patterns. For example, let us consider the decoding table shown in Fig. 2.9 for a receiver in the coverage of two transmitters. In this case, α_1 equals to 0.3 and α_2 equals to 0.9. There are 4 possible input combinations which produce 4 possible received patterns/outputs. The outputs are ordered from largest to smallest. If there is no noise, a receiver can reconstruct the bit patterns that were sent by the transmitters by comparing the y_i with the thresholds h_1, h_2, h_3 as shown in Fig. 2.9. For example, (1,0) was sent if $h_1 \leq y_j < h_2$. If the noise is large enough that it moves y_j across a threshold, then the decoding will result in error. Thus, a good decoding scheme should select the values of $h_1, h_2, \ldots$ to minimize the average symbol error. Fig. 2.10 shows another decoding table with $m = 2$, $n = 3$, and $\boldsymbol{\alpha} = (0.5, 0.7, 0.9)^T$.

The rule for decoding at a single receiver is as follows. Let $\mathbf{x}_1, \mathbf{x}_2, \ldots \mathbf{x}_K$ be K distinct transmitted patterns, where $K = m^n$ is the number of possible transmitted signal levels. Then if any received signal y_j is located in the range of $h_{i-1} \leq y_j < h_i$, $i \in [1, 2, \cdots, K]$, we say $\mathbf{x}_i$ is the transmitted pattern corresponding to the received signal y_j.

As in previous example, specific threshold values h_i can be chosen to minimize the average symbol error rate.

We have the following theorem regarding the optimal values of h_i's.

Theorem 2.1. *Let $p(\mathbf{x}_i)$ be the probability mass function of the input patterns and assume that the noise is i.i.d with probability density function $f(\cdot)$. Then*

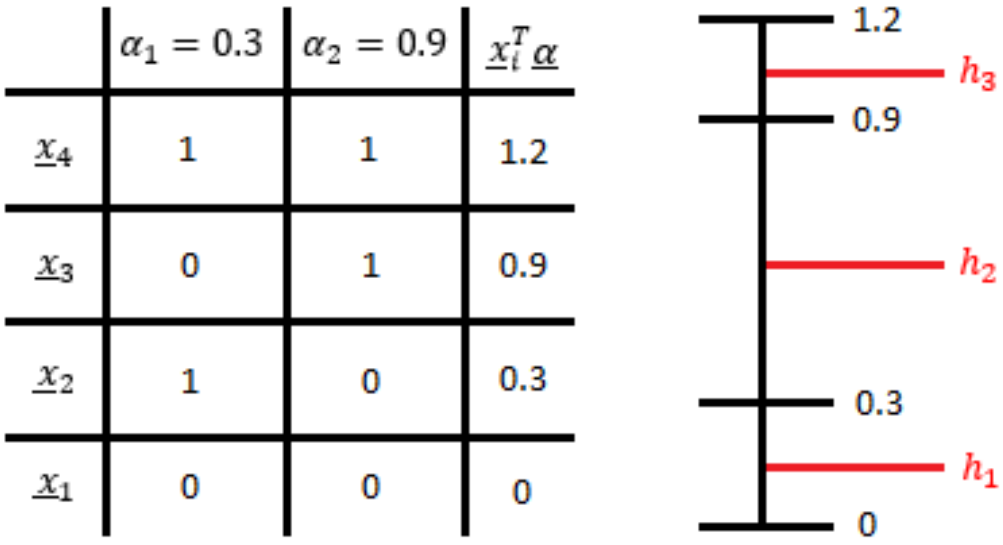

Figure 2.9: Decoding table for m=2 and n=2

the optimal thresholds, $h_1, h_2, \cdots, h_{K-1}$*, can be obtained by solving the following equation:*

$$p(\mathbf{x}_i) f(h_i - \mathbf{x}_i^T \boldsymbol{\alpha}) = p(\mathbf{x}_{i+1}) f(h_i - \mathbf{x}_{i+1}^T \boldsymbol{\alpha}), \tag{2.11}$$

as long as $p(\mathbf{x}_i) f(h_i - \mathbf{x}_i^T \boldsymbol{\alpha})$ *and* $p(\mathbf{x}_{i+1}) f(h_i - \mathbf{x}_{i+1}^T \boldsymbol{\alpha})$ *intersect within the range between* $\mathbf{x}_i^T \boldsymbol{\alpha}$ *and* $\mathbf{x}_{i+1}^T \boldsymbol{\alpha}$*.*

Especially when the source signals are uniformly distributed, then the optimal thresholds, $h_1, h_2, \cdots, h_{K-1}$*, must satisfy the following equation:*

$$f(h_i - \mathbf{x}_i^T \boldsymbol{\alpha}) = f(h_i - \mathbf{x}_{i+1}^T \boldsymbol{\alpha}). \tag{2.12}$$

	$\alpha_1 = 0.5$	$\alpha_2 = 0.7$	$\alpha_3 = 0.9$	$\underline{x}_i^T \underline{\alpha}$
$\underline{x}_8$	1	1	1	2.1
$\underline{x}_7$	0	1	1	1.6
$\underline{x}_6$	1	0	1	1.4
$\underline{x}_5$	1	1	0	1.2
$\underline{x}_4$	0	0	1	0.9
$\underline{x}_3$	0	1	0	0.7
$\underline{x}_2$	1	0	0	0.5
$\underline{x}_1$	0	0	0	0

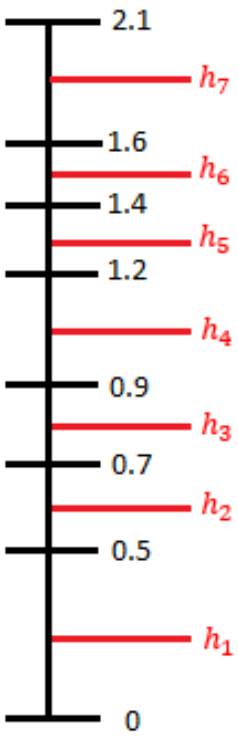

Figure 2.10: Decoding table m=2 and n=3

Furthermore, if $f(\cdot)$ is a symmetric double sided, non-increasing function, $f(\cdot)$ and $p(\mathbf{x}_i)$ should also satisfy $p(\mathbf{x}_i)f(0) \geq p(\mathbf{x}_{i+1})f((\mathbf{x}_i - \mathbf{x}_{i+1})^T\boldsymbol{\alpha})$ and $p(\mathbf{x}_i)f((\mathbf{x}_{i+1} - \mathbf{x}_i)^T\boldsymbol{\alpha}) \leq p(\mathbf{x}_{i+1})f(0)$.

Proof. With n transmitters, $K = m^n$ transmitted levels and the probability $p(\mathbf{x}_i)$ for each transmitted pattern $\mathbf{x}_i$, we then have the probability of error as

$$P(\varepsilon) = 1 - \sum_{i=1}^{K} p(\mathbf{x}_i)p(h_{i-1} \leq \mathbf{x}_i^T\boldsymbol{\alpha} + n < h_i)$$

$$= 1 - \sum_{i=1}^{K} p(\mathbf{x}_i)p(h_{i-1} - \mathbf{x}_i^T\boldsymbol{\alpha} \leq n < h_i - \mathbf{x}_i^T\boldsymbol{\alpha}). \tag{2.13}$$

Here we define $h_0 = -\infty$ and $h_K = \infty$.

Because the additive noise is i.i.d, we can rewrite Eq. (2.13) as

$$P(\varepsilon) = 1 - \sum_{i=1}^{K} p(\mathbf{x}_i)(\int_{h_{i-1}-\mathbf{x}_i^T\boldsymbol{\alpha}}^{h_i-\mathbf{x}_i^T\boldsymbol{\alpha}} f(\tau)\, d\tau. \tag{2.14}$$

By differentiating $P(\varepsilon)$ with respect to h_i and setting the equation to zero, we can find the optimal h_i to minimize $P(\varepsilon)$.

$$P_{h_i}^{'}(\varepsilon) = -(p(\mathbf{x}_i)f(h_i - \mathbf{x}_i^T\boldsymbol{\alpha}) - p(\mathbf{x}_{i+1})f(h_i - \mathbf{x}_{i+1}^T\boldsymbol{\alpha})) = 0 \tag{2.15}$$

$$\Rightarrow p(\mathbf{x}_i)f(h_i - \mathbf{x}_i^T\boldsymbol{\alpha}) = p(\mathbf{x}_{i+1})f(h_i - \mathbf{x}_{i+1}^T\boldsymbol{\alpha}), for\ i = 1, 2, \ldots, K-1. \tag{2.16}$$

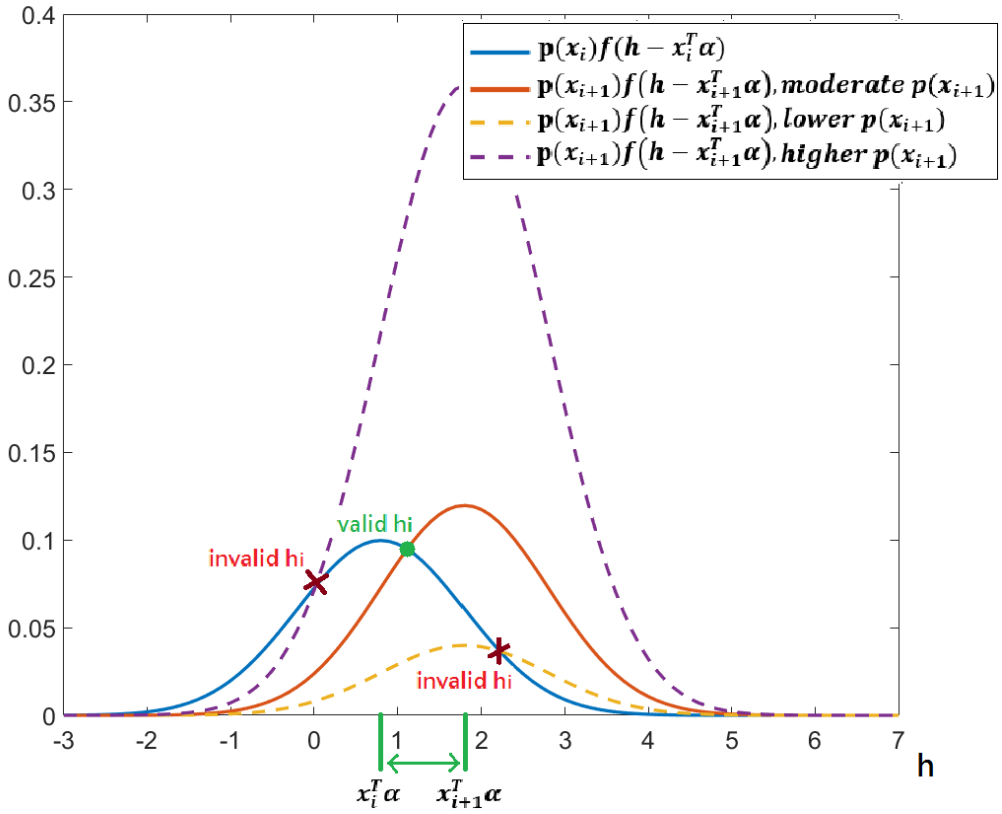

Figure 2.11: Illustration of the valid range for h_i.

To ensure that $h_0 < h_1 \leq h_2 \leq \cdots \leq h_i \leq \cdots \leq h_{K-1} < h_K$, $p(\mathbf{x}_i)f(h_i - \mathbf{x}_i^T\boldsymbol{\alpha})$ and $p(\mathbf{x}_{i+1})f(h_i - \mathbf{x}_{i+1}^T\boldsymbol{\alpha})$ should intersect within the range between $\mathbf{x}_i^T\boldsymbol{\alpha}$ and $\mathbf{x}_{i+1}^T\boldsymbol{\alpha}$, as shown in Fig. 2.11. Therefore, if $f(\cdot)$ is a symmetric double sided, non-increasing function, the distribution of $\mathbf{x}_i$ should satisfy the conditions $p(\mathbf{x}_i)f(0) \geq p(\mathbf{x}_{i+1})f((\mathbf{x}_i - \mathbf{x}_{i+1})^T\boldsymbol{\alpha})$ and $p(\mathbf{x}_i)f((\mathbf{x}_{i+1} - \mathbf{x}_i)^T\boldsymbol{\alpha}) \leq p(\mathbf{x}_{i+1})f(0)$. □

Fig. 2.12 and Fig. 2.13 show two examples for finding the thresholds h_i

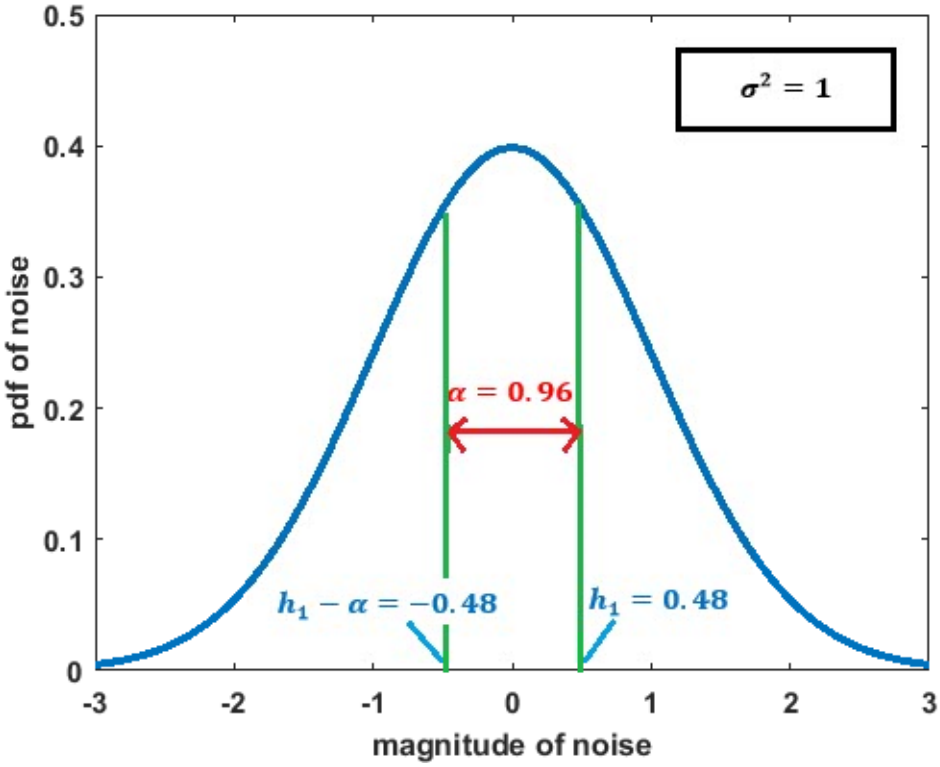

Figure 2.12: Optimal thresholds for Gaussian noise using two transmitters

graphically from the two different noise distributions. Both examples use $n = 1$, $m = 2$ and uniformly distributed transmitted patterns. As seen, h_i is obtained by looking for the specific positions that make $f(h_1 - 0 \cdot \alpha) = f(h_1 - 1 \cdot \alpha)$.

2.5 Conditions for Signal Irrecoverability

We note that even when there is no noise, certain $\boldsymbol{\alpha}$ values will likely result in decoding errors. Specifically, when two or more input patterns map into a single output value. Therefore, it is important to determine what $\boldsymbol{\alpha}$ values make

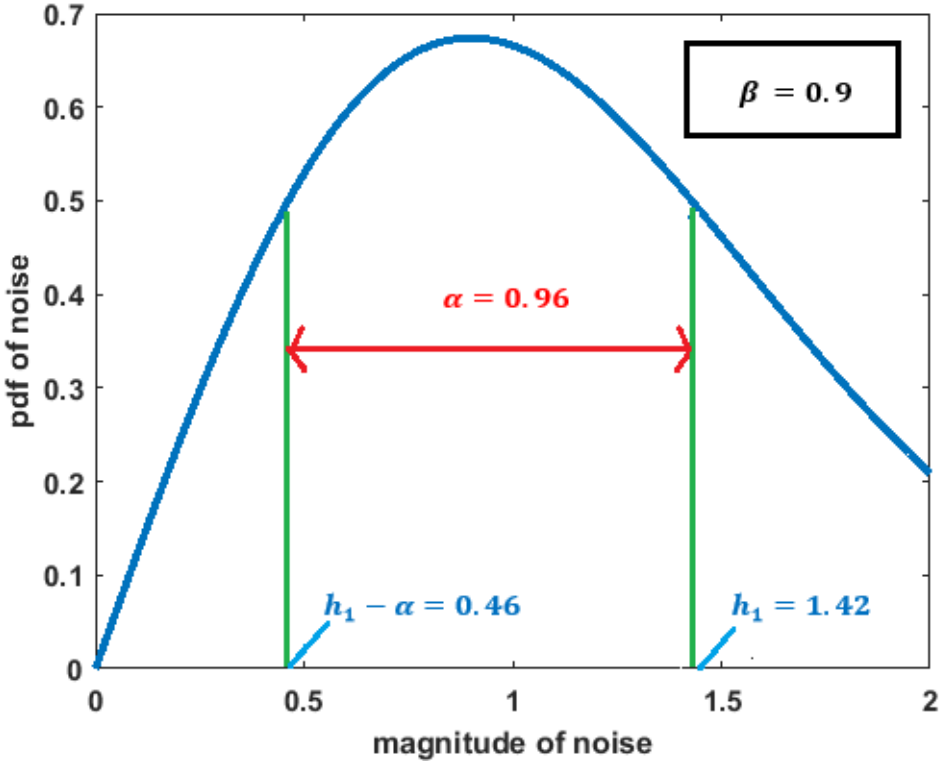

Figure 2.13: Optimal thresholds for Rayleigh noise using two transmitters

two signals indistinguishable. In order to solve this problem, first it's observed that two received signals can be expressed as y and y' where

$$y = x_1\alpha_1 + x_2\alpha_2 + ... + x_n\alpha_n \tag{2.17}$$

and

$$y' = x'_1\alpha_1 + x'_2\alpha_2 + ... + x'_n\alpha_n. \tag{2.18}$$

Even with infinite precision from the receiver, x and x' will still not be distinguishable if $y = y'$. Note, this can happen even if the transmitted signal sets x_i and x'_i are different.

In order to avoid the aforementioned situation, $y - y'$ must not equal 0. If the difference is 0, then the signals are indistinguishable. This can be expressed as follows:

$$y - y' = (x_1 - x'_1)\alpha_1 + (x_2 - x'_2)\alpha_2 + ... + (x_n - x'_n)\alpha_n = 0. \tag{2.19}$$

Let $b_i = x_i - x'_i$,

$$y - y' = b_1\alpha_1 + b_2\alpha_2 + ... + b_n\alpha_n = 0, \tag{2.20}$$

$$b_i \in [-(m-1), \cdots, -1, 0, 1, \cdots, (m-1)].$$

The variable b_i ranges from $-(m-1)$ to $(m-1)$ because $b_i = x_i - x'_i$ where x_i and x'_i both range from 0 to $m-1$. Therefore the minimum value is

$0-(m-1)=-(m-1)$ and the maximum value is $(m-1)-0=(m-1)$.

Now, by plugging all the permutations of b_i into Eq. (2.20), a matrix equation (21) is formed that can be used to find all the relationships among $\boldsymbol{\alpha}$ such that the receiver will not be able to distinguish between two signals.

$$\underbrace{\begin{bmatrix} b_{11} & \cdots & b_{1n} \\ \vdots & \ddots & \vdots \\ b_{(2m-1)^n 1} & \cdots & b_{(2m-1)^n n} \end{bmatrix}}_{\mathbf{B}} \begin{bmatrix} \alpha_1 \\ \vdots \\ \alpha_n \end{bmatrix} = \begin{bmatrix} 0 \\ \vdots \\ 0 \end{bmatrix} \tag{2.21}$$

The matrix $\mathbf{B}$ has a column for each transmitter with each row representing all possible permutations of the available signals. The matrix is of dimension $(2m-1)^n \times n$ because there are n transmitters and $(2m-1)^n$ possible permutations. Fig. 2.14 shows how to construct the matrix $\mathbf{B}$ for $m=2$ and $n=2$.

The following procedure can now be implemented to attain rows of the matrix $\mathbf{B}$ which have the potential of making Eq. (2.21) equal to 0. First, construct $\mathbf{B}$ with rows from all the permutations of b_i, as in Fig. 2.14(a). Then delete all rows with all positive or all negative values which results in Fig. 2.14(b). Treat 0 as both positive and negative. These rows would require negative α_j's which are not in the irrecoverable range. Finally, delete all rows that are multiples of each other. This is because these rows have the same relationships between α_j's. What's left is a unique set of ratios that represent all values of α_j's for which two different transmitted signals would result in an identical received

signal, as shown in Fig. 2.14(c). Therefore, any values of α_1 and α_2 that make the equation $\alpha_1 - \alpha_2$ equal 0 will make the two different transmitted signals indistinguishable at the receiver. Fig. 2.15 shows the lines that represent all pairs of α_1 and α_2 values that satisfy the equation sets for the case of $m = 3$ and $n = 2$., and therefore transmitted signals cannot be recovered at the receiver even without noise.

We summarize the procedure to obtain matrix $\mathbf{B}$ in Algorithm 1.

Algorithm 1 Determining Matrix $\mathbf{B}$

1: **for** each $i \in [1, (2m-1)^n]$ **do**
2: initialize each row of $\mathbf{B}$ with all permutations of $(b_1, b_2, \cdots, b_n)$
3: **end for**
4: **for all** rows of $\mathbf{B}$ **do**
5: delete rows with all positive/negative elements
6: **end for**
7: **for** remaining rows of $\mathbf{B}$ **do**
8: delete rows which are multiples of other rows
9: **end for**

2.6 Simulation and Discussion

In this section, we show numerical results to verify our proposed scheme. First, Fig. 2.16 shows the irrecoverable ranges for α_1 and α_2 as indicated by the points on the lines. This figure was generated by using Algorithm 1 with $m = 4$

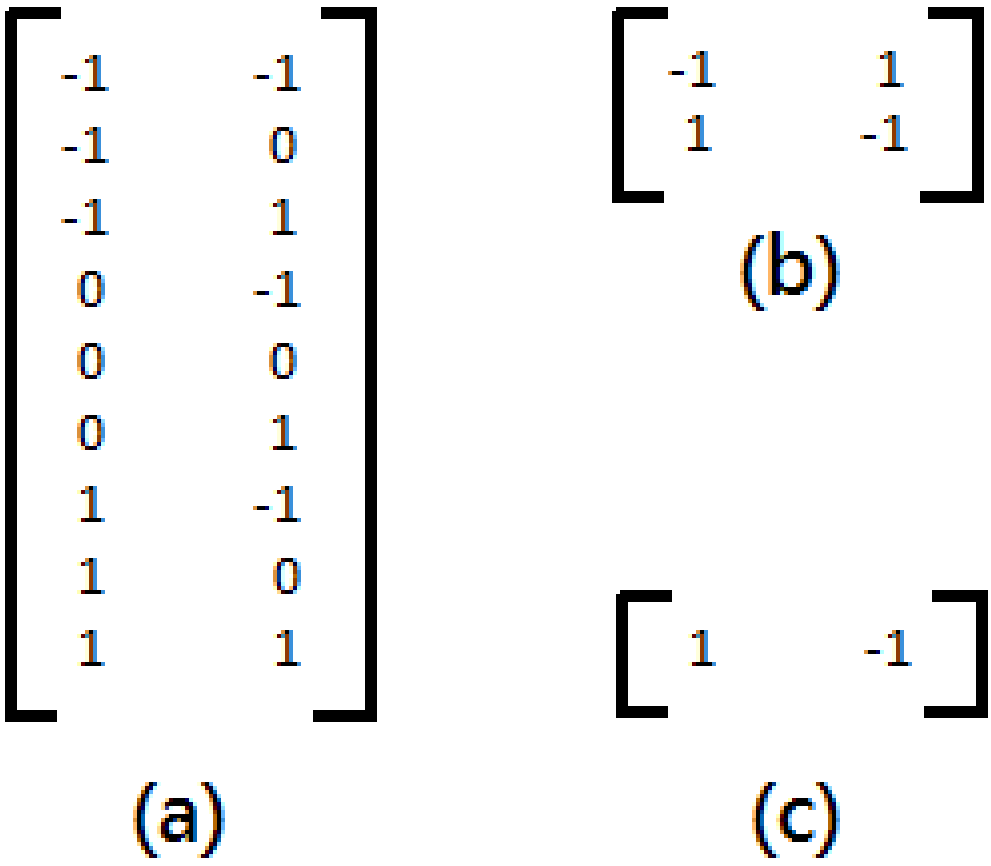

Figure 2.14: Example of steps for constructing the matrix **B**

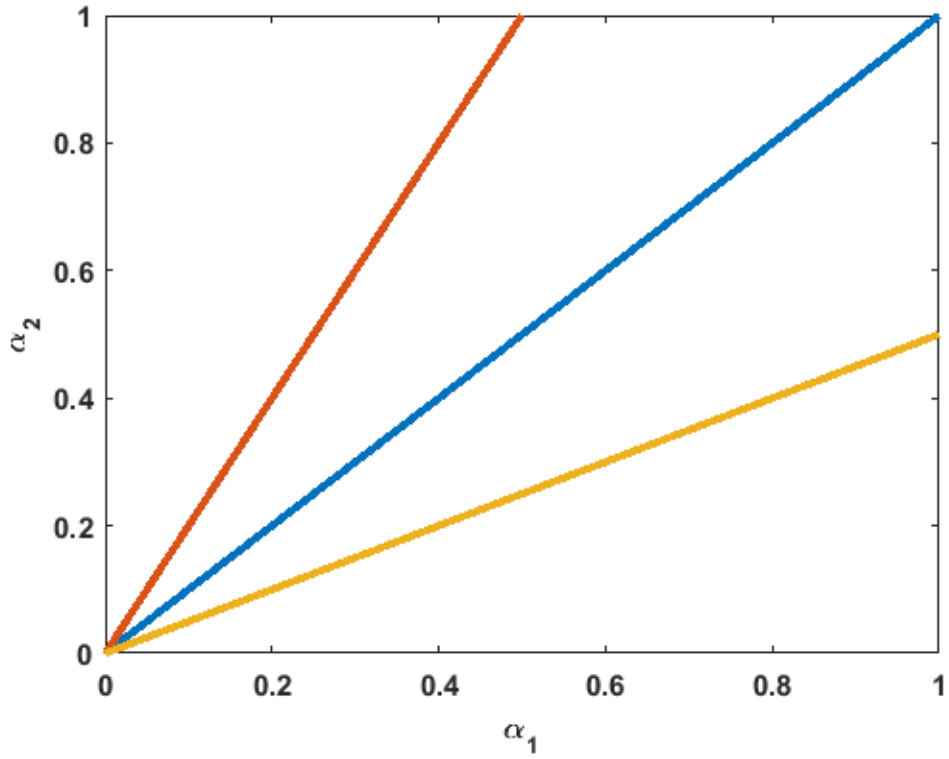

Figure 2.15: Invalid alpha values with m=3 and n=2

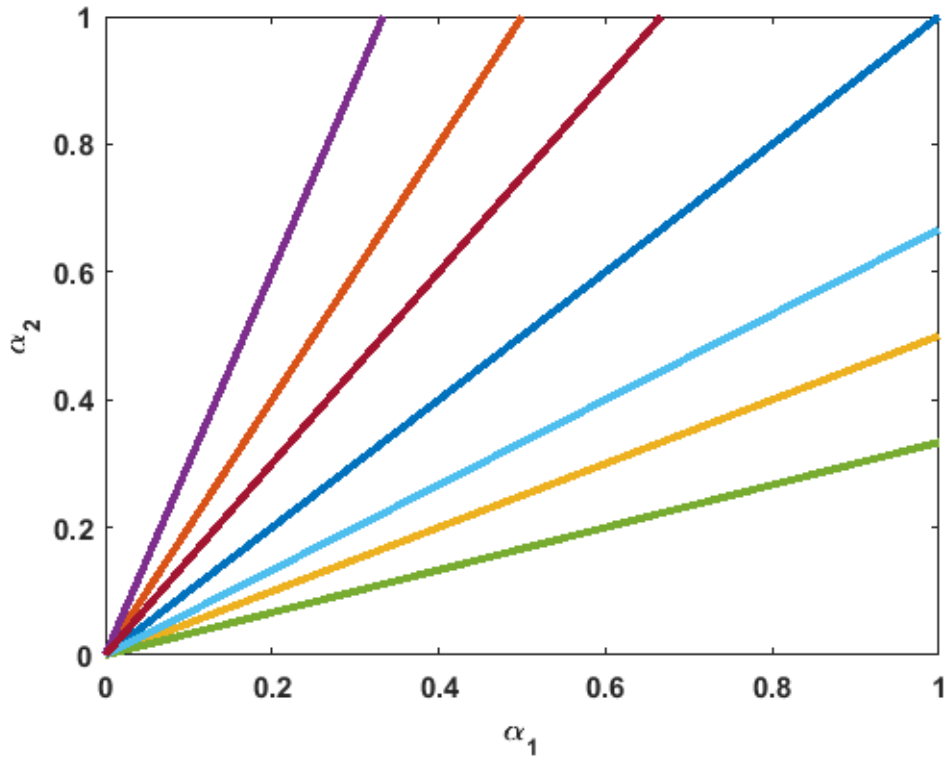

Figure 2.16: The range of α_1 and α_2 values for which perfect signal recovery is not possible, with m=4, n=2 and infinite precision.

and $n = 2$.

Fig. 2.16 assumes that the receiver can differentiate any two real numbers. In practice, a receiver has finite precision arithmetic, i.e., it can represent a real value with only a finite number of bits. In that case, it is difficult for a receiver to distinguish two values that are close to each other. As a result, the range of α_1 and α_2 for which the perfect reconstruction is not possible, will be enlarged. Fig. 2.17 shows such irrecoverable range of α_1 and α_2 for $m = 4$ and $n = 2$. Notice that the lines in Fig. 2.17 are much thicker than those of Fig. 2.16.

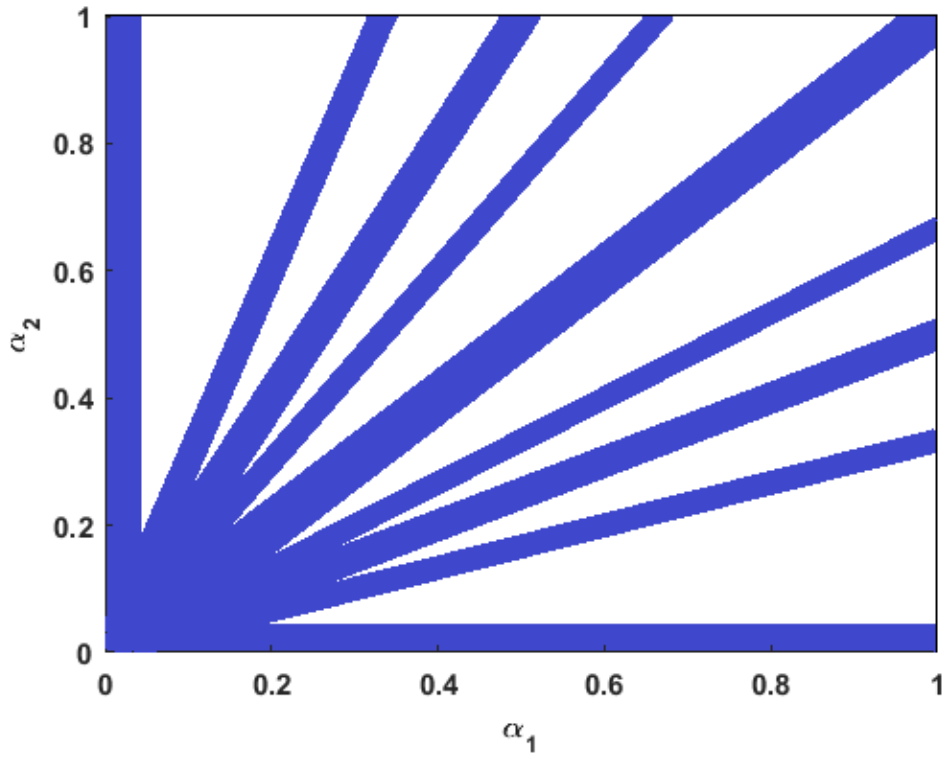

Figure 2.17: The range of α_1 and α_2 values for which perfect signal recovery is not possible, with m=4 and n=2.

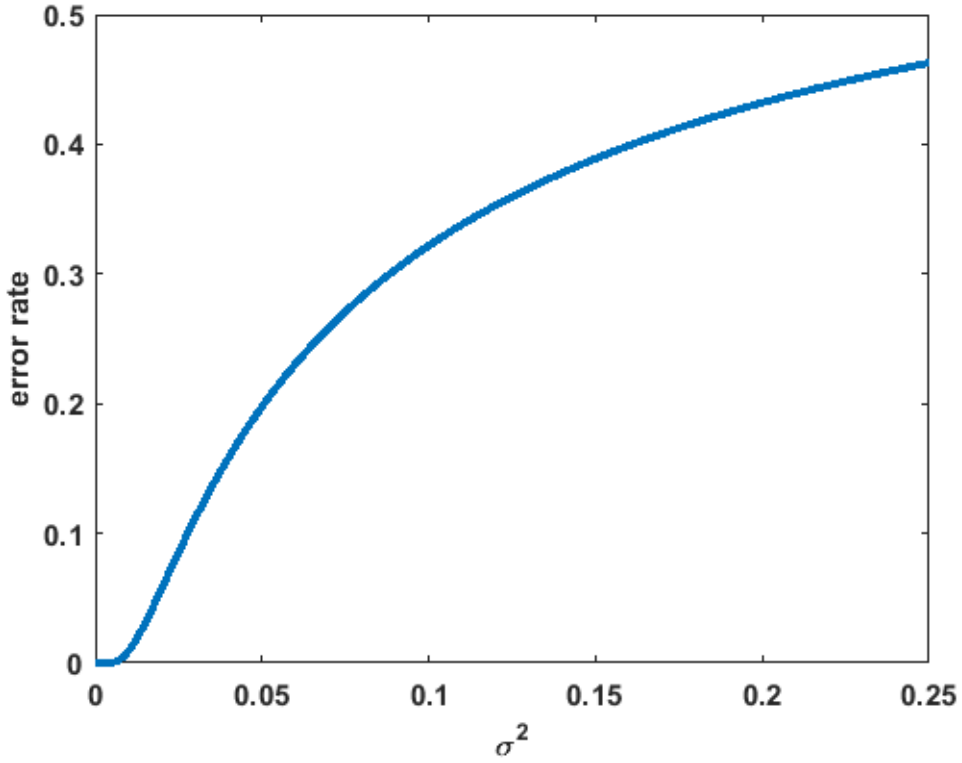

Figure 2.18: Bit error rates using optimal PAM decoding scheme for Gaussian noise as a function of its variance. $m = 2, n = 2, \alpha_1 = 0.5, \alpha_2 = 1$

We now show the bit error rates for symmetric and un-symmetric noises. Specifically, Fig. 2.18 shows the bit error rate for Gaussian noise [38] as a function of its variance. As seen, as the variance increases, the bit error rate increases accordingly. Similarly, Fig. 2.19 shows the bit error rate for Rayleigh noise [39] as a function of its mode. The bit error rates increase with the noise variance as predicted.

We now examine the bit error rates as a function of a receiver position for two transmitters. In particular, we consider the scenario where the receiver is

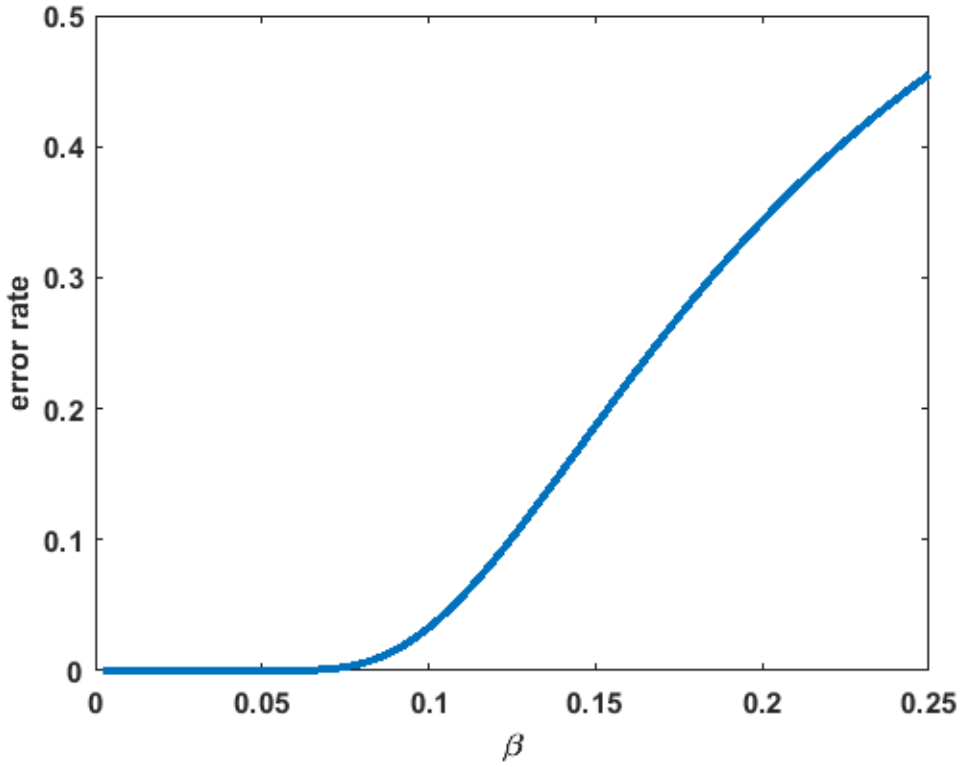

Figure 2.19: Bit error rates using optimal PAM decoding scheme for Rayleigh noise as a function of its mode. $m = 2, n = 2, \alpha_1 = 0.5, \alpha_2 = 1$

moving from the center of transmitter 2 to the center of transmitter 1. In this case, α_1 will increase while α_2 will decrease. Thus, we can plot the bit error rate vs. the ratio α_1/α_2. When the ratio = 1, i.e., $\alpha_1 = \alpha_2$, the receiver is at equal distances from both transmitters.

Fig. 2.20 to Fig. 2.22 show the bit error rates as functions of α_1/α_2 for under Gaussian noise with different variances. In all these figures, the bit error rates are 0.25 when $\alpha_1/\alpha_2 = 1$. This is intuitively plausible since the transmitted patterns 01 and 10 cannot be distinguished at the receiver. On the other hand, the patterns 11 and 00 can be distinguished easily since the thresholds for these symbols are quite far apart. As a result, we have the bit error rate roughly 0.25, assuming the transmitted patterns is uniformly distributed. It is also noted that the bit error rate is large when α_1/α_2 is small. This is because the transmitted patterns 00 and 10 results in similar received signal. Similarly, the transmitted patterns 01 and 11 will also result in the similar received signal.

We also investigated the relationships between BER(bit error rate) and the user's location. In Fig. 2.23, the BER is high when the user is near the edges of the cones. This is because near the edges, at least one light intensity is approximately 0. This makes recovering signals difficult. When the user is near the center of the overlapping area the BER is also high, this is because the light intensity from the two transmitters are the same. In this case, the receiver can only guess which transmitted signal set is transmitted. This is consistent with earlier results.

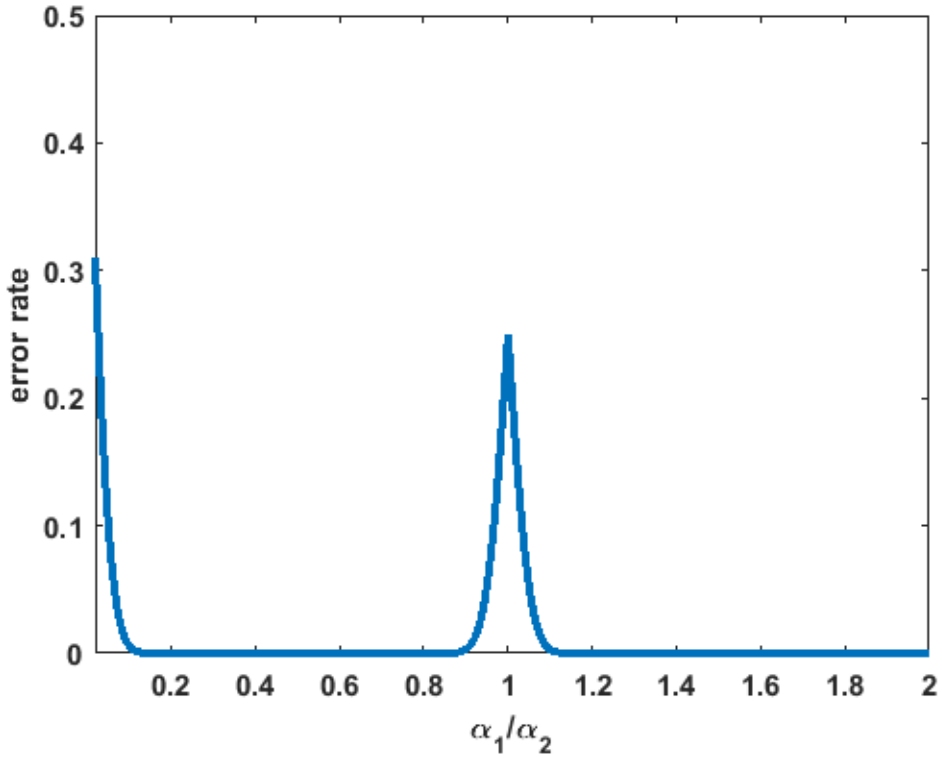

Figure 2.20: Bit error rate vs. the ratio of α_1/α_2. $\sigma^2 = 0.0001$

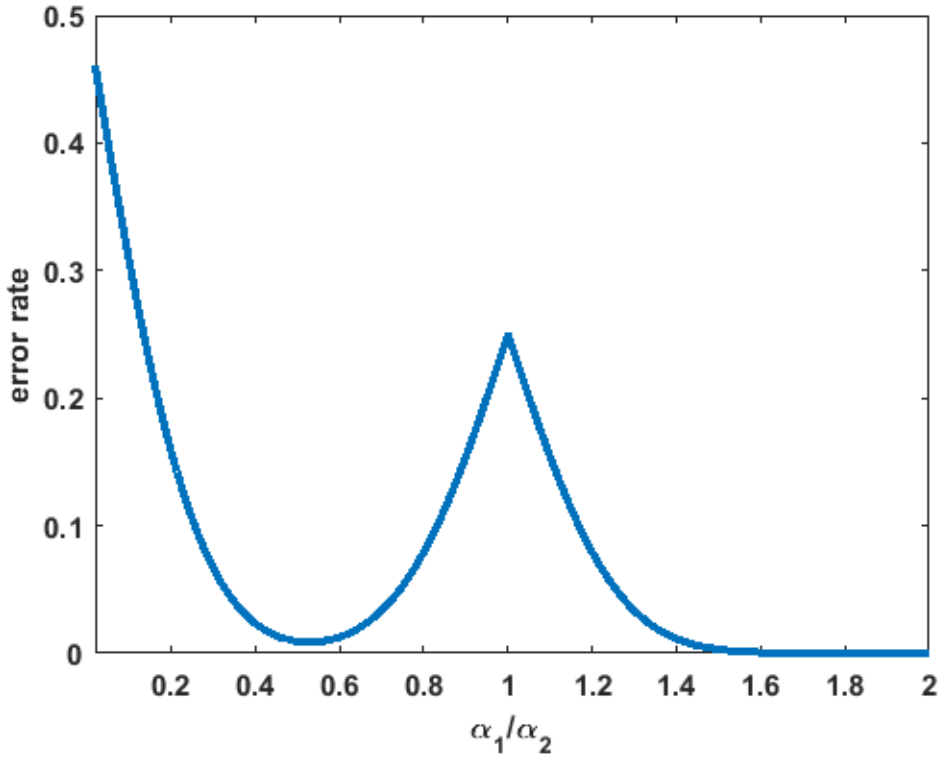

Figure 2.21: Bit error rate vs. the ratio of α_1/α_2. $\sigma^2 = 0.0025$

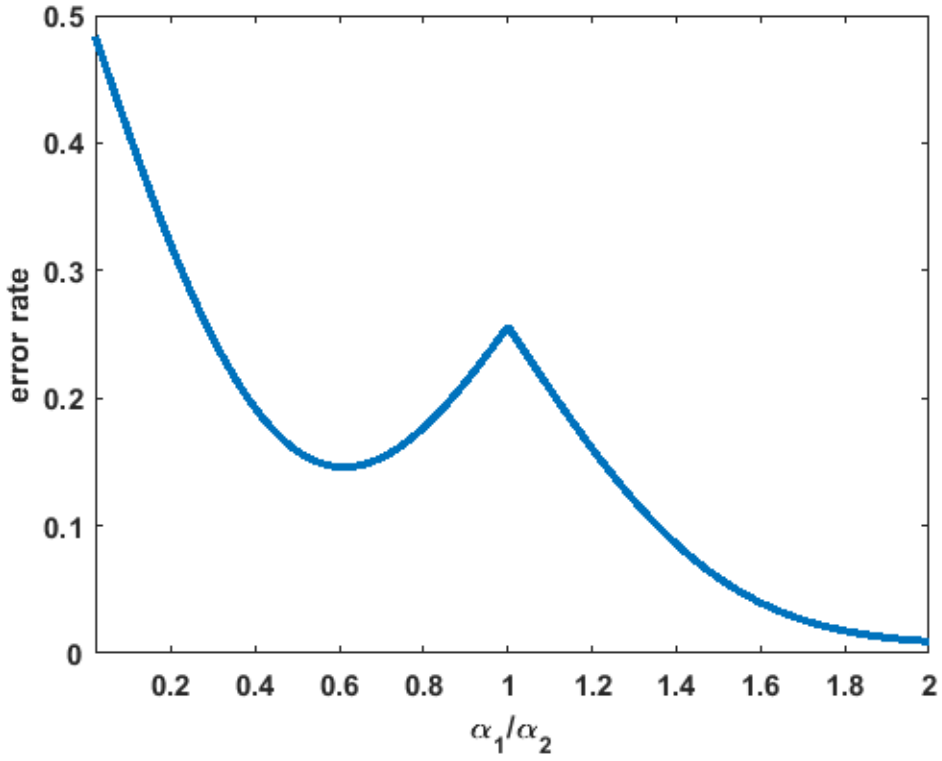

Figure 2.22: Bit error rate vs. the ratio of α_1/α_2. $\sigma^2 = 0.01$

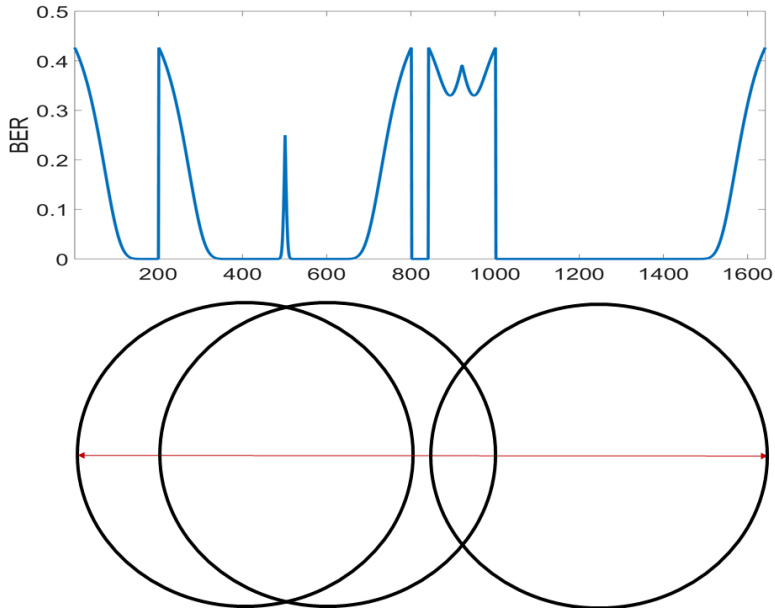

Figure 2.23: BER vs. user location

Chapter 3: Memory of FSO Response

Free Space Optical (FSO) communication technologies exploit the extremely large light spectrum to make it possible to transmit data fast. And our WiFO system is focused on how to transmit information quickly and reliably using On-Off Keying (OOK) modulation. However, FSO technologies, especially when using On-Off Keying modulation, the Light-Emitting-Diode (LED) transmitters produce an inherent non-linear distortion in the output. In particular, the LED acts as a band-limited channel between the inputs and outputs. As a result, high-frequency components of the input signal are attenuated, resulting in the distorted output, i.e., when the data rate is high, the output will be more distorted. And the distortion is generated inherently with LED, such that it is inevitable. Consequently, without any correction for the distortion, the bit error rate will be higher. While methods for distortion corrections are well explored, most of these techniques are general techniques, e.g., linear equalization that does not exploit the unique characteristics of LED-based transmitter response to reduce the bit error rate. Furthermore, linear equalization techniques are typically used for high-order modulation, e.g. PAM-16 where accurate decoding of different signal levels is crucial. On the other hand, when On-Off Keying modulation is used, linear equalization techniques offer minimal advantages while incurring other costs such as increasing power consumption and

lower speed which are due the requirement of an accurate Analog-to-Digital Converter(ADC).

In order to get a more reliable transmission with FSO technologies, in this chapter, a mathematical model is used to capture the distortion of LED output response in Section 3.1. And the memory property of the LED response is investigated and discussed in Sec 3.2, so that the a pre-shaping algorithm in Chapter 4 and a Memory Decoding Algorithm (MDA) in Chapter 5 can be proposed by utilizing the math model and memory property.

3.1 Math Model

The overall impulse response of an LED-based communication system depends on multiple factors. These include the characteristics of the LED at the transmitter, the photo-diode used at the receiver, the driver circuits associated with the transmitter and receiver, and propagation medium. In our application scenario, particularly the WiFO system [40], which we have been developing over several years, uses short and focused FSO transmissions. The FSO channel is used as an alternative of WiFi in the indoor and short-distance scenarios. As a result, multi-path fading due to light propagation is negligible. The primary signal distortion come from the LED, photo-diode, their driver circuits, and the attenuation due to the distance between the transmitter and the receiver. Therefore, although the impulse response of a considered FSO channel is device dependent, and can be empirically measured and calibrated, using LTI

techniques such as inverting the impulse response in the frequency domain is difficult to implement.

Fig. 3.1 shows the measured response at the receiver photo-diode when a pulse train is sent at $1.\overline{66}$ MHz. This follows the fact that the LED output pulse has an exponential rise and fall portions, as well as a little delay before the LED's full turn-on and turn-off. From physics, the characteristic time constant for the rise and fall portions of the pulse are related to the photon's net recombination time τ. Ideally, the rise time τ_R, (the time for the voltage to go from 10% to 90% of the maximum voltage of the light output), and the fall time τ_F (the time for the voltage to go from 90% to 10% of the maximum voltage), are the same and equal to 2.2τ [41]. In practice, the net recombination time τ itself depends on the circuit implementation to drive the LEDs and photo-diode. Thus, different values for τ_R and τ_F are often observed in real-world settings. Based on this, we use τ_a and τ_b for charging and discharging respectively to replace the photon's net recombination time, τ. Eq. (3.1) and Eq. (3.2) approximate the LED voltage responses while the sending bit is "1" and "0" respectively. V_{max} in Eq. (3.1) and Eq. (3.2) is the maximum response voltage of the LED, this value can be empirically measured at the receiver by sending multiple consecutive "1"s. τ_a and τ_b are the observed net recombination time with sending bit "1" and "0" respectively. By analyzing the measured data of the LED response, we can numerically obtain the parameters τ_a and τ_b. Eq. (3.1) is also the impulse response for an RC circuit, however, due to the different values observed for τ_a and τ_b, inverting Eq. (3.1) to cancel the channel is impractical. Fig. 3.2 and

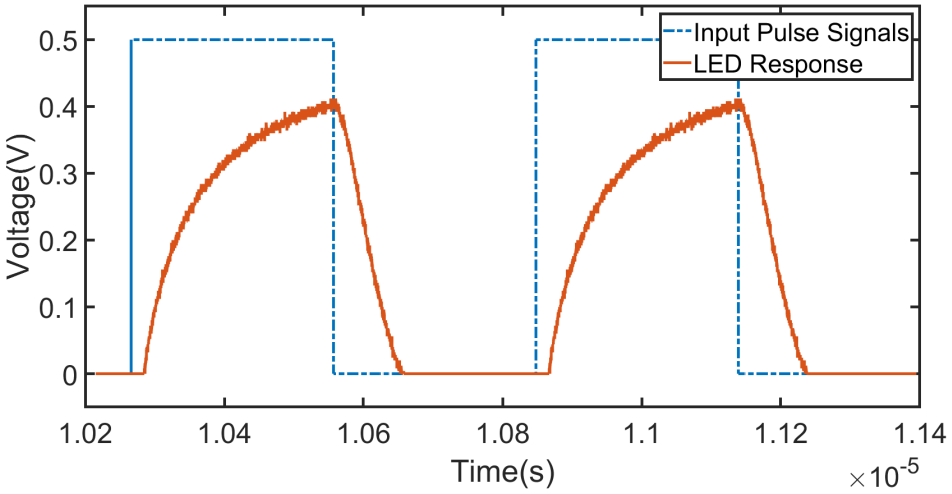

Figure 3.1: LED Pulse Response

Fig. 3.3 show the measured LED responses of a high speed infrared emitting diodes(850nm, VSMY2850) and the mathematically modeled response for the cases of 1M Hz and 25M Hz input pulse trains.

$$V_{response_1}(t) = V_{max} \cdot (1 - e^{-\frac{t}{\tau_a}}) \tag{3.1}$$

$$V_{response_0}(t) = V_{max} \cdot e^{-\frac{t}{\tau_b}} \tag{3.2}$$

3.2 k-Bit-Long Memory

Using the OOK modulation, the transmitted signal $x(t)$ can be considered as a telegraph pulse train that has only two distinct values, 0 and 1. We note

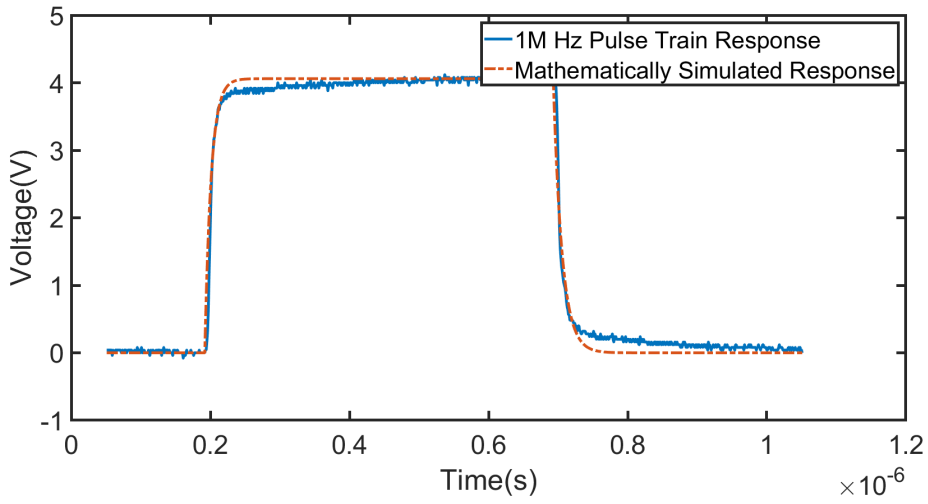

Figure 3.2: 1 MHz LED Pulse Response vs. Simulated Response

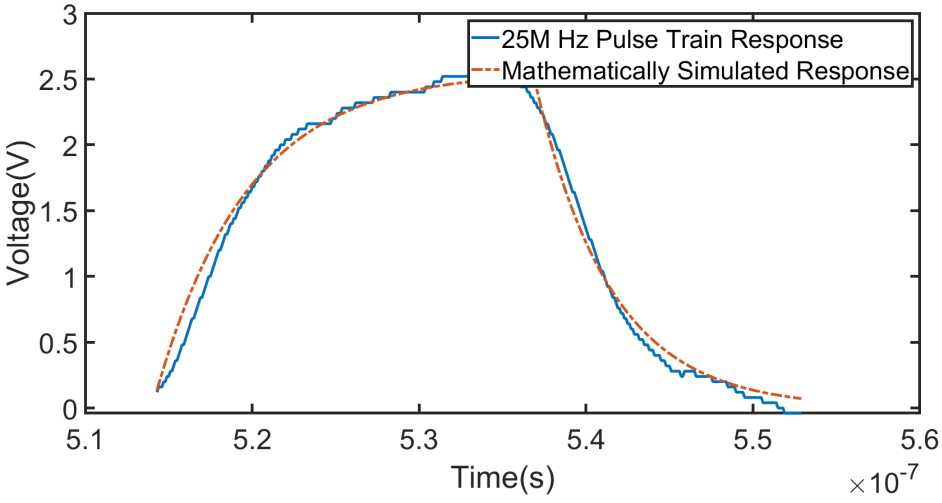

Figure 3.3: 25 MHz LED Pulse Response vs. Simulated Response

that for a given LED transmitter, the effective channel can be modelled as a band-limited channel. Thus, a transmitted signal whose significant amount of energy is in the high frequency band (outside the channel bandwidth) will be distorted greatly. If we assume that the rate of transmitted signal is within the bandwidth of the LED. In the time domain, it is equivalent to assuming that the sending rate is sufficiently low such that it only takes at most one sending duration, T, for the voltage to reach V_{max} from 0 as Fig. 3.4. Similarly, it also takes at most one sending duration, T, for the voltage to go from V_{max} down to 0. However, as the data rate increases, the voltage might not be able to reach the maximum or drop to 0 from the maximum in one sending duration, T, by sending a "1" or a "0". Fig. 3.5 is an example of that it takes at most $2T$ to charge from 0 voltage to V_{max} by sending two consecutive "1"s. Likewise, it also takes at most $2T$ to have the voltage drop to zero by sending two consecutive "0"s. Here two parameters, ΔT_{10} and ΔT_{01}, are introduced to compensate for the time offsets when the transitions happen and the voltages of the previous bits do not reach the maximum or the minimum. We also define T_{01}, T_{10} and the response $y(t)$ as follows.

- T_{01} : The last time stamp that a transition occurs in $x(t)$ from 0 to 1.
- T_{10} : The last time stamp that a transition occurs in $x(t)$ from 1 to 0.

With the definitions of T_{01}, T_{10}, and the LED responses in Eqs. (3.1)

and (3.2), the output $y(t)$ at the receiver can be expressed as:

$$y(t) = V_{max}(1 - e^{-\frac{t-T_{01}+\Delta T_{01}}{\tau_a}})x(t) + V_{max}e^{-\frac{t-T_{10}+\Delta T_{10}}{\tau_b}}(1 - x(t)). \tag{3.3}$$

T_{01}, T_{10}, ΔT_{01} and ΔT_{10} need to be updated whenever there is a transition in $x(t)$. Let's define x_i as the i^{th} sending bit. The updating rules are as follows.

$$\begin{cases} T_{01} = (i-1)T \\ \\ \Delta T_{01} = -\tau_a \ln(1 - \dfrac{y((i-1)T)}{V_{max}}) \end{cases} \quad \text{if } x_{i-1} = 0, x_i = 1$$

$$\begin{cases} T_{10} = (i-1)T \\ \\ \Delta T_{10} = -\tau_b \ln \dfrac{y((i-1)T)}{V_{max}} \end{cases} \quad \text{if } x_{i-1} = 1, x_i = 0 \tag{3.4}$$

We note that if the data rate is low enough to make the LED response go from 0 voltage to V_{max} and also drop voltage to zero within one sending duration, T, then the LED response only has one-bit-long memory. The upper left in Fig. 3.6 shows two LED responses of sending "000" and "100", which only differs in the first bits. But the responses of the second bits are still different, while the third bits' responses coincide with each other. The rest three sub-graphs in Fig. 3.6 also represent the same appearances that one bit can only affect its next bit. This explains that the LED response of the case that charging and discharging within one sending duration ,T, only has one-bit-long memory.

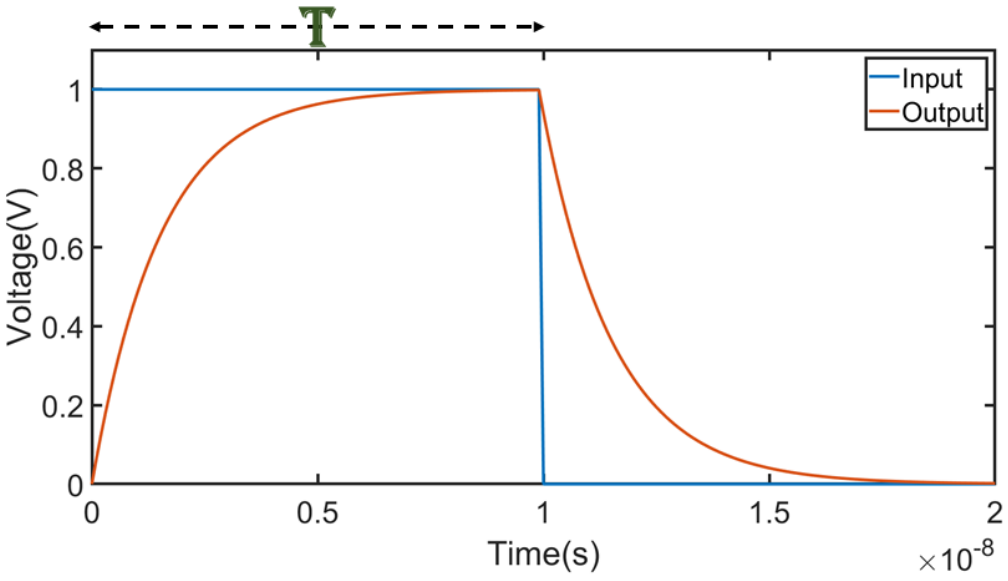

Figure 3.4: Low Sending Rate

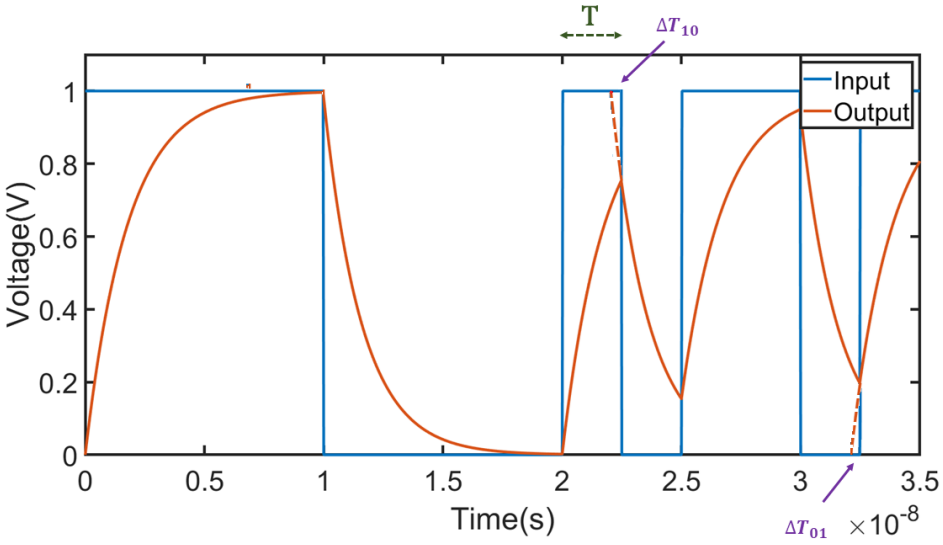

Figure 3.5: High Sending Rate

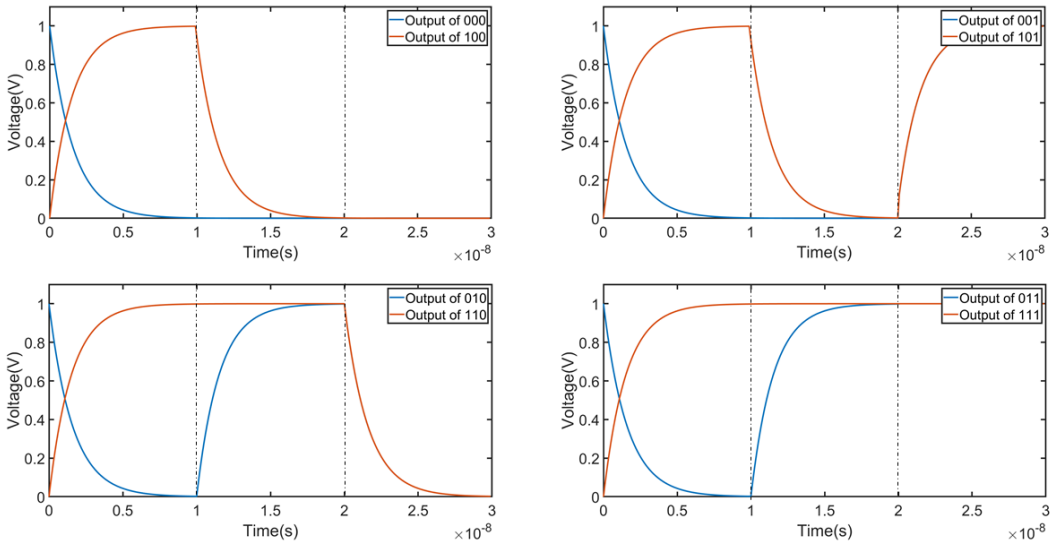

Figure 3.6: Illustration of 1-Bit-Long Memory

In other words, each bit is only affected by its previous one bit only.

Like previously mentioned, the data rate might increase so that the response voltage can not get fully charged(discharged) in one sending duration, T. Fig. 3.7 illustrates two examples of the case that the LED response takes at most two sending durations, T, to fully charged(discharged). The upper subgraph in Fig. 3.7 compares two LED responses of the inputs ”0010” and ”1010”, which only differs in the first bit. It could be seen that although only the first bits are different, the output curves of the second and third bits are still not the same, while the outputs of the fourth bits perfectly match with each other. The other example of sending bits ”0011” and ”1011” in Fig. 3.7 also shows that one bit has affection on only the next two bits but the fourth one. That is said, if it takes at most two sending durations, T, to get fully charged(discharged),

then the LED response has two-bit-long memory, which means every bit of LED response is related to its previous two bits.

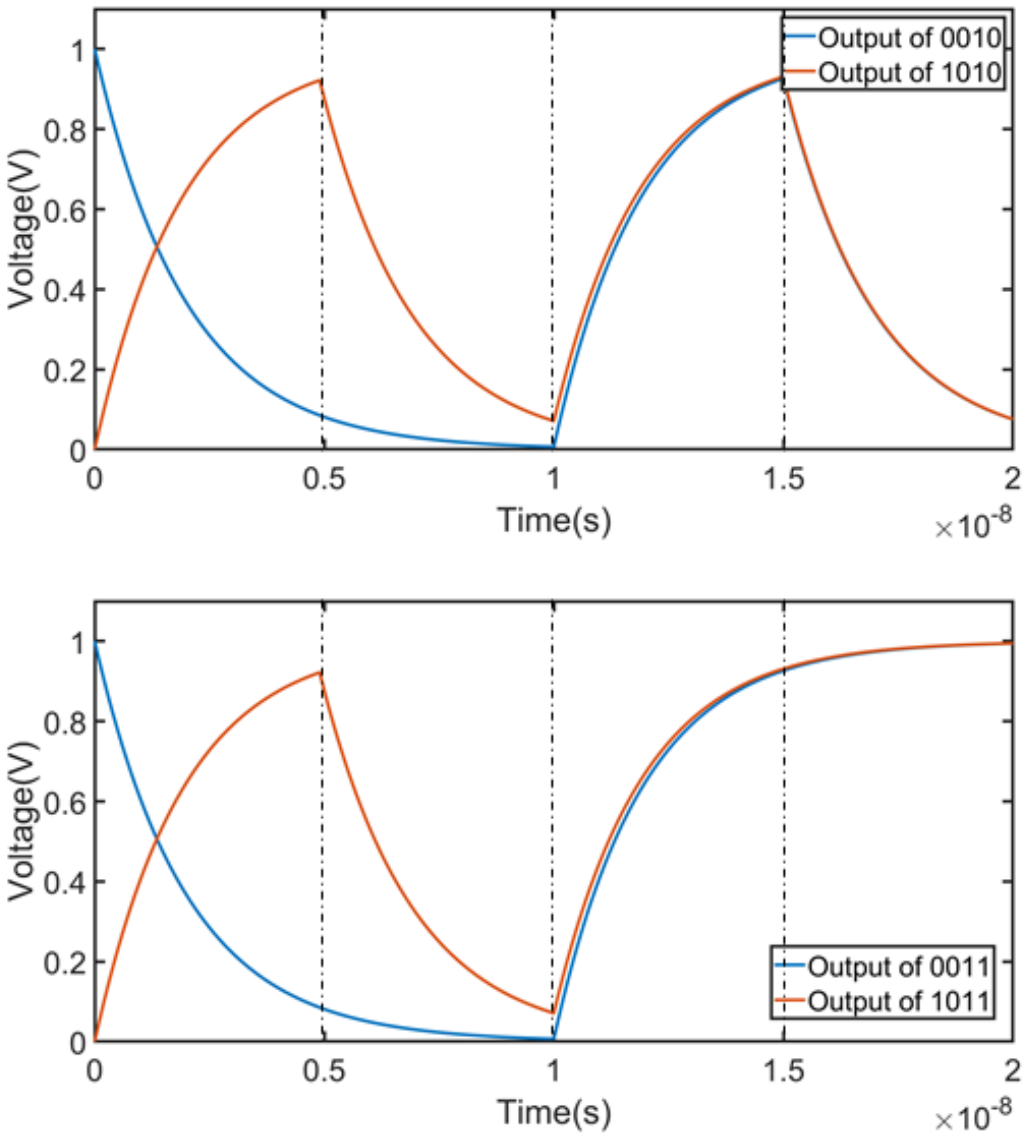

Figure 3.7: Illustration of 2-Bit-Long Memory

Chapter 4: Pre-shaping Technique for FSO Transmissions

The channel of LED transmissions is band limited and not a LTI system, so that a reliable high data rate transmission is not reachable. Usually, people implement a predistortion scheme at the transmitter and equalizer at the receiver for an optical channel to get promising transmissions and higher data rates [42] [43]. One of the factors that limits the performance of optical transmissions is the nonlinearity. Predistortion attempts to work with power amplifiers(PAs), which are inherently nonlinear devices, to make a nonlinear system into a linear system. However, Volterra series [44], the nonlinear model for the memory system, is not attractive in practice due to its complexity and large number of coefficients. Several linearization techniques have been studied to mitigate the effects of nonlinear distortion and to improve the nonlinearity of LEDs by predistortion [45]- [51]. In [47], an adaptive-learning-architecture (ALA) based predistortion method is proposed to estimate and compensate for LED nonlinearities as well as increase the spectral efficiency of a VLC system. [48] proposed an adaptive normalized least mean squares (NLMS) based predistorter that learns a scaling factor for predistortion and tracks changes in LED characteristics to mitigate the effects due to factors like temperature variation and aging. A Chebysev regression based nonlinear predistorter is also proposed in [49] to mitigate LED nonlinearity by learning a polynomial expansion of

the input electrical signal. The PA memory effects are also unwanted in communication systems, especially for those wider bandwidth applications such as wideband code-division multiple access (WCDMA) and wideband orthogonal frequency division multiplexing (WOFDM). Due to the limitation of memoryless predistortion, [50] proposed a memory polynomial model based predistorter. [51] shows that if the bias signal is distorted intentionally to compensate for the nonlinearity of the LED luminance, the performance of systems when using intensity modulation in combination with OFDM could be improved. Unlike other predistortion techniques, our proposed Adaptive Sending Duration Algorithm(ASDA) is a simple technique similar to the pulse width modulation (PWM) idea. While PWM techniques in which, bit 1 and 0 have different but fixed durations, the ASDA dynamically change the bit widths based on the incoming patterns. We note that PWM is widely used with micro-controllers to control analog devices with a digital signal. PWM has also been used to change the color or to control the brightness of an RGB LED by adjusting the duty cycle [52] [53] [54] [54] [56] [57]. In this chapter, we proposed a novel technique in time domain compliment to equalization to efficiently lower the bit error rate (BER).

4.1 Decoding Problem

In communication, hard decision decoding and soft decision decoding are the two main decoding methods at the receiving side. When a signal is sent

through the channel, the channel attenuates and adds noise to the signal. In the optical transmissions, the characteristics of LED itself make the received waveform distorted as well. Therefore, the receiver sees a distorted signal, which in our case is the red line in Fig. 3.1. A hard decision decoder determines if a bit is "0" or "1" based on a threshold value. At each sampling instant at the receiver, the hard decision decoder determines the bit to be "0" if the voltage falls below the threshold and "1" if the voltage is greater than the threshold. Now if we draw a decision threshold to decode the received signals as Fig. 4.1, T_1 is the duration of the response higher than the threshold to decode a bit as "1" and T_0 is the duration of the response below the threshold to decode a bit as "0". We can easily see that the periods for decoding "1" and "0" are not even, *i.e.*$T_1 \neq T_0$. Further more, they are not equal to the duration of sending one bit either, *i.e.*, $T \neq T_1 \neq T_0$. This would cause the sending bit of "1" to be mistakenly decoded as "0", if the sampling position at the receiver is deviated from the central by more than anticipated, and vice versa. As such, a clock and data recovery (CDR) module is usually used at the receiver as in [58]. The decoding problem gets worse when the sampling clock or the clock recovery at the receiver is not stable, therefore, resulting in poor bit error rate (BER). In [59], W. Xu, *et al.* proposed a predistortion waveform shaping scheme by creating an excess current when the LED is swiched on and off to compensate the LED rising time. In this paper, we proposed a different pre-shaping scheme to dissolve this unacceptable problem in optical transmissions, which has never been addressed until now.

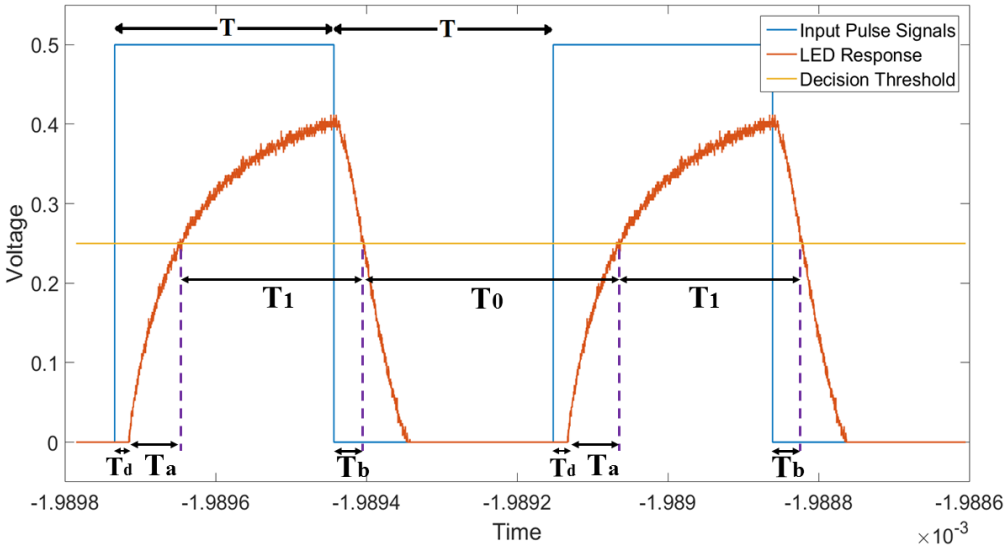

Figure 4.1: LED Pulse Response with Decision Threshold

4.2 Adaptive Sending Duration Algorithm

In Section 4.1, we described the decoding problem in LED optical transmissions. The problem arises from when the LED response gets distorted and thus the duration for decoding ”1” and ”0” is not even. To solve this problem, the main idea is to change the time periods for sending each bit so that the periods for decoding ”1” and ”0” are the same. We proposed solutions to this decoding problem in the following subsections by discussing two different scenarios. One is so that the LED gets full charged within one basic sending period for one bit, the other is so that the LED needs N basic sending periods to get full charged.

4.2.1 Fully Charging in One Cycle

To simplify the analysis, we start from the case that the LED response can reach the maximum voltage in one bit sending cycle as Fig. 4.1. And the voltage also drops down fast when discharging. So we can assume that the LED response always gets discharged down to zero within one basic sending cycle. In Fig. 4.1, T is one bit sending cycle while T_1 and T_0 are the periods for decoding "1" and "0", respectively, at the receiver. T_a is the region within the cycle for sending bit "1", but it would be wrongly decoded as "0". By the same token, T_b is the interval within the cycle for sending bit "0", but mistakenly decoded as "1". Once the threshold line is made, we can get T_a and T_b from Eq. (3.1) and Eq. (3.2). T_d is the delay for the input voltage to reach the LED Forward Voltage, which is usually omitted in practice. To analyze this, Fig. 4.1 shows that

$$T_1 = T - T_d - T_a + T_b \tag{4.1}$$

and

$$T_0 = T - T_b + T_d + T_a. \tag{4.2}$$

If we have N_1 consecutive "1"s and N_0 consecutive "0"s, we get

$$N_1 T_1 = N_1 T - T_d - T_a + T_b \tag{4.3}$$

and

$$N_0 T_0 = N_0 T - T_b + T_d + T_a. \tag{4.4}$$

Dividing N_1 and N_0 on both sides of Equations (4.3) and (4.4) respectively, the duration for decoding a "1" becomes

$$T_1 = T - \frac{T_d}{N_1} - \frac{T_a}{N_1} + \frac{T_b}{N_1} \tag{4.5}$$

and for decoding a "0" becomes

$$T_0 = T - \frac{T_b}{N_0} + \frac{T_d}{N_0} + \frac{T_a}{N_0}. \tag{4.6}$$

As described earlier, the key problem in LED optical transmission is that the periods for decoding "1" and "0" are not even. Therefore, our goal is to make T_1 equal to T_0 by adjusting the sending periods for each bit. Let T_{s1} and T_{s0} denote the average duration of sending bit "1" and bit "0" respectively and make $T_1 = T_0 = T_{fix}$. Rewriting equations (4.5) and (4.6), we get

$$T_{fixed} = T_1 = T_{s1} - \frac{T_d}{N_1} - \frac{T_a}{N_1} + \frac{T_b}{N_1} \tag{4.7}$$

and

$$T_{fixed} = T_0 = T_{s0} - \frac{T_b}{N_0} + \frac{T_d}{N_0} + \frac{T_a}{N_0}. \tag{4.8}$$

By rearranging equations (4.7) and (4.8), it's then easily solved to have

$$T_{s1} = T_{fixed} + \frac{T_d}{N_1} + \frac{T_a}{N_1} - \frac{T_b}{N_1} \tag{4.9}$$

and

$$T_{s0} = T_{fixed} + \frac{T_b}{N_0} - \frac{T_d}{N_0} - \frac{T_a}{N_0}. \tag{4.10}$$

Let T_{s1j} denote the duration of sending the j^{th} "1" in consecutive N_1 "1"s and T_{s0j} denote the duration of sending the j^{th} "0" in consecutive N_0 "0"s. From equations (4.9) and (4.10), if we have

$$N_1 = 1, \Rightarrow T_{s11} = T_{fixed} + T_d + T_a - T_b, \tag{4.11}$$

$$N_1 = 2, \Rightarrow 2T_{s1} = 2T_{fixed} + T_d + T_a - T_b \tag{4.12}$$

$$T_{s12} = 2T_{s1} - T_{s11} = T_{fixed}, \tag{4.13}$$

$$N_1 = 3, \Rightarrow 3T_{s1} = 3T_{fixed} + T_d + T_a - T_b \tag{4.14}$$

$$T_{s13} = 3T_{s1} - T_{s11} - T_{s12} = T_{fixed}, \tag{4.15}$$

$$\vdots$$

and

$$N_0 = 1, \Rightarrow T_{s01} = T_{fixed} + T_b - T_d - T_a, \tag{4.16}$$

$$N_0 = 2, \Rightarrow 2T_{s0} = 2T_{fixed} + T_b - T_d - T_a \tag{4.17}$$

$$T_{s02} = 2T_{s0} - T_{s01} = T_{fixed}, \tag{4.18}$$

$$N_0 = 3, \Rightarrow 3T_{s0} = 3T_{fixed} + T_b - T_d - T_a \tag{4.19}$$

$$T_{s03} = 3T_{s0} - T_{s01} - T_{s02} = T_{fixed}, \tag{4.20}$$

$$\vdots.$$

So, in practice, whenever sending the first "1" in consecutive "1"s, we set the duration T_{s11} to $T_{fixed} + T_d + T_a - T_b$, the sending duration of the rest "1"s can remain T_{fixed}. Similar rules can be applied to send "0"s.

4.2.2 Fully Charging in K Cycles

As the data rate increases, the LED response might not reach the maximum voltage by sending a single "1" due to the reduction in duration of sending each bit. Fig. 4.2 shows the scenario that the LED response needs four sending cycles, $(4T)$ to get the maximum voltage. If a decision line, TH, is drawn as the yellow line in Fig. 4.2, the new problem arises. The incorrect periods for

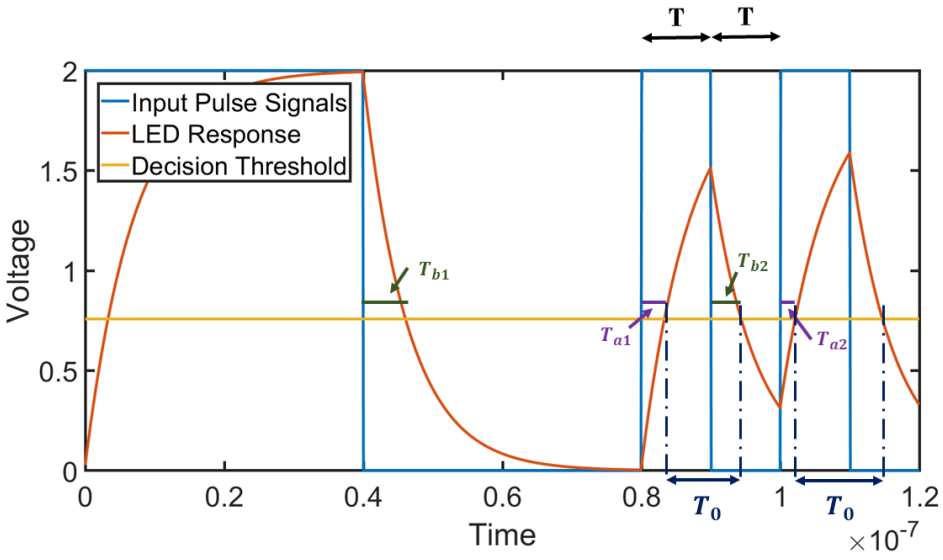

Figure 4.2: LED Pulse Response When Data Rate Increasing

decoding a "0" as a "1" are not always the same, *i.e.* $T_{b1} \neq T_{b2}$. For the same reason, $T_{a1} \neq T_{a2}$. Therefore, T_1 and T_0 do not remain the same either. This makes the results in Subsection 4.2.1 not applicable for this case.

From Eq. (3.3) and Eq. (3.4), we have

$$\begin{cases} T_a = -\tau_a \ln(1 - \dfrac{TH}{V_{max}}) - \Delta T_{01} \\ T_b = -\tau_b \ln(\dfrac{TH}{V_{max}}) - \Delta T_{10}. \end{cases} \tag{4.21}$$

Therefore, T_a and T_b here and in Eq.(4.9) and Eq.(4.10) are not always fixed due to ΔT_{01} and ΔT_{10}. We need to update T_a and T_b whenever ΔT_{01} and ΔT_{10} need to be updated. Supposed there are N_1 consecutive "1"s to be sent from i^{th} bit to $(i + N_1 - 1)^{th}$ bit, and the sender only knows the previous sent bits

and the current sending bit(causal system), below is how the sender adjusts the sending duration for each "1" it is going to send.

When the sender sees the first "1" at the i^{th} bit, it doesn't know if there are more "1"s in the next bits, so it assumes there is only one "1", i.e. $N_1 = 1$. Then the sending duration for sending the first "1", T_{s11} is defined as below.

$$N_1 = 1, \Rightarrow T_{s11} = T_{fixed} + T_d + T_a - T_b$$
$$= T_{fixed} + T_d + (-\tau_a \ln(1 - \frac{TH}{V_{max}}) + \tau_a \ln(1 - \frac{y((i-1)T_{fixed})}{V_{max}})) - (-\tau_b \ln(\frac{TH}{V_{max}}) + \tau_b \ln(\frac{y((i)T_{fixed})}{V_{max}})) \tag{4.22}$$

When the sender sees the second "1" at the $(i+1)^{th}$ bit, it knows that there is already a sent "1" before the current sending "1", but it still doesn't know if there are more "1"s in the next bits, so it now assumes there are two "1"s, i.e. $N_1 = 2$. Then the sending duration for sending the second "1", T_{s12} is obtained as below.

$$N_1 = 2, \Rightarrow 2T_{s1} = 2T_{fixed} + T_d + T_a - T_b$$
$$= 2T_{fixed} + T_d + (-\tau_a \ln(1 - \frac{TH}{V_{max}}) + \tau_a \ln(1 - \frac{y((i-1)T_{fixed})}{V_{max}})) - (-\tau_b \ln(\frac{TH}{V_{max}}) + \tau_b \ln(\frac{y((i+1)T_{fixed})}{V_{max}})) \tag{4.23}$$

$$\begin{aligned} T_{s12} &= 2T_{s1} - T_{s11} \\ &= T_{fixed} + \tau_b \ln(\frac{y((i)T_{fixed})}{V_{max}}) - \tau_b \ln(\frac{y((i+1)T_{fixed})}{V_{max}}) \\ &= T_{fixed} + \Delta T \end{aligned} \tag{4.24}$$

The ΔT in the above equation is the adjusted amount that needs to be

update whenever sending a bit. The same rule applies when the sender sees the third "1" at the $(i+2)^{th}$ bit.

$$N_1 = 3, \Rightarrow 3T_{s1} = 3T_{fixed} + T_d + T_a - T_b$$
$$= 3T_{fixed} + T_d + (-\tau_a \ln(1 - \frac{TH}{V_{max}}) + \tau_a \ln(1 - \frac{y((i-1)T_{fixed})}{V_{max}})) - (-\tau_b \ln(\frac{TH}{V_{max}}) + \tau_b \ln(\frac{y((i+2)T_{fixed})}{V_{max}})) \tag{4.25}$$

$$\begin{aligned} T_{s13} &= 3T_{s1} - T_{s11} - T_{s12} \\ &= T_{fixed} + \tau_b \ln(\frac{y((i+1)T_{fixed})}{V_{max}}) - \tau_b \ln(\frac{y((i+2)T_{fixed})}{V_{max}}) \\ &= T_{fixed} + \Delta T \end{aligned} \tag{4.26}$$

It can be summarized to when sending the n^{th} "1".

$$\begin{aligned} T_{s1n} &= nT_{s1} - T_{s11} - \cdots - T_{s1(n-1)} \\ &= T_{fixed} + \tau_b \ln(\frac{y((i+n-2)T_{fixed})}{V_{max}}) - \tau_b \ln(\frac{y((i+n-1)T_{fixed})}{V_{max}}) \\ &= T_{fixed} + \Delta T \end{aligned} \tag{4.27}$$

It is the same logic when there are N_0 consecutive "0"s from i^{th} bit to $(i + N_0 - 1)^{th}$ bit to be sent.

$$N_0 = 1, \Rightarrow T_{s01} = T_{fixed} + T_b - T_d - T_a$$
$$= T_{fixed} + (-\tau_b \ln(\frac{TH}{V_{max}}) + \tau_b \ln(\frac{y((i-1)T_{fixed})}{V_{max}})) - T_d - (-\tau_a \ln(1 - \frac{TH}{V_{max}}) + \tau_a \ln(1 - \frac{y((i)T_{fixed})}{V_{max}})) \tag{4.28}$$

$$N_0 = 2, \Rightarrow 2T_{s0} = 2T_{fixed} + T_b - T_d - T_a$$

$$= 2T_{fixed} + (-\tau_b \ln(\tfrac{TH}{V_{max}}) + \tau_b \ln(\tfrac{y((i-1)T_{fixed})}{V_{max}})) - T_d - (-\tau_a \ln(1 - \tfrac{TH}{V_{max}}) + \tau_a \ln(1 - \tfrac{y((i+1)T_{fixed})}{V_{max}})) \tag{4.29}$$

$$\begin{aligned} T_{s02} &= 2T_{s0} - T_{s01} \\ &= T_{fixed} + \tau_a \ln(1 - \frac{y((i)T_{fixed})}{V_{max}}) - \tau_a \ln(1 - \frac{y((i+1)T_{fixed})}{V_{max}}) \\ &= T_{fixed} + \Delta T \end{aligned} \tag{4.30}$$

$$N_0 = 3, \Rightarrow 3T_{s0} = 3T_{fixed} + T_b - T_d - T_a$$

$$= 3T_{fixed} + (-\tau_b \ln(\tfrac{TH}{V_{max}}) + \tau_b \ln(\tfrac{y((i-1)T_{fixed})}{V_{max}})) - T_d - (-\tau_a \ln(1 - \tfrac{TH}{V_{max}}) + \tau_a \ln(1 - \tfrac{y((i+2)T_{fixed})}{V_{max}})) \tag{4.31}$$

$$\begin{aligned} T_{s03} &= 3T_{s0} - T_{s01} - T_{s02} \\ &= T_{fixed} + \tau_a \ln(1 - \frac{y((i+1)T_{fixed})}{V_{max}}) - \tau_a \ln(1 - \frac{y((i+2)T_{fixed})}{V_{max}}) \\ &= T_{fixed} + \Delta T \end{aligned} \tag{4.32}$$

$$
\begin{aligned}
T_{s0n} &= nT_{s0} - T_{s01} - \cdots - T_{s0(n-1)} \\
&= T_{fixed} + \tau_a \ln(1 - \frac{y((i+n-2)T_{fixed})}{V_{max}}) - \tau_a \ln(1 - \frac{y((i+n-1)T_{fixed})}{V_{max}}) \\
&= T_{fixed} + \Delta T
\end{aligned}
\tag{4.33}
$$

Note that when it needs K cycles to fully charge and discharge the LED response, $\ln(\frac{y(jT_{fixed})}{V_{max}}) = 0$ and $\ln(1 - \frac{y(jT_{fixed})}{V_{max}}) = 0$ if $j \geq K$.

To summarize the above, we have

$$
\begin{aligned}
&T_{s11} = T_{fixed} + T_d + T_a - T_b \\
&= T_{fixed} + T_d + (-\tau_a \ln(1 - \tfrac{TH}{V_{max}}) + \tau_a \ln(1 - \tfrac{y((i-1)T_{fixed})}{V_{max}})) - (-\tau_b \ln(\tfrac{TH}{V_{max}}) + \tau_b \ln(\tfrac{y((i)T_{fixed})}{V_{max}}))
\end{aligned}
\tag{4.34}
$$

$$
\begin{cases}
T_{s1j} = T_{fixed} + \Delta T, \ for\ 1 < j \leq K \\
\Delta T = \tau_b \ln(\dfrac{y((i+j-2)T_{fixed})}{V_{max}}) - \tau_b \ln(\dfrac{y((i+j-1)T_{fixed})}{V_{max}})
\end{cases}
\tag{4.35}
$$

$$
T_{s1j} = T_{fixed}, \ for\ j \geq K+1 \tag{4.36}
$$

and

$$T_{s01} = T_{fixed} + T_b - T_d - T_a$$
$$= T_{fixed} + (-\tau_b \ln(\frac{TH}{V_{max}}) + \tau_b \ln(\frac{y((i-1)T_{fixed})}{V_{max}})) - T_d - (-\tau_a \ln(1 - \frac{TH}{V_{max}}) + \tau_a \ln(1 - \frac{y((i)T_{fixed})}{V_{max}})) \tag{4.37}$$

$$\begin{cases} T_{s0j} = T_{fixed} + \Delta T, \ for\ 1 < j \leq K \\ \Delta T = \tau_a \ln(1 - \dfrac{y((i+j-2)T_{fixed})}{V_{max}}) - \tau_a \ln(1 - \dfrac{y((i+j-1)T_{fixed})}{V_{max}}) \end{cases} \tag{4.38}$$

$$T_{s0j} = T_{fixed}, \ for\ j \geq K+1. \tag{4.39}$$

Eq. (4.34) to Eq. (4.39) can be further simplified as below.

$$T_{s11} = T_{fixed} + T_d - \tau_a \ln(\frac{V_{max} - TH}{V_{max} - y((i-1)T_{fixed})}) + \tau_b \ln(\frac{TH}{y((i)T_{fixed})}) \tag{4.40}$$

$$\begin{cases} T_{s1j} = T_{fixed} + \Delta T, \ for\ 1 < j \leq K \\ \Delta T = \tau_b \ln(\dfrac{y((i+j-2)T_{fixed})}{y((i+j-1)T_{fixed})}) \end{cases} \tag{4.41}$$

$$T_{s1j} = T_{fixed}, \ for\ j \geq K+1 \tag{4.42}$$

$$T_{s01} = T_{fixed} - \tau_b \ln(\frac{TH}{y((i-1)T_{fixed})}) - T_d + \tau_a \ln(\frac{V_{max} - TH}{V_{max} - y((i)T_{fixed})}) \quad (4.43)$$

$$\begin{cases} T_{s0j} = T_{fixed} + \Delta T, \ for\ 1 < j \leq K \\ \Delta T = \tau_a \ln(\frac{V_{max} - y((i+j-2)T_{fixed})}{V_{max} - y((i+j-1)T_{fixed})}) \end{cases} \quad (4.44)$$

$$T_{s0j} = T_{fixed}, \ for\ j \geq K+1 \quad (4.45)$$

When K equals to 1, the results above are equivalent to Subsection 4.2.1.

Finally, we summarize the algorithm for determining the duration of sending a block of N bits in Algorithm 2.

4.3 Simulation and Discussion

We can use Algorithm 2 to simulate the LED responses with the newly calculated adaptive sending duration. Fig. 4.3 and Fig. 4.4 are comparisons between the original LED response and the response with ASDA for $K = 1$ and $K = 2$ respectively. When K equals to 1, there is not big difference between two simulated LED responses. But it is apparent that the original LED's response width for each bit is not equal in Fig. 4.4, and ASDA LED response resolves this issue successfully.

Now we compare the BERs among ASDA, LMS Equalization and combined

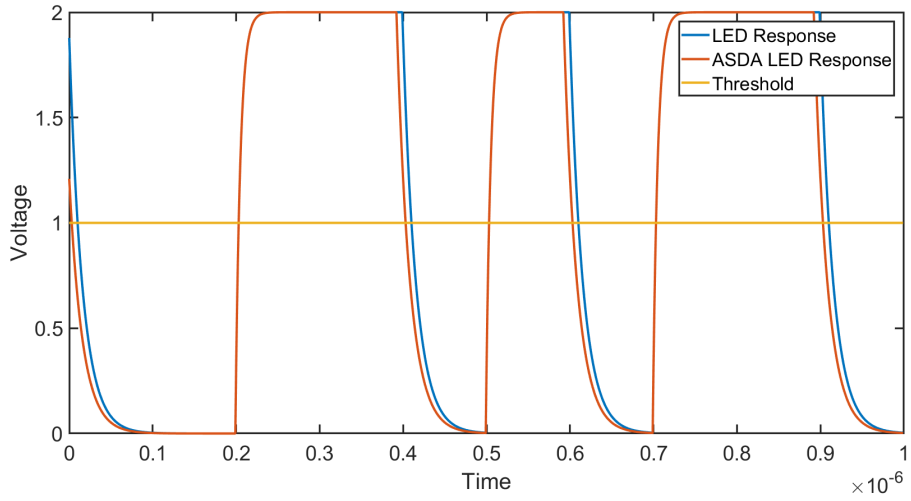

Figure 4.3: LED Responses With $K = 1$

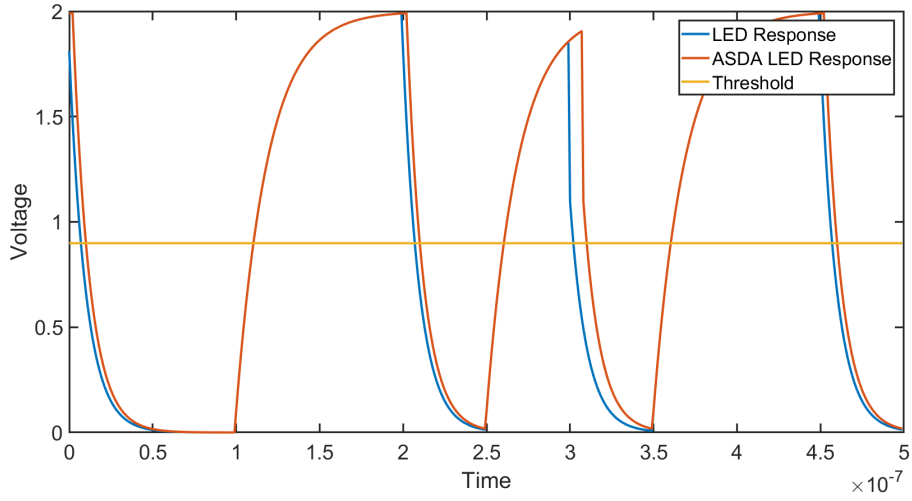

Figure 4.4: LED Responses With $K = 2$

ASDA with LMS Equalization. We use the parameters for the case $K = 1$ as following:

- Data Rate : $10M$ (Hz)
- T_{fixed} : 10^{-7} (s)
- V_{max} : 2 (V)
- Decision Threshold : 1 (V)
- ρ_a : 5.77×10^{-9} (s)
- ρ_b : 1.59×10^{-8} (s)
- Training Length : 100 (bits)
- Taps : 3
- Samples per Symbol : 3

Fig. 4.5 shows the BERs when sampling without clock jitter. Although ASDA alone doesn't really improve the BER compared with the original plain LED response, it got about 0.5dB gain with BER of 10^{-8} while working with Equalization.

For sampling the received signal, the clock jitter is always an issue. Therefore, we also simulated the scenarios when clock jitter is presented. Clock jitter [60] is the deviation from its ideal sampling position. Random jitter caused

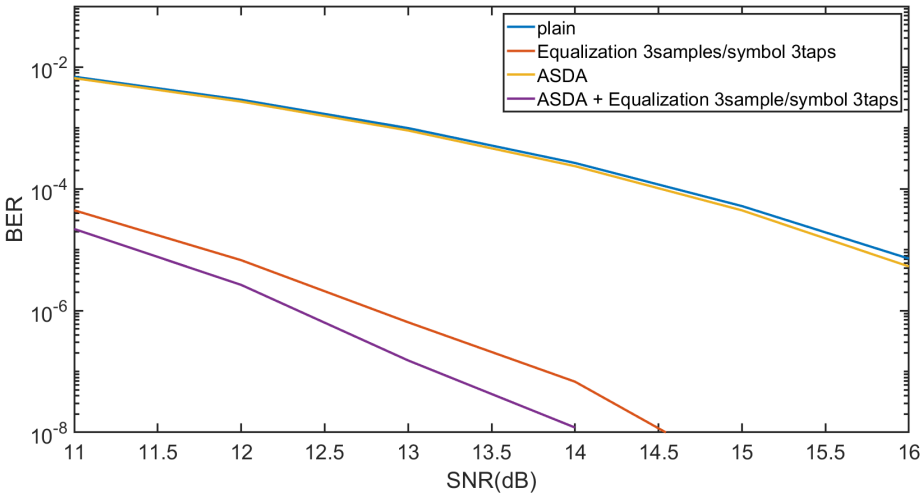

Figure 4.5: $K = 1$, *No Clock Jitter*

by thermal noise in an electrical circuit typically follows a normal distribution. Now, if we apply the clock jitter while sampling, our scheme combined with Equalization still has more than 0.5dB gain of BER at 10^{-7} compared to the one of Equalization alone when the noise distribution of clock jitter is $N(0, 4\%T_{fixed})$ in Fig. 4.6. Fig. 4.7 increases the standard deviation of clock jitter to $8\%T_{fixed}$, the bit error rates of all the schemes increase as expected, but ASDA alone outperforms the original plain LED response and the BER of Equalization alone crashes while the BER of Equalization with ASDA still remains low.

We also simulated the case for $K = 2$, below is the parameter settings:

- Data Rate : $20M$ (Hz)

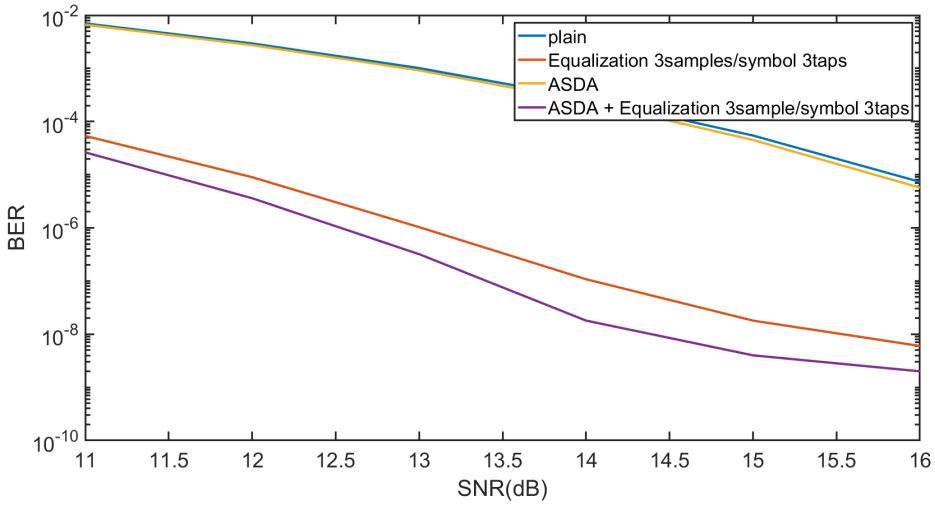

Figure 4.6: $K = 1$, $Clock\ Jitter \sim N(0, (4\%T_{fixed})^2)$

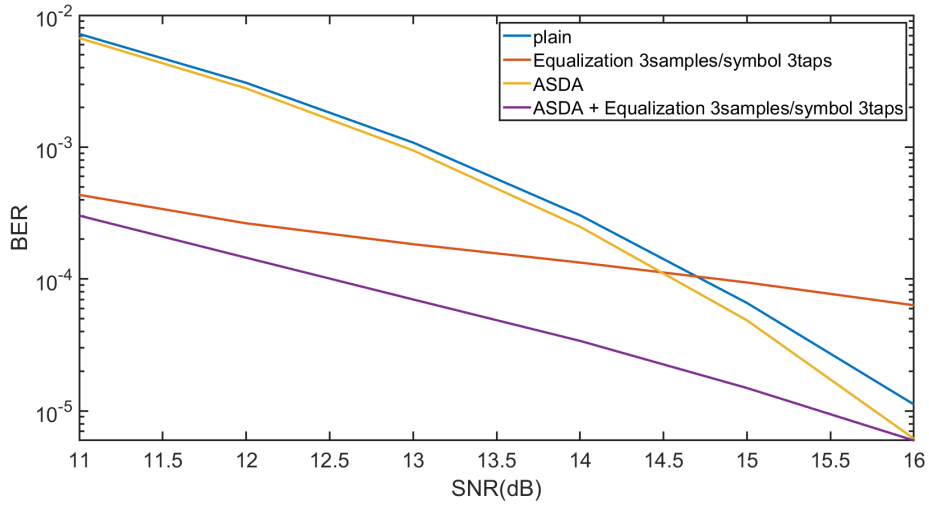

Figure 4.7: $K = 1$, $Clock\ Jitter \sim N(0, (8\%T_{fixed})^2)$

- T_{fixed} : 5×10^{-8} (s)
- V_{max} : 2 (V)
- Decision Threshold : 0.9767 (V)
- ρ_a : 1.343×10^{-8} (s)
- ρ_b : 1.6744×10^{-8} (s)
- Training Length : 100 (bits)
- Taps : 3
- Samples per Symbol : 3

Fig. 4.8 to Fig. 4.10 are the simulation results for the case $K = 2$ with/without clock jitter applied. We can see that even without coworking with an equalizer, the ASDAs improve the BERs a bit more than the case of $K = 1$. As the variance of the clock jitter increases, the performances of all decoding schemes decrease consistently. However, the ASDA combined with a linear equalizer still remains the lowest BER among all the decoding methods.

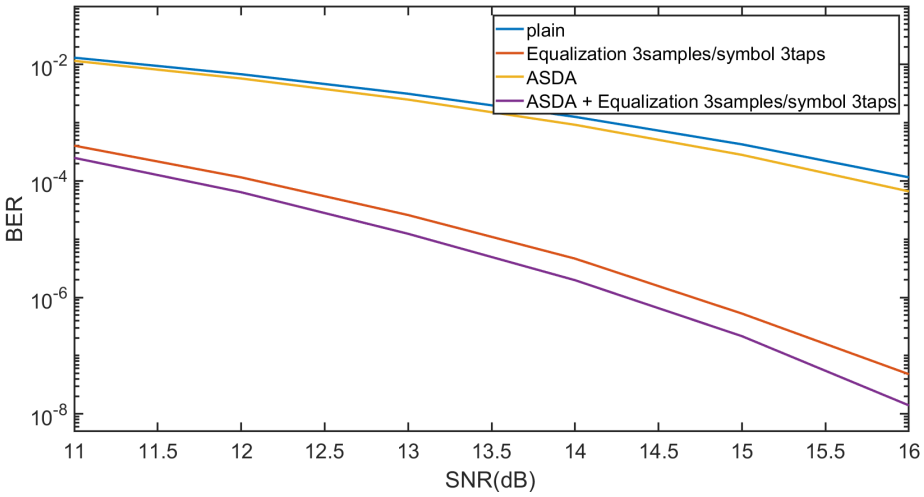

Figure 4.8: $K = 2$, *No Clock Jitter*

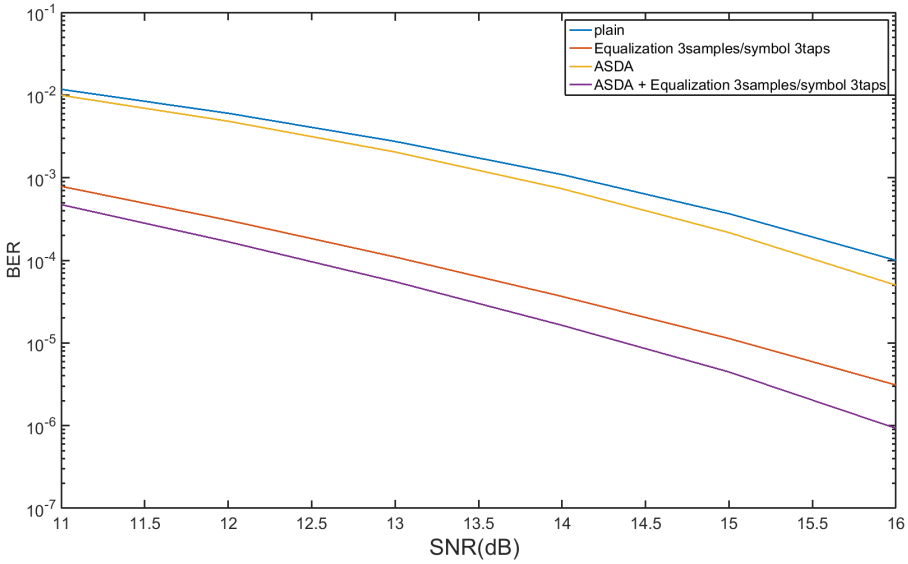

Figure 4.9: $K = 2$, *Clock Jitter* $\sim N(0, (4\%T_{fixed})^2)$

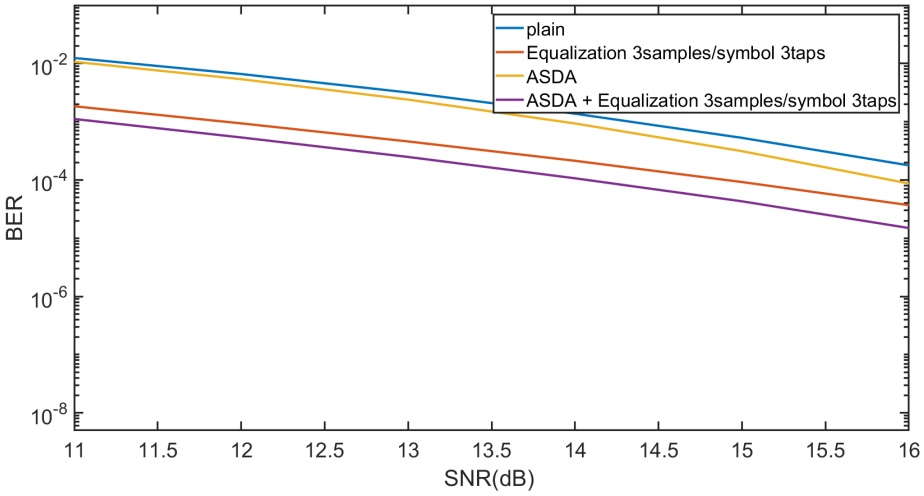

Figure 4.10: $K = 2$, $Clock\ Jitter \sim N(0, (8\%T_{fixed})^2)$

Algorithm 2 Adaptive Sending Duration Algorithm

Require: Known Parameters - K, T_{fixed}, T_d, N, $x_0 = 0$

$N_0 = 1$
$N_1 = 1$
for j from 1 to N **do**
    if $x_j == 1$ **then**
        if $x_(j-1) == 1$ **then**
            N_1++
            if $N_1 > K$ **then**
                $T_{sending} = T_{fixed}$
            else
                $\Delta T = \tau_b \ln(\frac{y((j-1)T_{fixed})}{y((j)T_{fixed})})$
                $T_{sending} = T_{fixed} + \Delta T$
            end if
        else
            $N_1 = 1$
            $T_a = -\tau_a \ln(\frac{V_{max}-TH}{V_{max}-y((j-1)T_{fixed})})$
            $T_b = -\tau_b \ln(\frac{TH}{y((j)T_{fixed})})$
            $T_{sending} = T_{fixed} + T_d + T_a - T_b$
        end if
    else ▷ $x_j == 0$
        if $x_(j-1) == 0$ **then**
            N_0++
            if $N_0 > K$ **then**
                $T_{sending} = T_{fixed}$
            else
                $\Delta T = \tau_a \ln(\frac{V_{max}-y((j-1)T_{fixed})}{V_{max}-y((j)T_{fixed})})$
                $T_{sending} = T_{fixed} + \Delta T$
            end if
        else
            $N_0 = 1$
            $T_a = -\tau_a \ln(\frac{V_{max}-TH}{V_{max}-y((j)T_{fixed})})$
            $T_b = -\tau_b \ln(\frac{TH}{y((j-1)T_{fixed})})$
            $T_{sending} = T_{fixed} + T_b - T_d - T_a$
        end if
    end if
end for

Chapter 5: Memory Decoding for FSO Transmissions

Methods for compensating the distortion during transmissions are well explored, especially in wireless and wired line communications. In wireline communication, the distortion is caused by high RC constant of the line, and in wireless communication, it is often caused by channel fading. There exists a wealth of techniques for correcting the distortion. These techniques generally fall into two approaches. In the first approach, a distorted received analog signal is linearized through a process of linear equalization before decoding the signals into bits. In the second approach, the transmitter pre-distorts the input signals to compensate for the distortion during the transmissions. This is the same concept as the ASDA algorithm we proposed in Chapter 4. In communication, the popular method is to use linear equalization to cancel the effect of distortion by the channel. For example, many adaptive MMSE equalizer schemes were proposed to suppress the multipath ISI (inter symbol interference) in [61]. [62] presents an effective analogue equalization to enhance the modulation bandwidth of an organic light emitting diode (OLED). We note that since the shapes of different distorted transmitted signals are known as in Chapter 3, a matched filter [63] [64] can be used at the receiver to detect the most probable transmitted signal to reduce the bit error rate. However, digital matched filters require a high precision analog-to-digital (ADC) con-

verter and more digital processing power to accurately match the shape. On the other hand, the algorithm called Memory Decoding Algorithm (MDA) [65] we proposed in this chapter only requires 1 or 2 samples per symbol. There is also analog implementation of matched filter, but the analog implementation is not sufficiently flexible (programmable) for our WiFO system. Both Partial Response Maximum Likelihood(PRML) [66] [67] and Maximum Likelihood Sequence Estimation (MLSE) employ coded schemes to improve the bit error rate at the expense of lower throughput. On the other hand, MDA does not use coding thus has less overhead.

The MDA is designed to be used by the receiver to reduce the bit error rate. Using this technique, there is no need for the transmitter to pre-distort the signal. Instead, based on the mathematical model of the channel response in Eqs. (3.1) and (3.2), MDA uses the maximum likelihood method for decoding the bits.With the relation between the input $x(t)$ and output $y(t)$ in Eq. (3.3) and the k-bit-long memory, we now propose a threshold decoding method using the previous decoded results as well as the adaptive thresholds to decode the current bit.

5.1 Memory Decoding Algorithm

We model the received signal as:

$$\tilde{y}(t) = y(t) + N(t), \tag{5.1}$$

where $N(t)$ is a white noise.

At receiver, $\tilde{y}(t)$ is sampled at some equal intervals, $(i-1)T+T_s$ for the i^{th} bit. The classical threshold decoding scheme decodes

$$\tilde{y}((i-1)T+T_s) = \begin{cases} 1 & \text{if } \tilde{y}((i-1)T+T_s) \geq \frac{V_{max}}{2}, \\ 0 & \text{otherwise.} \end{cases}$$

It can be shown that using a fixed threshold of $\frac{V_{max}}{2}$, is suboptimal. Therefore, we propose a novel decoding scheme that utilizes the "memory" property of LED response in Section 3.2. Before starting to decode, we need to specify how many bits of memory that we want to use for decoding models. In the following, we will explain how Memory Decoding Algorithm(MDA) works with one-bit-long memory and two-bit-long memory for examples in detail.

5.1.1 Decoding Models for One-Bit-Long Memory

Assuming that the memory only lasts for one bit duration, T, *i.e.,* $e^{-\frac{t}{\tau_a}} \cong 0$ and $e^{-\frac{t}{\tau_b}} \cong 0$ when $t \geq T$, from Fig. 5.1 we can see that the observed i^{th} received sample is simplified to

$$\tilde{y}_i = \begin{cases} 0 + N_i, & if\ x_{i-1} = 0\ and\ x_i = 0 \\ V_{max} \cdot e^{-\frac{T_s}{\tau_b}} + N_i, & if\ x_{i-1} = 1\ and\ x_i = 0 \\ V_{max} \cdot (1 - e^{-\frac{T_s}{\tau_a}}) + N_i, & if\ x_{i-1} = 0\ and\ x_i = 1 \\ V_{max} + N_i, & if\ x_{i-1} = 1\ and\ x_i = 1 \end{cases}, \tag{5.2}$$

where x_i denotes the i^{th} transmitted bit and N_i is a random variable repre-

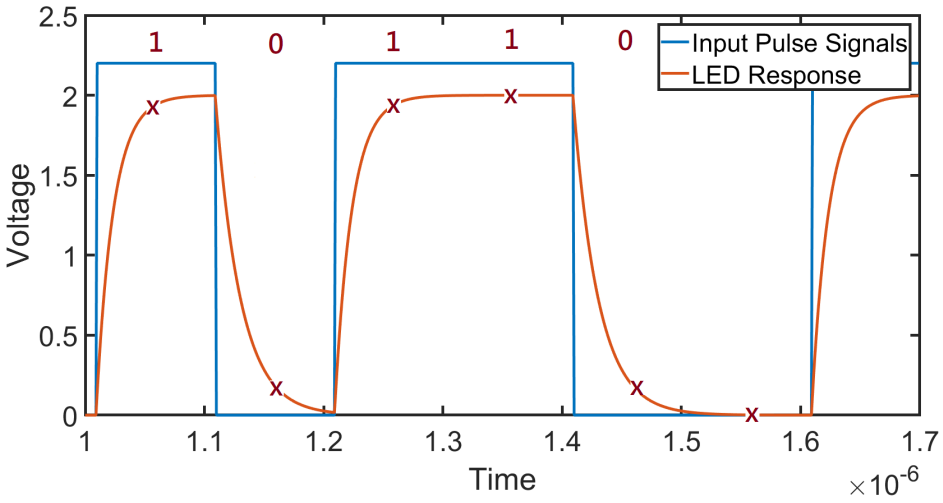

Figure 5.1: Illustration of Sampling and Math Models

senting the channel noise, which is independent of x_i and its response. Thus, each current bit depends on both the current and the previous bits. Applying the MLE (Maximum Likelihood Estimation) analysis, the decoding rule of current bit can be found as:

$$\hat{x}_i = \begin{cases} 1 & \text{if } \frac{f_{N_i}(\tilde{y}_i - y_i \mid x_{i-1}, x_i = 1, \tilde{y}_i)}{f_{N_i}(\tilde{y}_i - y_i \mid x_{i-1}, x_i = 0, \tilde{y}_i)} \geq 1, \\ 0 & \text{otherwise,} \end{cases} \tag{5.3}$$

where $f_{N_i}(\cdot)$ represents the probability density function of the noise, N_i. Fig. 5.2 is an example of decoding current bit when the previous bit is "1".

It is important to note that the proposed algorithm makes use of x_{i-1}, the correct transmitted bit in the previous time slot. However, x_{i-1} is not available at the receiver. To that end, we make the assumption that the decoded bit in the previous time slot, $\hat{x}_{i-1}$, is the same as the true transmitted bit,

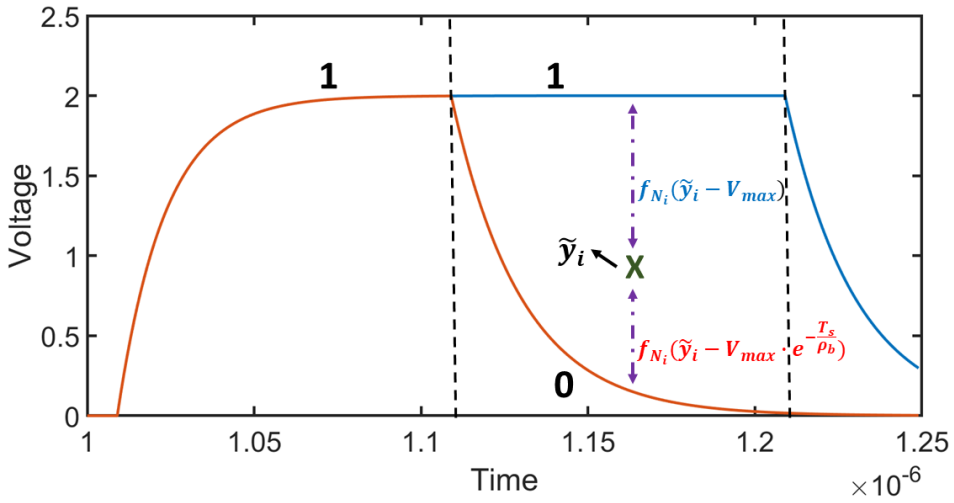

Figure 5.2: Example of MLE Decoding

x_{i-1}. Consequently, our algorithm uses $\hat{x}_{i-1}$ in place of x_{i-1} in Eq. (5.3). Although this approximation might introduce error propagation during decoding, our theoretical analysis and simulation will show that the error propagation is minimal.

The decoding algorithm based on Eq. (5.3) can be simplified to an adaptive threshold decoding algorithm involving two optimal thresholds TH_0 and TH_1. This is in contrast with the classical thresholding decoding algorithm where only one threshold is used. As an example, we derive the optimal thresholds TH_0 and TH_1 assuming an additive white Gaussian noise (AWGN) as follows.

Plugging $x_{i-1} = \hat{x}_{i-1} = 0$ and Eq. (5.2) in the inequality (5.3), we obtain

$$
\begin{aligned}
&\frac{f_{N_i}(\tilde{y}_i - y_i \mid x_{i-1}=0, x_i=1, \tilde{y}_i)}{f_{N_i}(\tilde{y}_i - y_i \mid x_{i-1}=0, x_i=0, \tilde{y}_i)} \geq 1 \\
\Rightarrow\ &\frac{f_{N_i}(\tilde{y}_i - V_{max}(1-e^{-\frac{T_s}{\tau_a}}))}{f_{N_i}(\tilde{y}_i - 0)} \geq 1 \\
\Rightarrow\ &\frac{\frac{1}{\sqrt{2\pi\sigma^2}} e^{-\frac{(\tilde{y}_i - V_{max}(1-e^{-\frac{T_s}{\tau_a}}))^2}{2\sigma^2}}}{\frac{1}{\sqrt{2\pi\sigma^2}} e^{-\frac{(\tilde{y}_i - 0)^2}{2\sigma^2}}} \geq 1 \\
\Rightarrow\ &\log_e\left(\frac{e^{-\frac{(\tilde{y}_i - V_{max}(1-e^{-\frac{T_s}{\tau_a}}))^2}{2\sigma^2}}}{e^{-\frac{(\tilde{y}_i - 0)^2}{2\sigma^2}}}\right) \geq \log_e(1) \\
\Rightarrow\ &\frac{(\tilde{y}_i)^2 - (\tilde{y}_i - V_{max}(1-e^{-\frac{T_s}{\tau_a}}))^2}{2\sigma^2} \geq 0 \\
\Rightarrow\ &\tilde{y}_i \geq \frac{V_{max}(1-e^{-\frac{T_s}{\tau_a}})}{2} = TH_0.
\end{aligned}
\tag{5.4}
$$

Applying the same rule and plugging $x_{i-1} = \hat{x}_{i-1} = 1$ and Equation (5.2) in the inequality (5.3), we obtain

$$
\begin{aligned}
&\frac{f_{N_i}(\tilde{y}_i - y_i \mid x_{i-1}=1, x_i=1, \tilde{y}_i)}{f_{N_i}(\tilde{y}_i - y_i \mid x_{i-1}=1, x_i=0, \tilde{y}_i)} \geq 1 \\
\Rightarrow\ &\frac{f_{N_i}(\tilde{y}_i - V_{max})}{f_{N_i}(\tilde{y}_i - V_{max}e^{-\frac{T_s}{\tau_b}})} \geq 1 \\
\Rightarrow\ &\frac{\frac{1}{\sqrt{2\pi\sigma^2}}e^{-\frac{(\tilde{y}_i - V_{max})^2}{2\sigma^2}}}{\frac{1}{\sqrt{2\pi\sigma^2}}\cdot e^{-\frac{(\tilde{y}_i - V_{max}e^{-\frac{T_s}{\tau_b}})^2}{2\sigma^2}}} \geq 1 \\
\Rightarrow\ &\log_e\left(\frac{e^{-\frac{(\tilde{y}_i - V_{max})^2}{2\sigma^2}}}{e^{-\frac{(\tilde{y}_i - V_{max}e^{-\frac{T_s}{\tau_b}})^2}{2\sigma^2}}}\right) \geq \log_e(1) \\
\Rightarrow\ &\frac{(\tilde{y}_i - V_{max}e^{-\frac{T_s}{\tau_b}})^2 - (\tilde{y}_i - V_{max})^2}{2\sigma^2} \geq 0 \\
\Rightarrow\ &\tilde{y}_i \geq \frac{V_{max}(1+e^{-\frac{T_s}{\tau_b}})}{2} = TH_1.
\end{aligned}
\tag{5.5}
$$

Using the optimal TH_0 and TH_1, the MDA based on models of one-bit-long memory for decoding a block of N bits is summarized in Algorithm 3.

Algorithm 3 Memory Decoding Algorithm Using Models of One-Bit-Long Memory

Require: Initial parameters : TH_0, TH_1, N, $\hat{x}_0 = 0$

1: **for** $i = 1$ to N **do**
2: **if** $\hat{x}_{i-1} == 0$ **then**
3: $Threshold = TH_0$
4: **else** ▷ $\hat{x}_{i-1} == 1$
5: $Threshold = TH_1$
6: **end if**
7: **if** $\tilde{y}_i \geq Threshold$ **then**
8: $\hat{x}_i = 1$
9: **else**
10: $\hat{x}_i = 0$
11: **end if**
12: **end for**

5.1.2 Decoding Models for Two-Bit-Long Memory

Supposed that the LED response has two-bit-long memory as Fig. 3.5, it means $e^{-\frac{t}{\tau_a}} \cong 0$ and $e^{-\frac{t}{\tau_b}} \cong 0$ when $t \geq 2T$. Therefore, the observed i^{th} received sample is approximated as

$$\tilde{y}_i = \begin{cases} 0 + N_i, & if\ x_{i-2} = 0,\ x_{i-1} = 0\ and\ x_i = 0 \\ V_{max} \cdot (1 - e^{-\frac{T_s}{\tau_a}}) + N_i, & if\ x_{i-2} = 0,\ x_{i-1} = 0\ and\ x_i = 1 \\ V_{max} \cdot e^{-\frac{T_s - \tau_b \ln \frac{y((i-1)T)}{V_{max}}}{\tau_b}} + N_i, & if\ x_{i-2} = 0,\ x_{i-1} = 1\ and\ x_i = 0 \\ V_{max} \cdot (1 - e^{-\frac{T_s+T}{\tau_a}}) + N_i, & if\ x_{i-2} = 0,\ x_{i-1} = 1\ and\ x_i = 1 \\ V_{max} \cdot e^{-\frac{T_s+T}{\tau_b}} + N_i, & if\ x_{i-2} = 1,\ x_{i-1} = 0\ and\ x_i = 0 \\ V_{max} \cdot (1 - e^{-\frac{T_s - \tau_a \ln 1 - \frac{y((i-1)T)}{V_{max}}}{\tau_a}}) + N_i, & if\ x_{i-2} = 1,\ x_{i-1} = 0\ and\ x_i = 1 \\ V_{max} \cdot e^{-\frac{T_s}{\tau_b}} + N_i, & if\ x_{i-2} = 1,\ x_{i-1} = 1\ and\ x_i = 0 \\ V_{max} + N_i, & if\ x_{i-2} = 1,\ x_{i-1} = 1\ and\ x_i = 1 \end{cases}, \tag{5.6}$$

where x_i and N_i denote the i^{th} transmitted bit and a random variable representing the independent channel noise respectively. Compared with one-bit-long memory in 5.1.1, it is obvious that each current received sample now depends on both the current and the previous two bits. Applying the same MLE (Maximum Likelihood Estimation) analysis in Eq.(5.3), four optimal thresholds would be obtained. If the independent channel noise is symmetric, for example, AWGN, the four thresholds of two-bit-long memory decoding are

$$TH_{00} = \frac{V_{max}(1 - e^{-\frac{T_s}{\tau_a}})}{2}, \tag{5.7}$$

$$TH_{01} = \frac{V_{max}(1 + e^{-\frac{T_s - \tau_b \ln (1 - e^{-\frac{T}{\tau_a}})}{\tau_b}} - e^{-\frac{T_s+T}{\tau_a}})}{2}, \tag{5.8}$$

$$TH_{10} = \frac{V_{max}(1 + e^{-\frac{T_s+T}{\tau_b}} - e^{-\frac{T_s-\tau_a \ln(1-e^{-\frac{T}{\tau_b}})}{\tau_a}})}{2} \tag{5.9}$$

and

$$TH_{11} = \frac{V_{max}(1 + e^{-\frac{T_s}{\tau_b}})}{2}. \tag{5.10}$$

Using the optimal TH_{00}, TH_{01}, TH_{10} and TH_{11}, the MDA based on models of two-bit-long memory for decoding a block of N bits is summarized in Algorithm 4.

Algorithm 4 Memory Decoding Algorithm Using Models of Two-Bit-Long Memory

Require: Initial parameters : TH_{00}, TH_{01}, TH_{10}, TH_{11}, N, $\hat{x}_{-1} = 0$, $\hat{x}_0 = 0$

for $i = 1$ to N **do**
  if $\hat{x}_{i-2} == 0$ **then**
    if $\hat{x}_{i-1} == 0$ **then**
      $Threshold = TH_{00}$
    else ▷ $\hat{x}_{i-1} == 1$
      $Threshold = TH_{01}$
    end if
  else ▷ $\hat{x}_{i-2} == 1$
    if $\hat{x}_{i-1} == 0$ **then**
      $Threshold = TH_{10}$
    else ▷ $\hat{x}_{i-1} == 1$
      $Threshold = TH_{11}$
    end if
  end if
  if $\tilde{y}_i \geq Threshold$ **then**
    $\hat{x}_i = 1$
  else
    $\hat{x}_i = 0$
  end if
end for

5.1.3 Decoding Models for N-Bit-Long Memory

What if the LED response has N-bit-long memory? According to Section 5.1.1 and Section 5.1.2, there are 2^N thresholds to be calculated in advance. It is barely possible while N is large. However, with Eq. (3.3) and Eq. (3.4), we can use the previous decoded bit $\hat{x}_{i-1}$ to replace the actual sending bit x_{i-1} and assume x_i as 1 and 0 respectively to update temporary T_{01}, ΔT_{01} and T_{10}, ΔT_{10} correspondingly whenever there is a transition between $\hat{x}_{i-1}$ and x_i. Then applying MLE(Maximum Likelihood Estimation) can decode the current received bit. The biggest difference between this decoding method and the rules described earlier is that it is required to apply MLE every time to decode each bit while the decoding rules using known information of k-bit-long memory compute thresholds beforehand once for decoding all received bits. Algorithm 5 for decoding a block of N bits explains each decoding step without knowing how long the memory is. T_{01} and T_{10} are set to $-\infty$, ΔT_{01} and ΔT_{10} are set to 0 because the sending signal, x_i, is assumed at rest initially.

Algorithm 5 Memory Decoding Algorithm Using Models of N-Bit-Long Memory

Require: Initial parameters : N, τ_a, τ_b, V_{max}, T, T_s, $f_{N_i}(\cdot)$, $T_{01} = T_{10} = -\infty$, $\Delta T_{01} = \Delta T_{10} = 0$, $\hat{x}_0 = 0$

for $i = 1$ to N **do**
  if $\hat{x}_{i-1} == 0$ **then**
    $T_{01}^{'} = (i-1)T$
    $\Delta T_{01}^{'} = -\tau_a \ln\left(1 - \frac{V_{max} e^{-\frac{(i-1)T - T_{10} + \Delta T_{10}}{\tau_b}}}{V_{max}}\right)$
    if $\frac{f_{N_i}(\tilde{y}_i - V_{max}(1 - e^{-\frac{(i-1)T + T_s - T_{01}^{'} + \Delta T_{01}^{'}}{\tau_a}}))}{f_{N_i}(\tilde{y}_i - V_{max} e^{-\frac{(i-1)T + T_s - T_{10} + \Delta T_{10}}{\tau_b}})} \geq 1$ **then**
      $\hat{x}_i = 1$
      $T_{01} = T_{01}^{'}$
      $\Delta T_{01} = \Delta T_{01}^{'}$
    else
      $\hat{x}_i = 0$
    end if
  else ▷ $\hat{x}_{i-1} == 1$
    $T_{10}^{'} = (i-1)T$
    $\Delta T_{10}^{'} = -\tau_b \ln \frac{V_{max}(1 - e^{-\frac{(i-1)T - T_{01} + \Delta T_{01}}{\tau_a}})}{V_{max}}$
    if $\frac{f_{N_i}(\tilde{y}_i - V_{max}(1 - e^{-\frac{(i-1)T + T_s - T_{01} + \Delta T_{01}}{\tau_a}}))}{f_{N_i}(\tilde{y}_i - V_{max} e^{-\frac{(i-1)T + T_s - T_{10}^{'} + \Delta T_{10}^{'}}{\tau_b}})} \geq 1$ **then**
      $\hat{x}_i = 1$
    else
      $\hat{x}_i = 0$
      $T_{10} = T_{10}^{'}$
      $\Delta T_{10} = \Delta T_{10}^{'}$
    end if
  end if
end for

5.2 Bit Error Rate Analysis

In this section, we provide analysis for the bit error rate of the proposed one-bit-long MDA using a Finite Markov Chain when the optical signals also have one-bit-long memory. First, we define the states, S_k, $k = 0, 1, \cdots, 7$, for a discrete-time stochastic process, X_n, $n = 0, 1, 2, \cdots$, in the Markov Chain, where S_k represents a tuple consisting of previously decoded bit, previously sent bit, and current transmitted bit, i.e., $(\hat{x}_{i-1}, x_{i-1}, x_i)$. We order the states S_k as follows: S_0 is defined as $(0, 0, 0)$, S_1 is defined as $(1, 0, 0)$, S_2 is defined as $(0, 1, 0)$, $\cdots$, and S_7 is defined as $(1, 1, 1)$. To construct the transition matrix P for the Markov chain, we compute the transition probabilities, $P\{X_n \mid X_{n-1}\}$. For example, let us compute $P\{X_n = S_1 \mid X_{n-1} = S_0\}$. Using the optimal TH_0 and TH_1 we derived previously and Eq. (5.2), we have:

$$\begin{aligned} & P\{X_n = S_1 \mid X_{n-1} = S_0\} \\ &= \frac{1}{2} \cdot P(\tilde{y}_i \geq TH_0 \mid \hat{x}_{i-1} = 0,\ x_{i-1} = 0,\ x_i = 0) \\ &= \frac{1}{2} \cdot P(N_i \geq TH_0) \\ &= \frac{1}{2} \cdot \{1 - F_{N_i}(TH_0)\}, \end{aligned} \tag{5.11}$$

where $F_{N_i}(\cdot)$ denotes the cumulative distribution function of the random variable, N_i. The transition matrix P is then obtained as

$$P = \begin{bmatrix}
\frac{1}{2}F_{N_i}(TH_0) & \frac{1}{2}\{1-F_{N_i}(TH_0)\} & 0 & 0 & \frac{1}{2}F_{N_i}(TH_0) & \frac{1}{2}\{1-F_{N_i}(TH_0)\} & 0 & 0 \\
\frac{1}{2}F_{N_i}(TH_1) & \frac{1}{2}\{1-F_{N_i}(TH_1)\} & 0 & 0 & \frac{1}{2}F_{N_i}(TH_1) & \frac{1}{2}\{1-F_{N_i}(TH_1)\} & 0 & 0 \\
\frac{1}{2}F_{N_i}(l) & \frac{1}{2}\{1-F_{N_i}(l)\} & 0 & 0 & \frac{1}{2}F_{N_i}(l) & \frac{1}{2}\{1-F_{N_i}(l)\} & 0 & 0 \\
\frac{1}{2}F_{N_i}(m) & \frac{1}{2}\{1-F_{N_i}(m)\} & 0 & 0 & \frac{1}{2}F_{N_i}(m) & \frac{1}{2}\{1-F_{N_i}(m)\} & 0 & 0 \\
0 & 0 & \frac{1}{2}F_{N_i}(s) & \frac{1}{2}\{1-F_{N_i}(s)\} & 0 & 0 & \frac{1}{2}F_{N_i}(s) & \frac{1}{2}\{1-F_{N_i}(s)\} \\
0 & 0 & \frac{1}{2}F_{N_i}(u) & \frac{1}{2}\{1-F_{N_i}(u)\} & 0 & 0 & \frac{1}{2}F_{N_i}(u) & \frac{1}{2}\{1-F_{N_i}(u)\} \\
0 & 0 & \frac{1}{2}F_{N_i}(q) & \frac{1}{2}\{1-F_{N_i}(q)\} & 0 & 0 & \frac{1}{2}F_{N_i}(q) & \frac{1}{2}\{1-F_{N_i}(q)\} \\
0 & 0 & \frac{1}{2}F_{N_i}(r) & \frac{1}{2}\{1-F_{N_i}(r)\} & 0 & 0 & \frac{1}{2}F_{N_i}(r) & \frac{1}{2}\{1-F_{N_i}(r)\}
\end{bmatrix}, \tag{5.12}$$

where

$$\begin{aligned}
l &= TH_0 - V_{max}e^{-\frac{T_s}{\tau_b}} \\
m &= TH_1 - V_{max}e^{-\frac{T_s}{\tau_b}} \\
s &= TH_0 - V_{max}(1-e^{-\frac{T_s}{\tau_a}}) \\
u &= TH_1 - V_{max}(1-e^{-\frac{T_s}{\tau_a}}) \\
q &= TH_0 - V_{max} \\
r &= TH_1 - V_{max}.
\end{aligned} \tag{5.13}$$

It can be shown that P is irreducible and aperiodic. Therefore, there exists a unique stationary probability vector $\bar{\boldsymbol{\pi}}$ satisfying

$$\bar{\boldsymbol{\pi}}P = \bar{\boldsymbol{\pi}} \tag{5.14}$$

and

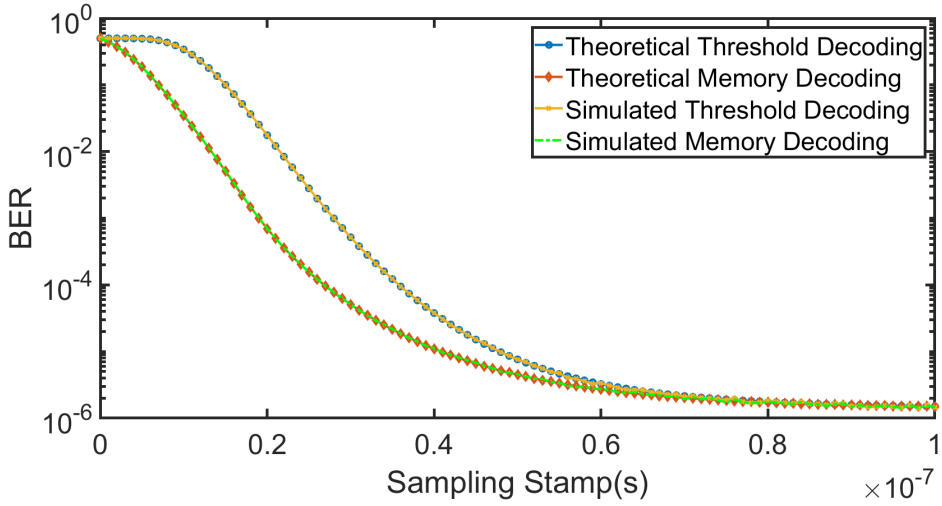

Figure 5.3: Classical Threshold Decoding vs. Memory Decoding Algorithm

$$\sum_i \pi_i = 1. \tag{5.15}$$

Solving Eq. (5.14) and Eq. (5.15) gives a unique vector $\bar{\boldsymbol{\pi}}$. The average bit error rate, BER, can be computed by summing up the stationary probabilities corresponding to all the states S_k where $\hat{x}_{i-1}$ is different from x_{i-1}. In this case, we have:

$$BER = \pi_1 + \pi_2 + \pi_5 + \pi_6. \tag{5.16}$$

Fig. 5.3 shows the comparisons of theoretical and simulated BERs for the normal threshold decoding and memory decoding scheme with SNR = 16 dB.

Similar techniques could be applied to analyse BERs for MDA with k-bit-long memory.

5.3 Simulation and Discussion

In this section, we show the simulation results for the proposed MDA vs. LMS equalization with Additive white Gaussian noise applied. We discuss the performances of one-bit-long memory, three-bit-long memory and five-bit-long memory signals with/without clock jitter. The training bits are used to determine τ_a and τ_b at the receiver for MDA and to train LMS equalization algorithm. Each figure in this section shows the BER vs. SNR when AWGN applied for a number of decoding schemes: classical threshold decoding with a fixed threshold, LMS equalization, and MDA with 1-bit-long, 2-bit-long and N-bit-long memory decoding models. The fixed threshold for classical threshold decoding is half of the voltage that the received signal can reach by sending a single "1". We simulated for both one and two samples per symbol.

5.3.1 One-Bit-Long Memory

The simulation parameters for one-bit-long memory optical signals are shown below.

- Data Rate : 100 MHz
- V_{max} : 2 V
- τ_a : 1.77×10^{-9} s
- τ_b : 1.59×10^{-9} s

- Length of training bits : 100 bits
- Threshold of Classic Threshold Decoding : 1 V

Fig. 5.4 shows the BER vs. SNR when AWGN applied with no clock jitter. For one sample per symbol, LMS equalization has almost exactly the same BER with normal threshold decoding, this is because the linear equalization is unable to recover the signals with just one sample per symbol. MDA with one sample per symbol improves the BER a bit compared with the other two schemes. Note that the BERs of MDA with 1-bit-long, 2-bit-long and N-bit-long memory decoding models are the same, is because the optical signals have only one-bit-long memory. Thus, the BERs can not benefit from 2-bit-long and N-bit-long decoding models. Sampling twice for each symbol can definitely help decoding. The BERs of both classical threshold decoding and LMS equalization reduce from 5.5×10^{-5} (one sample/symbol) to about 10^{-6} (two samples/symbol) with SNR of 15 dB. Furthermore, the BERs of MDAs reduce from 3.8×10^{-5} (one sample/symbol) to about 8.4×10^{-8} (two samples/symbol) with the same SNR level. As seen, using MDA results in the lowest bit error rates at the same level SNR. The difference is more pronounced as SNR increases. Fig. 5.5 and Fig. 5.6 simulate the scenarios when the clock jitter follows a zero mean normal distributions with standard deviations 2% of T and 4% of T respectively. The simulated results show that MDAs still consistently have lower bit error rates than the other schemes when clock jitter increases.

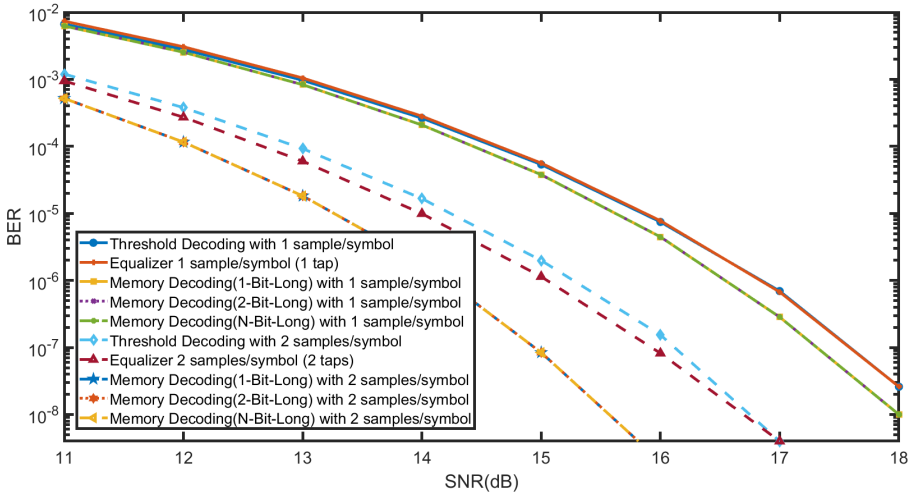

Figure 5.4: BER vs. SNR for Decoding 1-Bit-Long Memory Signals, No Clock Jitter

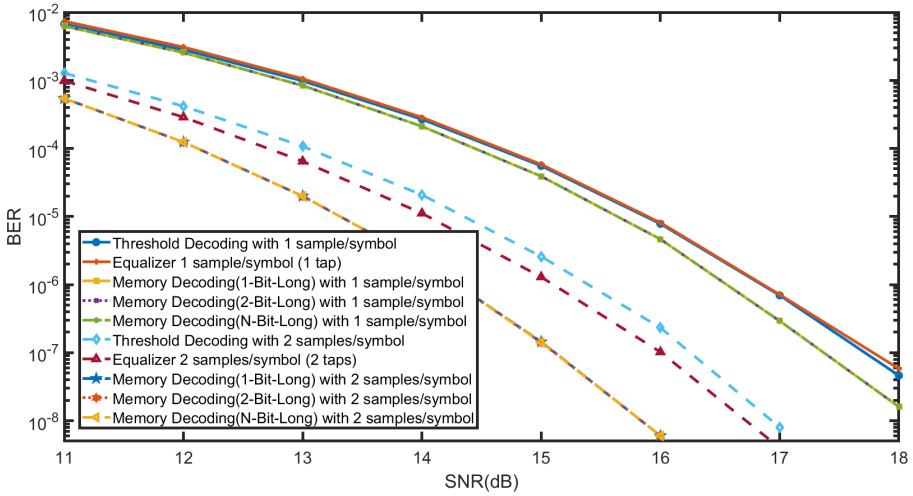

Figure 5.5: BER vs. SNR for Decoding 1-Bit-Long Memory Signals, Clock Jitter $\sim N(0, (2\%T)^2)$

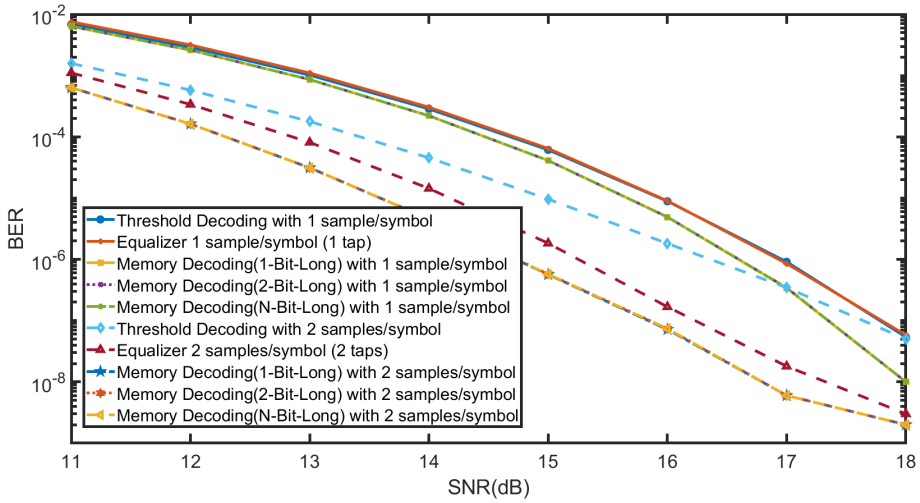

Figure 5.6: BER vs. SNR for Decoding 1-Bit-Long Memory Signals, Clock Jitter $\sim N(0, (4\%T)^2)$

5.3.2 Three-Bit-Long Memory

The simulation parameters for three-bit-long memory optical signals are shown below.

- Data Rate : 100 MHz
- V_{max} : 2 V
- τ_a : 5.31×10^{-9} s
- τ_b : 4.77×10^{-9} s
- Length of training bits : 100 bits
- Threshold of Classic Threshold Decoding : 0.85 V

Fig. 5.7 though Fig. 5.9 are the simulated results for the optical signals having three-bit-long memory with/without clock jitter applied. Because of the three-bit-long memory that the signals have, for both one sample and two samples per symbol cases, MDAs with 2-bit-long and N-bit-long memory models outperform the MDA with only 1-bit-long decoding model. This is because the decoding models with more bit memory can fit the signals better. As the SNR increases, the equalizer with one sample per symbol and the classic threshold decoding schemes with one sample and two samples per symbol still fail to decode. This is saying, as the data rates increases, the optical signals get distorted and have more memory, such that the normal decoding mechanisms are unable to adapt the distortion. Therefore, even with higher SNR, normal decoding is still infeasible. By contrast, MDAs get lower BERs consistently as SNR increases even the the clock jitter applied.

5.3.3 Five-Bit-Long Memory

The simulation parameters for five-bit-long memory optical signals are shown below.

- Data Rate : 100 MHz
- V_{max} : 2 V
- τ_a : 8.85×10^{-9} s
- τ_b : 7.95×10^{-9} s

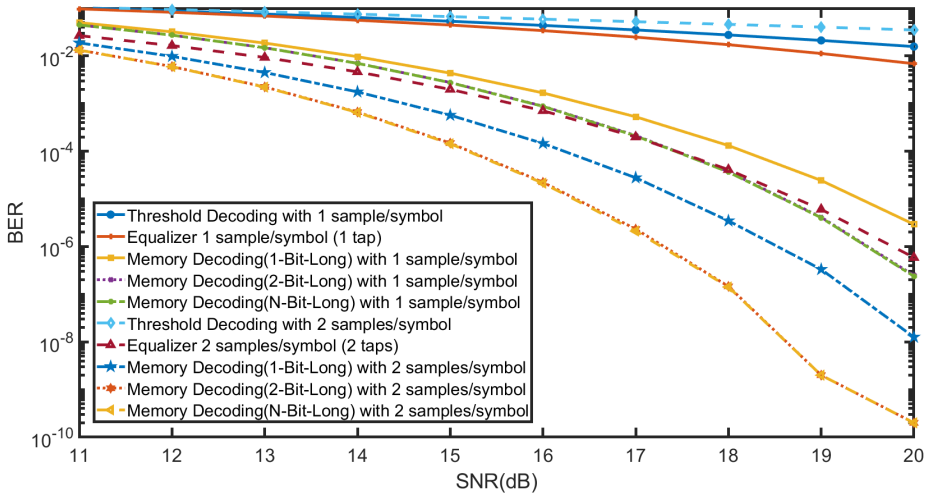

Figure 5.7: BER vs. SNR for Decoding 3-Bit-Long Memory Signals, No Clock Jitter

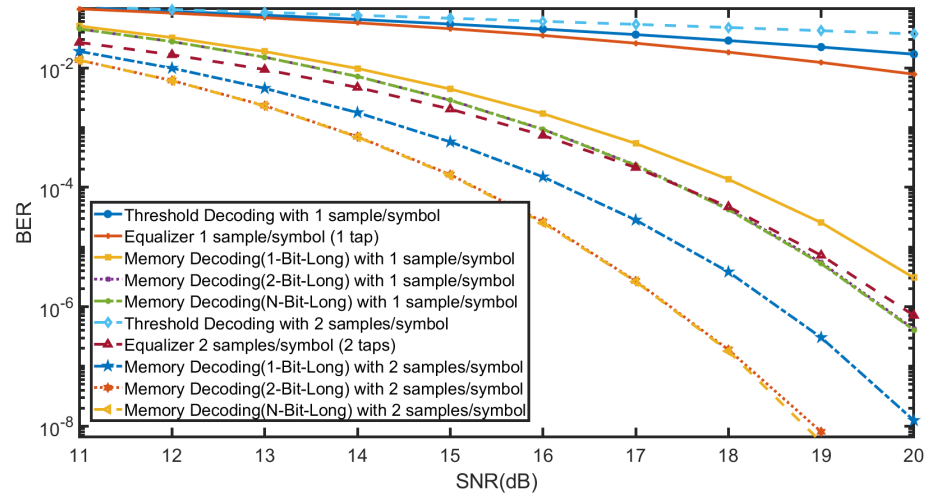

Figure 5.8: BER vs. SNR for Decoding 3-Bit-Long Memory Signals, Clock Jitter $\sim N(0, (2\%T)^2)$

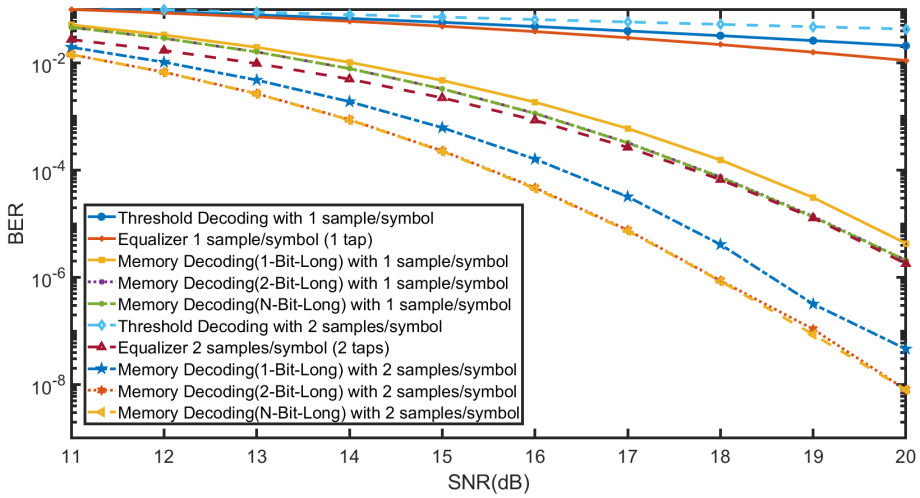

Figure 5.9: BER vs. SNR for Decoding 3-Bit-Long Memory Signals, Clock Jitter $\sim N(0, (4\%T)^2)$

- Length of training bits : 100 bits
- Threshold of Classic Threshold Decoding : 0.68 V

When the memory of the optical signals increases to five bits, only MDAs with 2-bit-long and N-bit-long memory models and the equalizer with two samples per symbol can attain lower BERs. The reason that the classic threshold decoding doesn't work has been explained earlier. The BER of MDA of 1-bit-long decoding model is higher than 10^{-2} when SNR is 22 dB, and even sampling twice per symbol can not improve the BER. This is because the 1-bit-long memory decoding model fails predicting the five-bit-long memory signals. This is also the reason that MDA with N-bit-long decoding model outperforms MDA with 2-bit-long decoding model. The MDA with N-bit-long decoding model fits the five-bit-long memory signals better than the 2-bit-long decoding model.

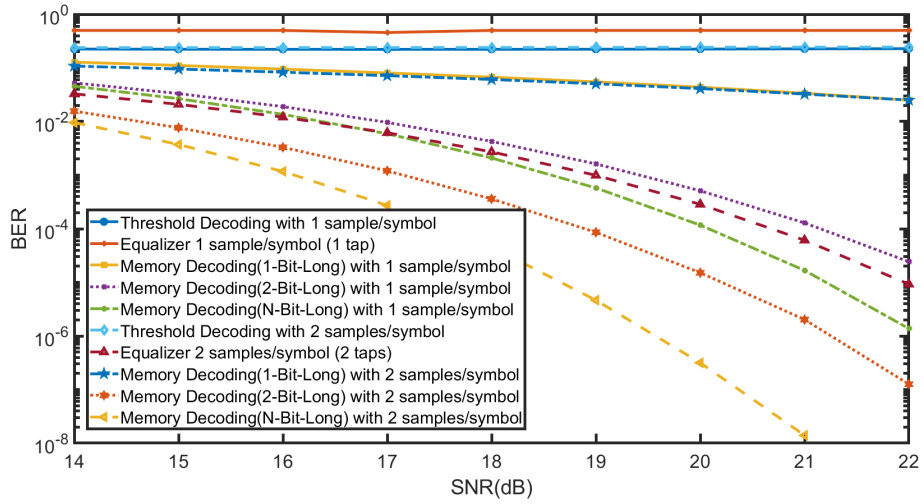

Figure 5.10: BER vs. SNR for Decoding 5-Bit-Long Memory Signals, No Clock Jitter

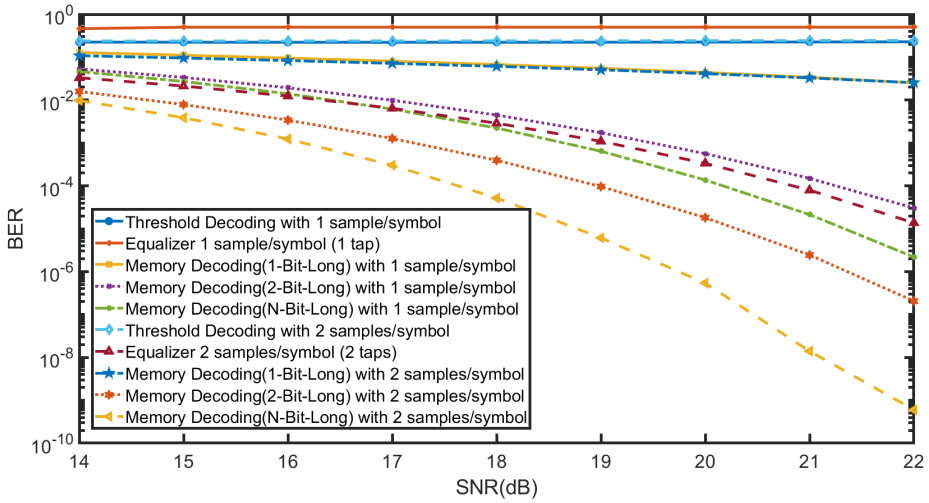

Figure 5.11: BER vs. SNR for Decoding 5-Bit-Long Memory Signals, Clock Jitter $\sim N(0, (2\%T)^2)$

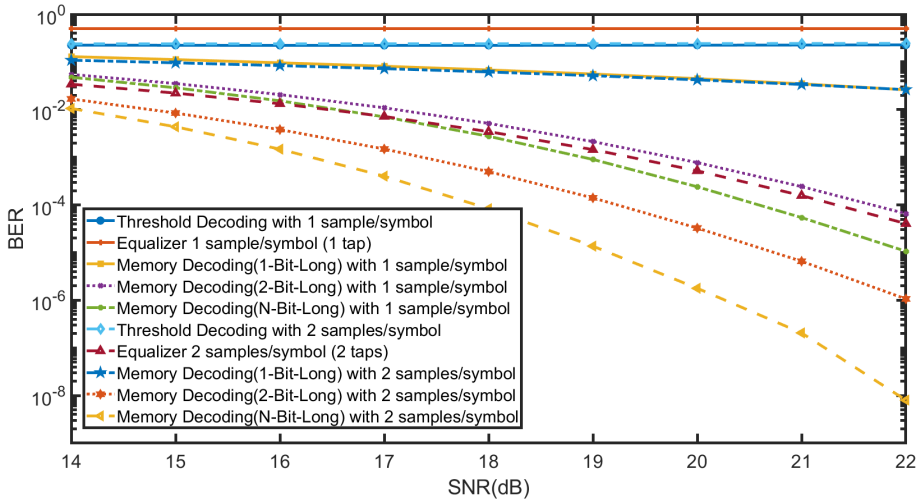

Figure 5.12: BER vs. SNR for Decoding 5-Bit-Long Memory Signals, Clock Jitter $\sim N(0, (4\%T)^2)$

Chapter 6: Conclusion

This chapter is a conclusion made to summarize the previous chapters. In Chapter 1, it briefly introduced the motivation, related work and the architecture of the novel WiFO system based on the FSO technologies. Video demos also successfully verify the feasibility of this novel system. In Chapters 2 , a reformed system for the scenario of overlapping light cones is addressed by mathematical models. We also proposed an optimal PAM decoding scheme for WiFO. The proposed PAM decoding scheme estimates the channel parameters, then uses them to determine the optimal thresholds to recover the transmitted signals and to minimize the bit error rate. Furthermore, we characterize the conditions on the channel parameters for signal irrecoverability. Simulations and theoretical analyses are provided to validate the proposed scheme. 3 utilizes the mathematical model from RC circuits to capture the distortion of optical response. The simulation shows that the math model fits the real optical response well for both low and high data rates. The memory property of optical response is also discussed in this chapter. This memory property plays a key role in Chapter 4 and Chapter 5 to successfully reduce BERs. In Chapter 4, we proposed a pre-shaping scheme by adjusting the sending duration for each bit. This so called Adaptive Sending Duration Algorithm(ASDA) successfully reduce BERs when working with a linear equalizer at the receiver. Chapter 5 utilized

a mathematical model from Chapter 3 to capture the distortion of the output for a given input. Based on the mathematical model, we developed a technique that effectively reduces the bit error rate when On-Off Keying modulation is used. This so called Memory Decoding Algorithm (MDA) is used at a receiver that exploits the distortion model to reduce the bit error rates via maximum likelihood decoding principle. Both theoretical analyses and simulation results show that the proposed technique outperforms the conventional methods such as linear equalization techniques, which require more samples and taps to get lower BER.

Bibliography

[1] Thomas Barnett, Jr., Shruti Jain, Usha Andra and Taru Khurana, "Cisco Visual Networking Index (VNI) Global and Americas/EMEAR Mobile Data Traffic Forecast, 2017–2022," at *https://www.cisco.com*

[2] J. Mitola III, G.Q. Maguire Jr., "Cognitive radio: making software radios more personal," in *Personal Communications, IEEE 6, 4 (1999), 13–18.*

[3] Qin Zhao, B.M. Sadler, "A survey of dynamic spectrum access," at *Signal Processing Magazine, IEEE 24, 2007, 79 –89.*

[4] Report of the spectrum efficiency working group "FC Spectrum Policy Task Force," at *http://www.fcc.gov/sptf/reports.html*

[5] Z. Ghassemlooy, S. Arnon, M. Uysal, Z. Xu, and J. Cheng, "Emerging optical wireless communications advances and challenges," in *IEEE J. Sel. Areas Commun., vol. 33, no. 9, pp. 1738–1749, Sep. 2015.*

[6] P. H. Binh and V. D. Trong, "500 MBIT/s OOKNRZ transceiver for 50 m GI-POF using 100 MHz RC-led," in *Microw. Opt. Technol. Lett., vol. 57, no. 4, pp. 826–830, 2015*

[7] P. Binh, V. Trong, P. Renucci, and X. Marie, "Improving OOK modulation rate of visible LED by peaking and carrier sweep-out effects using n-Schottky diodes-capacitance circuit," in *J. Lightw. Technol., vol. 31, no. 15, pp. 2578–2583, Apr. 2013*

[8] A. Jovicic, J. Li, and T. Richardson, "Visible light communication: Opportunities, challenges and the path to market," in *IEEE Commun. Mag., vol. 51, no. 12, pp. 26–32, Dec. 2013*

[9] B. Lin, X. Tang, Z. Ghassemlooy, C. Lin, and Y. Li, "Experimental demonstration of an indoor VLC positioning system based on OFDMA," in *IEEE Photon. J., vol. 9, no. 2, Apr. 2017, Art. no. 7902209.*

[10] O. Bouchet, M. El Tabach, M. Wolf, D. O'brien, G. Faulkner, J.W. Walewski, S. Randel, M. Franke, S. Nerreter, K.-D. Langer, J. Grubor and T. Kamalakis, "Hybrid wireless optics (hwo): Building the next generation home network," in *CNSDSP 2008*, pp. 283-287, 2008.

[11] H. Wu, B. Hamzeh and M. Kavehrad, "Achieving carrier class availability of fso link via a complementary rf link," in *Signals, Systems and Compputers, 2004. Conference Record of the Thirty-Eighth Asilomar Conference*, vol. 2, pp. 1483-1487, Nov. 2004.

[12] S. Bloom and W. Hartley, "The last-mile solution: hybrid FSO radio," in *AirFibber Inc.*, May. 2002.

[13] I. Kim and E. Korevaar, "Availability of free space optics (fso) and hybrid fso/rf systems," in *Proc. Optical Wireless Commun. IV*, Aug. 2001.

[14] H. Al Hajjar, B. Fracasso and D. Leroux, "Indoor optical wireless gbps link dimensioning," in *National Fiber Optic Engineers Conference, Anaheim, CA*, Mar. 17-21 2013.

[15] K. Wang, A. Nirmalathas, C. Lim and E. Skafidas, "Ultra-broadband indoor optical wireless communication system with multimode fiber," in *Optics Letters*, vol. 37, pp. 1514-1516, 2012.

[16] M. Kavehrad, "Sustainable energy-efficient wireless applications using light," in *IEEE Communication Magazine*, pp. 66-73, 2010.

[17] Z. Zhan et al., "1.2 Gbps non-imaging MIMO-OFDM scheme based VLC over indoor lighting LED arrangments," in *Proc. Opto-Electron. Commun. Conf., Shanghai, China, 2015, pp. 1–3.*

[18] A. Eslami, S. Vangala and H. Pishro-Nik, "Hybrid channel codes for efficient fso/rf communication systems," in *Communications, IEEE Transactions*, vol. 58, pp. 2926-2938, Oct. 2010.

[19] Y. Tang, M. Brandt-Pearce and S. Wilson, "Link adaptation for throughput optimization of parallel channels with application to hybrid fso/rf systems," in *Communications, IEEE Transactions*, vol. 60, pp. 2723-2732, Sep. 2012.

[20] N. Letzepis, K. Nguyen, A. Guillen i Fabregas and W. Cowley, "Outage analysis of the hybrid free-space optical and radio-frequency channel," in *Selected Areas in Communications, IEEE Journal*, vol. 27, pp. 1709-1719, Dec. 2009.

[21] F. Ahdi and S. Subramaniam, "Optimal placement of fso links in hybrid wireless optical networks," in *Global Telecommunications Conference (GLOBECOM 2011), 2011 IEEE*, pp. 1-6, Dec. 2011.

[22] A. Abdulhussein, A. Oka, T. T. Nguyen and L. Lampe, "Rateless coding for hybrid free-space optical and radio-frequency communication," in *Wireless Communications, IEEE Transactions*, vol. 9, pp. 907-913, Mar. 2010.

[23] D. Wang and A. Abouzeid, "Throughput capacity of hybrid radio-frequency and free-space-optical (rf/fso) multi-hop networks," in *Information Theory and Applications Workshop, 2007*, pp. 3-10, Jan. 2007.

[24] H. Kaushal and G. Kaddoum, "Underwater optical wireless communication," in *IEEE Access, vol. 4, pp. 1518–1547, 2016.*

[25] M. Kavehrad, Z. Hajjarian, and A. Enteshari, "Energy-efficient broadband data communications using white LEDs on aircraft powerlines," in *Proc. Integr. Commun., Navig. Surveillance Conf., Bethesda, MD, USA, 2008, pp. 1–8.*

[26] P. Luo, Z. Ghassemlooy, H. Le Minh, E. Bentley, A. Burton, and X. Tang, "Performance analysis of a car-to-car visible light communication system," in *Appl. Opt., vol. 54, no. 7, pp. 1696–1706, 2015.*

[27] H. Haas, L. Yin, Y. Wang and C. Chen, "What is LiFi," in *Journal of Lightware Technology.*

[28] Di Wang and Alhussein A. Abouzeid, "Throughput and delay analysis for hybrid radio-frequency and free-space-optical (rf/fso) networks," in *Wirel. Netw.*, vol. 17, no. 4, pp .877-892, May 2011.

[29] F. E. Doany et al., "Terabit/s-class optical pcb links incorporating 360gb/s bidirectional 850 nm parallel optical transceivers," in *J. Lightwave Technol.*, vol. 30, pp .560-571, 2012.

[30] A. T. Hussein, J. M. H. Elmirghani, "Mobile Multi-gigabit Visible Light Communication System in Realistic Indoor Environment," in *Journal of Lightwave Technology, vol. 33, pp. 3293-3307, 2015.*

[31] I. Stefan, H. Haas, "Hybrid Visible Light and Radio Frequency Communication Systems," in *IEEE 80th Vehicular Technology Conference., pp. 1-5, 2014.*

[32] M. Z. Afgani, H. Haas, H. Elgala, D. Knipp, "Visible Light Communication Using OFDM," in *2nd International Conference on Testbeds and Research Infrastructures for the Development of Networks and Communities., TRIDENTCOM (2006) 6–134.*

[33] Q. Wang, T. Nguyen and A. Wang, "Channel capacity optimization for an integrated wi-fi and free-space optic communication system(wififo)," in *17th ACM MSWIM 2014*, ACM, 2014.

[34] T. Duong, D. Nguyen and T. Nguyen, "Location assisted coding(LAC): Embracing interference in free space optical commnucations," in *ACM MsWiM, 2015.*

[35] YJ. Chu, T. Nguyen and Z. Stark, "WiFO: Hybrid WiFi and Free-Space Optical Communication System with PAM Optimal Decoding," in *ICCCN, 2016.*

[36] Wikipedia, "Manchester code," in *https://en.wikipedia.orgwiki/Manchester_code*

[37] G. Einarsson, "rinciples of Lightwave Communications," in *John Wiley and Sons, 1996.*

[38] Wikipedia, "Additive White Gaussian Noise," in *https://en.wikipedia.org/wiki/Additive_white_Gaussian_noise*

[39] Wikipedia, "Rayleigh Distribution," in *https://en.wikipedia.org/wiki/Rayleigh_distribution*

[40] S. Liverman, Q. Wang, Y.J. Chu, A. Borah, S. Wang, A. Natarajan, A. Wang and T. Nguyen, "WiFO: A hybrid communication network based on integrated free-space optical and WiFi femtocells," in *Computer Communications, vol. 132, pp. 74-83, November 2018.*

[41] S.O. Kasap, "Optoelectronics and Photonics: Principles and Practices," in *Prentice Hall, Jan 1, 2001.*

[42] H. Li, X. Chen, J. Guo, and H. Chen, "A 550 Mbit/s real-time visible light communication system based on phosphorescent white light LED for practical high-speed low-complexity application," in *Opt. Exp., vol. 22, no. 22, pp. 27203–27213, 2014.*

[43] M. Zhang, "A visible light communications system with 220 MHz bandwidth based on pre-emphasis and postequalization technologies," in *Proc. Asia Commun. Photon. Conf., Shanghai, China, 2014, Paper ATh3A.116.*

[44] Cheng, C.M., Peng, Z., Zhang, W. and Meng, Guang "Volterra-series-based nonlinear system modeling and its engineering applications: A state-of-the-art review," in *Vol. 87, Mechanical Systems and Signal Processing, Nov. 2016.*

[45] K. Asatani, and N. Tatsuya, "Linearization of LED Nonlinearity by Predistortions," in *IEEE Journal of Solid-State Circuits, Vol. SC-13, No. 1, Feb. 1978.*

[46] K. Asatani, and T. Kimura, "Nonlinear phase distortion and its compensation in l.e.d direct modulation," in *Electron. Eltt., vol. 13, pp. 162-163, 1977.*

[47] P. Aggarwal, R. Ahmad, V. A. Bohara and A. Srivastava, "Adaptive Predistortion Technique for nonlinear LED with Dimming Control in VLC system," in *2017 IEEE International Conference on Advanced Networks and Telecommunications Systems (ANTS), pp. 1-6, 2017.*

[48] J. K. Kim, K. Hyun, and S. K. Park, "Adaptive predistorter using NLMS algorithm for nonlinear compensation in visible-light communication system," in *2017 Electronics Letters, vol. 50, no. 20, pp. 1457-1459, Sept. 2014.*

[49] R. Mitra, and V. Bhatia, "Chebyshev Polynomial-Based Adaptive Predistorter for Nonlinear LED Compensation in VLC," in *IEEE Photonics Technology Letters, vol. 28, no.10, pp. 1053-1056, May 2016.*

[50] L. Ding, G. T. Zhou, D. R. Morgan, Z. Ma, J. S. Kenney, J. Kim, and C. R. Giardina, "A robust digital baseband predistorter constructed using

memory polynomials," in *IEEE Transactions on Communications, vol. 52, no.1, pp. 159-165, Jan 2004.*

[51] H. Elgala, R. Mesleh, and H. Haas, "Predistortion in optical wireless transmission using OFDM," in *Proc. 9th Int Conf. Hybrid Intell. Syst.(HIS), vol.2, pp. 184-189, Aug. 2009.*

[52] A. V. Kudryashov, A. S. Kalinina, and G. N. Yagovkin, "Pulse width modulated LED light control and vision adaptation," in *International Conference on Industrial Engineering, Applications and Manufacturing, pp. 1-4, May, 2017.*

[53] S. Mahadeokar and M. Sardeshmukh, "Energy efficient PWM Dimmable Smart Digital LED driver," in *International Conference on Energy Systems and Applications, pp. 306-311, 2015.*

[54] K. Cho, W. Oh, Y. Oh and C. In, "A new high resolution PWM dimming strategy for LED lightings," in *IEEE International Conference on Industrial Technology (ICIT), pp. 581-584, Feb. 2018.*

[55] A. Sepahvand, A. Kumar, M. Doshi, V. Yousefzadeh, J. Patterson, K. K. Afridi and D. Maksimovic, "Current control and PWM dimming in an automotive LED driver based on a Ćuk converter," in *IEEE 18th Workshop on Control and Modeling for Power Electronics (COMPEL), pp. 1-8, July. 2017.*

[56] M. Zhou, L. Cheng, D. Lv, Z. Hong and B. Y. Liu, "A dual-path, current-sensing resistor-free boost LED driver with fast PWM dimming," in *Twenty-Eighth Annual IEEE Applied Power Electronics Conference and Exposition (APEC), pp. 848-853, Mar. 2013.*

[57] A. Mirvakili and V. J. Koomson, "High efficiency LED driver design for concurrent data transmission and PWM dimming control for indoor visible light communication," in *IEEE Photonics Society Summer Topical Meeting Series, pp. 132-133, July 2012.*

[58] D. Dalton et al., "A 12.5-Mb/s to 2.7-Gb/s continuous-rate CDR with automatic frequency acquisition and data-rate readback," in *IEEE J. Solid-State Circuits, vol. 40, no. 12, pp. 2713-2725, Dec. 2005.*

[59] W. Xu, M. Zhang, D. Han, Z. Ghassemlooy, P. Luo, and Y. Zhang, "Real-time 262-Mb/s visible light communication with digital predistortion waveform shaping," in *IEEE Photon. J., vol. 10, no. 3, Jun. 2018, Art. no. 7903610.*

[60] Wikipedia, "Jitter," in *https://en.wikipedia.org/wiki/Jitter*

[61] Y. Yi, K. Lee, Y. M. Jang, J. Cha, J. Y. Kim and K. Lee, "Indoor LED-Based identification systems using adaptive MMSE equalizer for optical multipath dispersion reduction," in *International Conference on ICT Convergence Sept. 2011. pp. 95-100 ITCT 2011.*

[62] H. Le Minh, Z. Ghassemlooy, A. Burton and P. A. Haigh, "Equalization for organic light emitting diodes in visible light communications," in *2011 IEEE GLOBECOM Workshops (GC Wkshps), Dec. 2011.*

[63] P. A. Humblet, "Design of optical matched filters," in *Proc. IEEE GLOBECOM'91, vol. 2, Dec. 2–5, 1991, pp. 1246–1250.*

[64] T. Matsumoto and S. Matsufuji, "Theoretical analysis of BER performance in ASK-SS and M-ary/ASK-SS systems using compact matched filter bank for an optical ZCZ code over AWGN channels," in *Proc. of the 5th International Workshop on Signal Design and its Applications in Communications, pp. 161-164, 2011.*

[65] Y. Chu and T. Nguyen, "Memory Decoding Algorithm for FSO Transmission," in *91st Vehicular Technology Conference (VTC Spring), IEEE, 2020.*

[66] Sun-How Jiang and Feng-Hsiang Lo, "PRML process of multilevel run length-limited modulation recording on optical disk," in *IEEE Trans. on Magnetism, vol. 41, no. 2, pp. 1070-1072, Feb. 2005.*

[67] J. Edwards et al., "A 12.5 Gbps analog timing recovery system for PRML optical receivers," in *IEEE RFIC Symp., Jun. 2009.*